2-2-2016

Numerical modeling of nonlinear mode interaction in semiconductor lasers and amplifiers to generate slow/fast light

Hemashilpa Kalagara

Hemashilpa Kalagara
Candidate

Electrical & Computer Engineering
Department

The dissertation is approved, and it is acceptable in quality and form for publication on microfilm:

Approved by the Dissertation Committee:

Dr. Marek Osinski , Chairperson

Dr. Peter G. Eliseev

Dr. Mansoor Sheik- Bahae

Dr. Ganesh Balakrishnan

NUMERICAL MODELING OF NONLINEAR MODE INTERACTION IN SEMICONDUCTOR LASERS AND AMPLIFIERS TO GENERATE SLOW/FAST LIGHT

BY

HEMASHILPA KALAGARA

B.E., Electronics & Instrumentation Engineering, Birla Institute of Technology and Science, Pilani, 2008

DISSERTATION

Submitted in Partial Fulfillment of the
Requirements for the Degree of

Doctor of Philosophy
Engineering

The University of New Mexico
Albuquerque, New Mexico

December 2015

ACKNOWLEDGMENTS

I sincerely thank Dr. Marek Osiński, my advisor and dissertation chair for giving me the opportunity to work on this project. He is not only a great scientist, but a visionary and an inspiration to me. I am also extremely grateful to Dr. Peter Eliseev who is my co-advisor and also the innovator of this idea along with Dr. Osiński. Dr. Eliseev has been my driving force throughout this study, and without him this dissertation would not exist. I'm highly privileged to work with such a brilliant researcher and a great human being. I also thank my committee members, Dr. Mansoor Sheik-Bahae and Dr. Ganesh Balakrishnan for their advice and valuable comments regarding my dissertation. I sincerely thank Dr. Gennady Smolyakov for his support during the span of my PhD. I also thank my colleagues in the Center for High Technology Materials, especially my group member Fei-Hung Chu for his help and support.

I am extremely grateful to my mother, Vasantha; her unconditional love and sacrifices have helped me arrive at where I am today. I am also thankful to my friends Pankaj Ahirwar, Inian Subramanian, Rahul Jaiswal, Thomas Rotter, Ashwin Rishinaramangalam, Romica Kerketta, Anusha Tejomurtula, Abhishek Reddy, and Ezhi Subramanian, without whose encouragement and support this degree would not have been possible. I'm also grateful to my father Venkata Rao Kalagara, brother Sunil Kalagara, sister-in-law Swetha Bezawada and my nephew Ivaan Kalagara for their love and support.

Dedicated to my mother, Vasantha

NUMERICAL MODELING OF NONLINEAR MODE INTERACTION IN SEMICONDUCTOR LASERS AND AMPLIFIERS TO GENERATE SLOW/FAST LIGHT

by

Hemashilpa Kalagara

B.E., Electronics & Instrumentation Engineering, Birla Institute of Technology and Science, Pilani, 2008

Ph.D., Engineering, University of New Mexico, 2015

ABSTRACT

The nonlinear interaction (NLI) between modes in a semiconductor laser or amplifier is one of the techniques to obtain slow light ($n_g >> 1$), fast light ($-1 < n_g < 1$), phase conjugated reflection (also known as backward light ($n_g < 0$)) and supercontinuum emission (also known as critically anomalous dispersion ($n_g = 0$)), where n_g is the group index. In the nonlinear interaction (NLI) mechanism, the interaction between a driving wave (mode) which is of sufficiently high intensity, and a probe wave (mode) results in modification of complex permittivity of the probe wave, if the frequency detuning between the two waves falls into the spectral range of parametric interaction. Consequently, in the vicinity of a strong driving wave (mode), the optical parameters such as the phase index, group index, linewidth, and the gain of a neighboring probe (weak) wave are strongly perturbed. The unusual perturbation of group index leads to slow light, fast light and backward propagating light depending on the frequency detuning between the two waves. Fast light can have important applications in interferometry, to make very sensitive interferometric sensors for detection of nano displacement, ultra-low vibration, rotation rate and even very weak gravitational waves. The

slope sensitivity of an active integrated ring laser gyro (RLG) is directly proportional to the size of the ring and inversely proportional to the group index of the medium filling the cavity. By reducing n_g in the nonlinear regime of laser operation, slope sensitivity can be improved by manifolds without having to increase the size of the gyro, which will lead to monolithic integration.

In this dissertation work, the numerical modeling and simulation of NLI in semiconductor ridge waveguide (RWG) lasers is performed and perturbations of phase index, group index, gain, linewidth are calculated. The modeling is based on "theory of nonlinear interaction of waves" developed for plane waves and is applied to RWG lasers. The RWG laser structures are based on GaN/InGaN, GaAs/AlGaAs, InGaAs/GaAs/AlGaAs, InGaAsP/InP material systems, to cover the most important spectral range of semiconductor lasers starting from $\lambda = 0.4$ μm to $\lambda = 1.55$ μm, respectively. The photonic design software RSoft's FemSIM that uses finite element method is used for design and modeling of NLI in RWG and calculation of effective phase index. The induced dispersion and effective group index n_g are then calculated by differentiation of the effective phase index of guided probe wave over the optical frequency. The calculations indicate that the magnitude of NLI depends on the driving wave intensity, frequency detuning between driving and probe waves, lifetime of carriers in the laser system, optical confinement factor, driving wave wavelength and linewidth broadening factor of the laser structure.

An important result of this work is observation of frequency points where n_g passes zero line, known as the points of *critically anomalous dispersion* (CAD). In the spectral vicinity of CAD points, superluminal group velocity is observed, which can be used for improving the sensitivity of ring laser gyros and other interferometric sensors. In this dissertation, we established possibility of superluminal behavior ($-1 < n_g < 1$) through NLI in all of the above mentioned RWG laser structures, and obtained the conditions necessary to

observe this behavior. Also, the CAD frequencies are plotted by varying the driving wave intensities, where the data form a closed loop. The closing of the loop is due to suppression of NLI with an increase in driving wave intensity; at high intensities, the stimulated recombination rate increases, leading to an increase in overall relaxation rate, which in turn decreases the NLI. The CAD loops are calculated for all the RWG lasers mentioned above. The CAD loops provide information on lower and upper threshold intensity of the driving wave, and on frequency detuning between the driving and probe waves for observation of superluminal group velocity. Another important result is that the perturbed linewidth increases infinitely at the CAD point, leading to supercontinuum emission or white light, which can be exploited for very broadband laser emission applications.

We also fitted our numerically calculated perturbed delay and advance due to NLI with the experimental data of perturbed delay and advance of an optical pulse in a semiconductor optical amplifier based on InGaAsP/InP, and identified the CAD point for the very first time.

TABLE OF CONTENTS

LIST OF FIGURES

LIST OF TABLES

Chapter 1
Introduction

1.1. Motivation and applications

The physics of semiconductor lasers combines several interacting sub-systems, namely optical, electronic, electrical, thermal and lattice-mechanical systems. The optical sub-system seems to be the most complicated one due to significant nonlinearity of the semiconductor medium. In this dissertation, our interest is on a relatively new sphere of physical problems in the optical sub-system associated with anomalous propagation of laser emission. It is due to nonlinear interaction (NLI) between the spectral modes in a semiconductor laser or two travelling waves in a semiconductor amplifier in close spectral vicinity [Bogatov 1975], [Uskov 2005].

In the NLI phenomenon, the interaction between two waves, with one of them being at sufficiently high intensity, called the driving wave, results in modification of optical parameters such as phase index, group index, gain , linewidth at the probe wave frequency [Bogatov 1975], [Eliseev 2005a], [Eliseev 2005b]. The group velocity v_g of the probe wave, especially, is significantly modified resulting in slow light ($v_g << c$), fast light ($v_g > c$), backward propagating light ($v_g < 0$) and critically anomalous dispersion (CAD) or supercontinuum emission where, theoretically, $v_g \rightarrow \infty$ [Eliseev 2006]. Using traditional wave mechanics, it is difficult to predict the behavior of optical elements and systems in the anomalous (negative) dispersion regime. The difficulty is due to change in the physical meaning of optical parameters and in the interpretation of group velocity where the commonly-accepted technique of measurement of group velocity failed to give meaningful results [Milonni 2004], [Boyd 1992].

Semiconductor lasers are extensively used in “sensing applications” due to coherent emission of the very compact laser diodes. The possibility to increase the group velocity beyond *c* using NLI can be used for improving the sensitivity of interferometer-based laser sensors for detection of nano-displacement, ultra- low vibration, rotation rate (i.e, ring laser gyroscopes) and even gravitational waves.

The mechanism of NLI was first observed in [Bogatov 1975] in the form of spectrally-asymmetric gain suppression in an external cavity semiconductor laser and similar results were observed in [Ishikawa 1982], [Ogaswara 1988a],[Ogaswara 1988b] and [Yamada 1989] that also focused on the perturbation of gain. However, in [Bogatov 1975] the perturbed permittivity has also been calculated, so the perturbation of refractive index can be predicted . The perturbation of refractive index was calculated in [Eliseev 2005]. An important feature of this type of nonlinear perturbation is relatively very small perturbation of phase index which is sufficient enough to result in significant modification of the group index. This can be explained by narrow frequency range where the phase index perturbation occurs. Thus, the induced dispersion is quite large, and it is comparable or even larger than the background dispersion.

1.2. Theory of coherent population oscillation (CPO) related to the wave interaction in lasers

1.2.1. The mechanism of nonlinear interaction (NLI) of waves

The nonlinear interaction (NLI) of waves in semiconductor lasers is inevitable process because exchange of photons takes place between, either travelling waves in semiconductor optical amplifier, or between modes of laser emission in the laser oscillator. It acts in addition to the usual mode competition for the pumping power. The interaction of two (or more) waves results in oscillation (“vibration”) of the carrier density according to the wave

interference pattern. The local carrier density is subjected to spatial and temporal variations so the process can be considered as a particular case of *coherent population oscillation* (CPO) [Palinginis 2005]. The CPO is the predominating process of NLI in semiconductor media because of very strong influence of carrier density on the complex refraction index. This mechanism is prominent in semiconductor lasers also due to relatively large recombination lifetime of carriers, ~1 ns in contrast to ~1 ps for the intraband relaxation. The CPO is assumed to be mechanism of not only the two-wave NLI but also three-wave, four-wave and six-wave mixing phenomena. Especially, the six-wave NLI is found to be one of the mechanisms for lateral instability of laser beam in laser diodes.

A general NLI phenomenon consists of the following steps: (i) formation of dynamic spatial structure of intensity due to interference of interacting waves; (ii) formation of the dynamic structure of the dielectric permittivity in the medium; (iii) nonlinear scattering of driving wave on the dynamic structure of dielectric permittivity with generation of photons at shifted wavelength, particularly, at frequency of another interacting wave; (iv) modification of refractive index and coefficient of gain at probe wave frequency.

1.2.2. Estimation of NLI related perturbation of refractive index

Preliminary calculations of perturbed refractive index have been performed in [Eliseev 2005] and the perturbation δn is in the range of 10^{-4}-10^{-3}. The spectrum of the perturbation is a "bump" around the frequency of the driving wave. If the "bump" is localized in the range of about 1 GHz, the induced dispersion is as large as 10^{-13}-10^{-12} s, whereas background dispersion is about 10^{-15} s (here background dispersion means linear, unperturbed part of the dispersion). Earlier calculations of NLI were for plane waves taking into account material parameters of index and its dispersion. However in real laser structures one deals with guided waves propagating in multilayer structures. The modal parameters will be substantially modified, according to optical model of single-spatial-mode. The magnitude of

optical gain also decreases according to the optical confinement parameter Γ. Separate analysis is needed to calculate the NLI in real lasers, simple multiplication of δn due to plane wave approach with Γ is not accurate.

In this dissertation study, we performed numerical modeling of NLI in ridge-waveguide (RW) laser structures based on various material systems. The RSoft FemSIM which we used allows us to find the modal refractive index that is a weighted average value of indices involved in the structure (in proportion to the fraction of modal field propagating in all layers). We understand that the NLI occurs only in active layers where the modal field interacts with the matter. Thus, there should be correlation between the magnitude of the NLI and parameter Γ. Also, calculations are performed accounting for the lateral confinement. The RW geometry is chosen because of its advantage in precise control of lateral confinement and because of technological advances and popularity of the RW stripe geometry in industries and laboratories**.** The results of these calculations will be discussed in chapters 5, 6 and 7.

The main goals of this dissertation are :

(i) To understand and predict the behavior of laser with modes operating under anomalous conditions ($dn/d\nu < 0$) due to parametric wave interaction (NLI)

(ii) To understand the mysterious behavior of laser systems at critically anomalous dispersion (CAD) points where $n_g = 0$ and $v_g \rightarrow \infty$

(iii) Operating in the unusual regimes of light propagation such as slow light, fast light, critically anomalous dispersion (CAD) (also called as white light cavity resonance) and reflected light

(iv) Numerical modeling and simulation of NLI in tightly-confined guided waves in the ridge waveguide (RW) geometry

(v) Development of theory for making monolithically integrated ring laser based gyroscopes using nonlinear Sagnac effect

Fig.1.1 shows the effects of NLI and the potential applications of these effects.

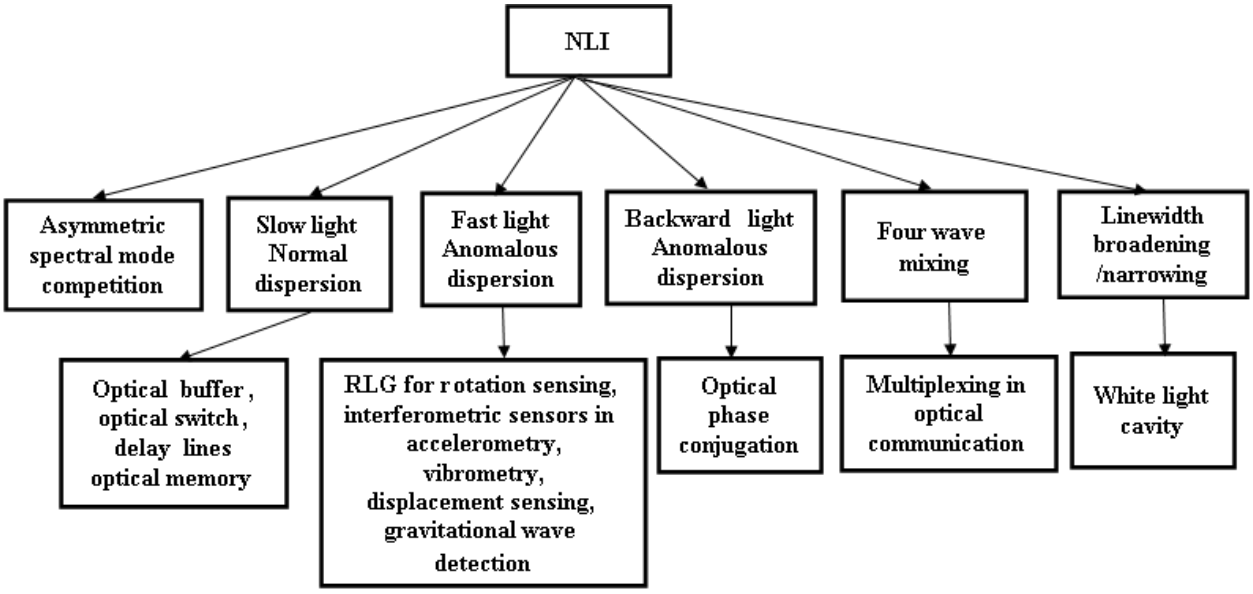

Fig.1.1. Effects of NLI and their potential applications

Chapter 2

Nonlinear optics of semiconductor lasers

2.1. Introduction

The semiconductor laser is highly nonlinear, when compared with other types of lasers. The laser operation by itself is a nonlinear process, which is evident from the rate equations used to describe its electrical and optical performance. The gain saturation mechanism is one of the basic nonlinear processes. In addition, nonlinear mechanisms such as hole burning, nonlinear gain, etc. exist that influence the gain in semiconductors. These phenomena are incorporated into the rate equations by additional terms. In this project, we consider the phenomenon of "nonlinear interaction" (NLI) of modes or waves. Due to this phenomenon, the *eigen-functions* representing modes of electromagnetic field in the semiconductor medium do not obey the orthogonality principle. Hence, we cannot consider our laser system in the multimode regime, comprising of independent modes. In the NLI mechanism, due to the exchange of photons between different modes, the behavior of saturation and competition of spectral and spatial components of the laser emission is modified. We continue to use the term "mode" for those field formations that can be identified as simplest components of individual frequency and configuration.

One of the most important features of semiconductor laser media is influence of carrier density on the refractive index of the medium. The two main effects behind the influence are:

1) Absorption saturation and inversion at the edge of intrinsic absorption

2) Shift of plasma resonance frequency

These mechanisms will be explained in more detail in the later sections. An increase of carrier density leads to a decrease of the refractive index n at the laser frequency according to both mechanisms. The property of semiconductors to have a variable index, depending on

carrier density N was well known. In the early papers on the theory of semiconductor lasers, it was mentioned that the gradient of dopant density can be used to obtain an internal optical reflection [Basov 1961]. This effect is crucial for the formation of guided waves in the semiconductor lasers. The waveguide theory of semiconductor laser structures taking into account carrier-dependent index is given in [Eliseev 1970]. The theory of optical filamentation in semiconductor lasers which is based on carrier-dependent index is given in [Thompson 1972].

The differential index which is given by the equation, $\sigma = \frac{dn}{dN}$, is in the range of 10^{-21}-10^{-20} cm^3 for a semiconductor medium. This quantity provides significant change of the index when carrier density change is in the range of 10^{17}-10^{19} cm^{-3}. The observation of optical bistability is an indication of very high nonlinearity in semiconductors when compared to other well-known transparent dielectrics. In materials where self-focusing was observed for the first time, the coefficient of nonlinearity, n_2 is found to be in the range of 10^{-16}-10^{-18} cm^2/W. Whereas, the parameter n_2 is found to be -0.003 cm^2/W in InSb [Miller 1979], and -$4x10^{-4}$ cm^2/W [Gibbs 1979] in GaAs. Such giant nonlinearity leads to a resonant-like "bump", at spectral vicinity of the intrinsic absorption edge.

Another parameter widely used in the theory of nonlinear effects is the *linewidth enhancement factor*

$$\alpha = -\frac{\mathrm{Re}(d\varepsilon / dN)}{\mathrm{Im}(d\varepsilon / dN)} = -\frac{4\pi}{\lambda}\frac{dn/dN}{dg/dN} \qquad (2.1)$$

where, ε is the complex dielectric permittivity of material filling the laser cavity, *dn*/*dN* is the differential index and *dg/dN* is the differential gain. The factor α, which is also referred to as coefficient of *amplitude-phase coupling*, indicates the relationship between change in refractive index and optical gain. The quantity $\xi = 1/\alpha$ has been first introduced in [Bogatov 1975]. Later, in it was shown that the factor α plays a substantial role in the broadening of

laser spectral line and is commonly known as *linewidth enhancement factor* [Henry 1982]. In many cases, linewidth enhancement factor is used at particular laser wavelength, since it is not constant over the lasing spectral range of each laser structure. The spectral variations of linewidth enhancement factor have been considered in [Osinski 1987].

In the following sections about nonlinear optics, we will consider nonlinear phenomena associated with interaction of waves in the semiconductor medium with externally pumped optical gain (carrier injection through a *p-n* junction or by optical pumping).

2.2. Nonlinear gain

The NLI produces a change of optical gain in the semiconductor active medium according to intensity of electromagnetic wave propagating in the medium. The probe wave gets spectrally-asymmetric gain or attenuation that is dependent on intensity of driving wave, as shown in [Bogatov 1975]. Thus, this effect is an example of nonlinear gain. However, in the theory of semiconductor lasers, the term "nonlinear gain" is used frequently for gain suppression due to high intensity of laser emission at the same optical frequency. In other words, the behavior is nothing but the nonlinear self-action of the laser emission. The effective gain at the lasing frequency is described by the familiar equation,

$$g(S) = \frac{g_0}{1+\varepsilon S} \approx g_0(1-\varepsilon S) \tag{2.2}$$

where, S is the photon density, ε is the nonlinear gain coefficient. The product εS is assumed to be small, $\varepsilon S << 1$. Thus, it is necessary to distinguish the nonlinear gain at the lasing frequency and at frequencies in the vicinity of lasing frequency.

2.3. Nonlinear optical self-action

There are several mechanisms of nonlinear self-action. The result is change of refractive index and/or gain due to influence of the laser emission intensity.

1) The calculated effect of NLI predicts change of gain when the probe frequency and drive frequency coincide. This result is not reliable because the assumptions are not fulfilled in this case. Moreover, the procedure of calculation does not include accounting for phenomena characteristic to very close frequencies of interacting waves, namely, frequency locking, line-shape overlapping, etc.

2) The primary effect of saturation of gain under influence of the light intensity (both in laser and in amplifier) is treated by the rate equations. This is quite strong effect that explains limitation of light amplification in dependence with pumping rate.

3) In addition to this global saturation of gain and carrier density, it is necessary to take into account further increase of carrier density in the stationary laser regime. It is well known fact that the optical gain is stabilized (pinned) above the threshold. This leads automatically to the pinning of carrier density. Actually it was noticed that the pinning of carrier density at the threshold is not perfect, as the optical gain gets additional suppression at higher pump rate, so this gain becomes sensitive to the intensity of light. This behavior can be due to combination of several mechanisms. One is the spectral hole-burning. In this case, the distribution of carriers over energy scale is deviated from the quasi-equilibrium (the Fermi-Dirac functions). The distribution “hole” grows along with the increase of emission intensity. Thus, the gain in the “hole” gets suppression that is not accounted for in traditional rate equations. Another mechanism is carrier heating due to laser emission. The elementary process is similar to light absorption by free carriers. The result is, increase of temperature T_e of electron-hole gas along with an increase of the light intensity. Due to substantial dependence of gain on temperature, an increase of T_e leads to a suppression of gain.

In the physics of semiconductor lasers, the phenomena of gain saturation and suppression have been accounted in the rate-equation in two steps: the global saturation of gain (and inverted population) is treated by basic rate equation whereas the "nonlinear gain" is considered as addition to stimulated recombination term. Namely, the actual gain *g* is equal to $g_0/1+\varepsilon S$, where g_0 is the unsuppressed gain when there is no laser action, S is the photon density in the laser regime, and ε is a phenomenological parameter of nonlinear gain. Typical values of ε were obtained from experimental data which range from $5\text{x}10^{-18}$ to 10^{-15} cm^3.

2.4. Self-focusing and optical bistability

Another self-action nonlinear effect is self-focusing (or self-defocusing, depending on the sign of the change of the refractive index at an increase of the light intensity). The expression for self focusing is given by

$$n(I) = n_0 + n_2 I \tag{2.3}$$

where, *I* is intensity of light, n_0 is the refractive index at low intensity, n_2 is the nonlinear coefficient of refractive index. The expression for n_2 is given by the formula

$$n_2 = \eta(dn/dN)\alpha\tau/h\nu \tag{2.4}$$

where η is the coefficient representing relative portion of photoelectric absorption, *dn*/*dN* is the differential index, α is the coefficient of absorption, τ is the lifetime of excess carriers [Eliseev 1987]. The quantity *dn/dN* is negative in GaAs and in similar semiconductors, and this corresponds to the effect of self-defocusing with incident light. The attenuation of the laser beam passing the semiconductor sample has been used to determine the intensity threshold of nonlinear propagation in different materials [Bahae 1989], [Bahae 1990].

In active medium of the laser, coefficient of absorption α, is negative. Thus in the case of laser, coefficient n_2 becomes positive. This corresponds to self-focusing and related phenomena of spatial instability of emitted beam [Bachert 1978] .The self-focusing occurs as

a result of increase of the refractive index in a region of the wave front where the intensity is higher than average value. The "bump" of refractive index works as a lens for further increase of local intensity. When the focusing overcomes the diffraction, the process leads to filamentation of the emission pattern [Thompson 1972]. This is one of the important origins of spotty near-field in the broad-area laser diodes. Each optical filament is dynamic field formation of high intensity guided wave located along the axis of the cavity. The intensity threshold of the filamentation is quite low in broad-area diodes, but is significantly higher in the case of ridge-waveguide single-mode structure, where lateral confinement is initially provided. Signs of the occurrence of the optical filamentation is spotty or deformed near field (deviation from uniformity or from the fundamental mode profile), distortion of the far-field pattern, and also deviation of *L-I* characteristic from linearity (power kinks or discontinuities).

The optical bistability is a nonlinear effect observed in passive Fabry-Perot ethalon [Gibbs 1979] and also in diode lasers with an external selective feedback [Bazhenov 1981]. The bistable operation is a phenomenon associated with nonlinear resonance in the diode cavity (change of refractive index and resonant frequency along with an increase of intensity) if the lasing frequency is fixed by external feedback. Observed features are output power jumps and power hysteresis.

2.5. Phenomenon of induced dispersion of the refractive index

As it has been discussed above, a strong electromagnetic wave produces perturbation of the dielectric function in spectral vicinity of the strong (driving) wave. Corresponding perturbation of refractive index produces modification of spectral characteristics (shifts of modal resonances, change of mode-beating frequencies, etc.). The point of interest for us is the change of phase index leading to change of group velocity v_g (and group index $n_g = c/v_g$). This influence is origin of unusual phenomena of light propagation such as slow light ($n_g >>$

n), fast light ($n_g < 1$) and backward propagating light ($n_g < 0$). The possibility to use the nonlinear interaction of modes in semiconductor lasers to obtain slow/fast light has been stated in [Uskov 2005], [Eliseev 2006].

Chapter 3

Analysis of theory of nonlinear interaction (NLI) and feasibility of superluminal group velocity

3.1. Introduction

The nonlinear mode interaction (NMI) in semiconductor lasers occurs due to formation of a dynamic grating of carrier density in the nonlinear medium. This mechanism was shown to be involved in asymmetric suppression of spectral modes in semiconductor lasers [Bogatov 1975], [Eliseev 1987], in splitting of lines in the mode-beating spectra of semiconductor lasers [Eliseev 2005a], and also in the multi-wave mixing [Uskov 2005], and other nonlinear phenomena in semiconductors. The mechanism has been shown to provide optical perturbations leading to the slow or fast light phenomena [Bogatov 1975], [Eliseev 2005]. In [Uskov 2005], the same mechanism was calculated for the light slowing in optical amplifiers.

3.2. Nonlinear interaction (NLI) as an origin for induced dispersion of refractive index

It has been shown that optical perturbation produced by a strong electromagnetic wave in a nonlinear medium effects both gain and refractive index [Bogatov 1975], [Eliseev 2005a], [Eliseev 2005b]. The effect on the phase index n leads to induced dispersion of n and consequently results in substantial modification of the wave propagation. The induced variation of n is rather small ($\delta n << n$), since the variation occurs in a very narrow spectral range, the modification of group index is rather high. The frequency range where the NLI takes place is of the order of relaxation rate of carriers. The local value of the induced dispersion is easily much higher than the background (“linear”) dispersion. The perturbed component of the index n has a “bump” with positive and negative slopes on both sides of the

driving frequency. It corresponds to positive dispersion at low photon energy side and negative dispersion at higher photon energy side. At proper conditions, the dynamic contribution to the total index dispersion can modify the group index in such a manner, that in frequency range below driving frequency, one gets slowed propagation of light whereas at frequency range above the driving frequency, one gets a superluminal propagation. The goal of our project is to define conditions necessary to obtain such perturbation and find the corresponding frequency ranges for slow and superluminal propagation of light in RW laser devices operating in 0.4-1.55 μm range.

3.3. Interference pattern in the nonlinear medium

An important element of the NLI-model is interference of interacting waves. The first demonstration of interaction was associated with observation of spectrally-asymmetric mode suppression around the predominating mode in two-mode external cavity laser [Bogatov 1974]. Later, these observations were theoretically interpreted in [Bogatov 1975] taking into account the interference of interacting modes, and the formation of dynamic grating in the active medium corresponding to the interference pattern. The grating of local intensity of the electromagnetic waves produces grating of carrier density due to interconnection between carrier density and complex refractive index. The intensity determines the local rate of stimulated emission, i.e. an increase in intensity leads to decrease of local carrier density, and decrease of local optical gain leading to an increase of local refractive index. The grating contains oscillations at the beating frequency of two interacting waves and spatial variations according to the difference of wave vectors. Hence, it is justified to say that a dynamic grating of the complex dielectric permittivity ε is formed. The stability of the interference pattern depends on degree of coherence of the interacting waves, and sufficient coherence of waves provides stable dynamic grating of ε. Thus, the interference pattern and corresponding

dynamic carrier grating are associated with coherent oscillations of excess carrier density, which is famously known as the *coherent oscillation of population*, CPO.

Let us consider the interaction of two waves propagating in an amplifying medium. The two waves are represented as follows:

$$E_{dr} = E_{dr0}\exp(-i\omega_0 t + ik_0 r) \tag{3.1}$$

$$E_{pr} = E_{pr0}\exp(-i\omega t + ikr) \tag{3.2}$$

where, E_{dr0} and E_{pr0} are amplitudes, ω_0 and ω are angular frequencies, k_0 and k are wave vectors of driving and probe waves respectively. It is assumed that the $E_{dr0} >> E_{pr0}$. The superposition of these waves produces spatio-temporal grating of local intensity, according to the expression

$$|E|^2 = |E_{dr0}|^2 + |E_{pr0}|^2 + 2E_{dr0}E_{pr0}\exp(i\Omega t - i(k_0 - k)r)\ , \tag{3.3}$$

where, $\Omega = \omega_0 - \omega$ is an angular frequency detuning between driving and probe wave. In laser, the predominating mode of emission is considered as the driving wave and the subsidiary mode as probe or weak wave. The probe wave is the neighboring longitudinal mode, the detuning Ω, is the intermodal spacing given by the expression

$$\Omega = \frac{c}{2n_g L} \tag{3.4}$$

The main feature of this approach is analysis of the cross term in equation (3.3) that is commonly ignored when multimode theory is developed, based on the addition of intensities. In reality, the cross term produces perturbation of population of excess carriers as they are subjected to spatial-temporal oscillations, also known as CPO.

The local balance of excess carriers can be represented by the expression:

$$dN/dt = -N/\tau + G - B(N)|E|^2 \tag{3.5}$$

where, N is the local carrier density, τ is the carrier lifetime, G is the pumping rate (injection through the *p-n* junction), $B(N)$ is the coefficient of stimulated recombination. A feature of semiconductor media is mobility and diffusion of excess carriers that can smoothen the spatial variation of the population. The smoothening can be quite effective in wiping out the effect of standing wave in resonators. The spatial periodicity of nodes of the standing wave is $\lambda/2n$ and is about 124 nm in GaAs. Therefore, the diffusion length which is about 1 μm can wipe out the short-period grating. On another hand, the influence of diffusion is reduced if the grating period is comparable to the cavity length. The diffusion can be neglected in the near-degenerate case.

The conditions for the near degenerate case where diffusion can be ignored are:

$$\Omega << \omega \tag{3.6}$$

and

$$D << \frac{\Omega}{\left|k - k_0\right|^2} \tag{3.7}$$

Here, D is the ambipolar diffusion coefficient of excess carriers, Ω is angular frequency detuning between driving and probe wave, k_0 and k are wave vectors of driving and probe waves respectively. The solution for oscillating part of carrier density is given by

$$\delta N = \frac{-B(N - N_0)E_{dr0}E_{pr0}\exp(-i\Omega t - i(k_0 - k)r)}{i\Omega + 1/\tau + B\left|E_{dr0}\right|^2} \tag{3.8}$$

This oscillation of the population excites spatial-temporal variations of optical parameters of the medium, which are components of the complex dielectric permittivity, ε of the medium. The relationship between change in permittivity and change in carrier density in the linearized form is as follows:

$$\delta\varepsilon(r,t) = \frac{\partial\varepsilon}{\partial N}\delta N(r,t) \tag{3.9}$$

This is the dynamic grating of complex permittivity due to the interference of interacting waves. The real part gives refractive index grating and the imaginary part gives the gain/absorption grating.

3.4. Transformation of photon energy due to dynamic grating of complex permittivity

The propagation of electromagnetic wave through a medium with dynamic grating is accompanied by transformation of some part of photons to combined frequencies or photon energies. The wave interaction occurs by photon exchange between the waves. In the case of one strong (driving) wave and one subsidiary (probe) wave, the NLI leads to transforming of photon of driving wave into photons of probe wave. This transformation of photon energy is very similar to the frequency shift in acousto-optic convertor. If secondary photon flow is directed in the same direction as the probe wave, the probe wave experiences additional gain. If the secondary photon flow is directed in opposite direction to probe wave, the probe wave is suppressed. In the simplest case of two mode interaction, the mixing of two frequencies, ω_{dr} and ω_{pr} produces signals at the following combination frequencies: ω_{dr}, ω_{pr}, $\omega_{dr} - \omega_{pr}$, $\omega_{dr} + \omega_{pr}$, $2\omega_{dr} - \omega_{pr}$, $2\omega_{pr} - \omega_{dr}$, etc. Signal at $\omega_{dr} + \omega_{pr}$, is of very high frequency, and the corresponding spatial variations in semiconductor medium will be wiped out by carrier diffusion (in contrast to laser with immobile ions in crystals). Other combination frequencies are as a result of mutual interaction and leads to appearance of new (mirror-like) lines of emission (also considered as the four-wave mixing). Our case of two wave interaction is close to near-degenerate four-wave mixing (NDFWM), as both the waves propagating in same direction have very slight frequency difference (which is called the detuning frequency).

The perturbation of complex permittivity produced by driving wave at the frequency of probe wave, according to [Eliseev 2005b] is given by:

$$\delta\varepsilon = -B|E_0|^2 (N - N_0) \frac{d\varepsilon''}{dN} \frac{\alpha + i}{\gamma + \Omega} \tag{3.10}$$

where, B is the stimulated recombination coefficient (in units of m^2/V^2s), E_0^2 is the driving wave intensity, N is the carrier density, N_0 is the transparency carrier density, ε" is the imaginary part of complex dielectric permittivity, α is the linewidth enhancement factor, γ is the relaxation rate of the carriers and Ω is the angular frequency detuning between the driving and probe wave and is given by $\Omega = 2\pi(\nu_0 - \nu_1)$, where, ν_0 and ν_1 are frequencies of driving and probe waves respectively.

This expression leads to spectrally-asymmetric gain. The equation for additional gain is as follows:

$$\delta g = -2\pi B|E_0|^2 (N - N_0) \frac{d\varepsilon''}{dN} \frac{\left(1 + \frac{\alpha\Omega}{\gamma}\right)}{n_{eff} c \left(1 + \frac{\Omega^2}{\gamma^2}\right)} \tag{3.11}$$

where, B is the stimulated recombination coefficient (in units of m^2/V^2s), E_0^2 is the driving wave intensity, N is the carrier density, N_0 is the transparency carrier density, ε" is the imaginary part of complex dielectric permittivity, α is the linewidth enhancement factor, γ is the relaxation rate of the carriers and Ω is the angular frequency detuning between the driving and probe wave and is given by $\Omega = 2\pi(\nu_0 - \nu_1)$, where, ν_0 and ν_1 are frequencies of driving and probe waves respectively . The spectral shape of the gain is given by the expression:

$$F(\Omega) = \frac{1 + \frac{\alpha\Omega}{\gamma}}{1 + \frac{\Omega^2}{\gamma^2}} \tag{3.12}$$

The expressions (3.11) and (3.12) describe the magnitude and spectral shape of nonlinear gain in the plane wave approximation. In practice, the interacting modes are always guided waves. As the NLI occurs only in active layer, the magnitude of NLI in real laser structures

is smaller when compared to the interaction in plane waves. In the following chapters, the technique to calculate the NLI in the guided modes of RW is discussed.

The gain is suppressed for shorter-wavelengths and it is amplified for longer-wavelengths. The mechanism of gain perturbation is associated with generation of photons at probe wave frequency by scattering of the driving wave on the dynamic grating, as explained above. Hence, the probe wave experiences additional gain for longer-wavelengths and it experiences attenuation for shorter-wavelengths.

According to Kramers Kroing relations, the probe wave also experiences perturbation in refractive index due to perturbation in gain. The perturbation of the refractive index at the probe wave is given by the following equation [Eliseev 2005]:

$$\delta n = \mathrm{Re}(\delta\varepsilon)/2n = -B|E_0|^2 (N - N_0)\frac{d\varepsilon''}{dN}\frac{(\alpha + \frac{\Omega}{\gamma})}{2n\gamma(1+\frac{\Omega^2}{\gamma^2})} \tag{3.13}$$

where, ε is the complex dielectric permittivity, n is the phase index, B is the stimulated recombination coefficient (in units of m^2/V^2s), E_0^2 is the driving wave intensity, N is the carrier density, N_0 is the transparency carrier density, ε" is the imaginary part of complex dielectric permittivity, α is the linewidth enhancement factor, γ is the relaxation rate of the carriers and Ω is the angular frequency detuning between the driving and probe wave and is given by $\Omega = 2\pi(\nu_0 - \nu_1)$, ν_0 and ν_1 are frequencies of driving and probe waves respectively . The total relaxation rate, γ is expressed as the sum of spontaneous relaxation rate, γ_0 and stimulated relaxation rate. It is given by equation 3.14, that shows the influence of intensity of driving wave, on the total relaxation probability, where γ_0 is initial relaxation rate, B is stimulated recombination coefficient (in units of m^2/V^2s), and $|E_0|^2$ is intensity of driving wave.

$$\gamma = \gamma_0 + B|E_0|^2 \tag{3.14}$$

The dependence on intensity is a very important factor that leads to broadening of the perturbation band and also in decrease of the magnitude of the nonlinear effect.

3.5. Intermodal spacing

The resonance wavelength in a Fabry-Perot cavity is given by

$$\lambda_q = \frac{2nL}{q} \tag{3.15}$$

where, n is the refractive index at λ_q, L is the cavity length, q is the number of order of resonance called as the longitudinal index. The above equation is valid at $L >> \lambda$, therefore $q >> 1$ and usually the exact value of q is unknown. The most common approach is to exclude q from the resulting final expressions.

The direct differentiation of λ_q w.r.t q gives

$$\frac{d\lambda_q}{dq} = \frac{2L}{q}\frac{dn_q}{dq} - \frac{2L}{q^2}n_q = \frac{\lambda_q}{n_q}\left(\frac{dn_q}{dq} - \frac{\lambda_q}{2L}\right)$$

We substitute dn_q/dq by $(dn_q/d\lambda_q)(d\lambda_q/dq)$ and solve the equation with respect to $d\lambda_q/dq$.

The result is given by

$$\frac{d\lambda_q}{dq} = \frac{-\lambda_q^{\,2}}{2n_q L\left[1 - \left(\frac{\lambda_q}{n_q}\right)\left(\frac{dn_q}{d\lambda_q}\right)\right]} = \frac{-\lambda_q^{\,2}}{2n_g L} \tag{3.16}$$

Where,

$n_g = n_q\left[1 - \left(\frac{\lambda_q}{n_q}\right)\left(\frac{dn_q}{d\lambda_q}\right)\right]$ is the group index that is well known in the form of $n - \lambda\frac{dn}{d\lambda}$.

Taking dq = 1, we obtain the spectral spacing between neighboring longitudinal modes, which is given by:

$$|\Delta\lambda| = \lambda_q^{\,2}/(2n_g L) \tag{3.17}$$

The expression (3.16) is derived accounting for first order dispersion $dn/d\lambda$. More general expression which includes the second order dispersion term is solution of the square equation for $\Delta\lambda$:

$$(\Delta\lambda)^2(\lambda/2n)(d^2n/d\lambda^2) - \Delta\lambda[1-(\lambda/n)(dn/d\lambda)] + \lambda^2/2nL = 0 \qquad (3.18)$$

The solutions are as following:

$$\Delta\lambda_{1,2} = [(\lambda/n)(d^2n/d\lambda^2)]^{-1}\{[1-(\lambda/n)(dn/d\lambda)] \pm \{[1-(\lambda/n)(dn/d\lambda)]^2 + (\lambda^3/n^2L)(d^2n/d\lambda^2)]^{1/2}\} \qquad (3.19)$$

Usually, the second order dispersion term ($d^2n/d\lambda^2$) is used for determination of dispersion of group index, for example, in calculation of the pulse width increase in optical-fiber communication. It is a factor limiting the transmission bandwidth. Also, the second derivative leads to non-equidistance of longitudinal modes in semiconductor lasers.

In the case of the NLI, the dispersion parameters and the group index can vary significantly within the single intermodal spacing. Expression (3.17) is very useful to analyze influence of the NLI on the intermodal spacing and on the mode-beating behavior (known as phenomenon of splitting of microwave beat spectra). If the NLI-related change of the phase index is positive, the frequencies of modes neighboring to the driving mode, shift in one direction with respect to the strong or driving mode. In this case, the longer wavelength mode is attracted to the strong or driving mode whereas shorter wavelength mode is "repulsed" from the driving mode. In the mode beating spectrum, this shifts lead to splitting of the main beating line [Eliseev 2005a].

3.6. Difference between laser oscillator regime and laser amplifier regime

The magnitude of NLI is measured as the extra gain or extra absorption occurring due to the NLI at the background of linear components of gain or attenuation. The magnitude of the NLI is dependent on the operation regime, as the modal gain behaves in different manner in oscillator and in amplifier. In the oscillator regime, the optical gain is pinned at a threshold

value. This is valid for first order approximation in the laser operating in the steady state. In the transient states, the rule is not valid. The gain pinning is the result of the saturation of carrier density at the threshold value, as the effective lifetime in the laser regime decreases to maintain the balance of optical emission and optical losses. In second order approximation, one has to account for the nonlinear gain at the laser frequency which is the mechanism reducing the gain at the same carrier density. Therefore, the fulfilling of threshold condition in the oscillator requires an increase of carrier density at the same pumping current. In general, this process leads to sub-linearity of the *L-I* curve at high pumping and also to reduction of the laser efficiency. But, optical gain will remain unchanged. In other words, the steady-state gain in the oscillator does not depend on the intensity of the interacting waves. We do not consider the next order of approximation accounting for the multi-photon absorption here.

The laser oscillator can be used as an amplifier in vicinity of the laser threshold (just below the threshold). The laser operates as a resonant (or regenerate) amplifier for waves tuned to the laser mode. More interesting phenomenon is when the device operates as travelling-wave amplifier. The difference between the oscillator and amplifier is that there is no optical feedback in amplifier. Such amplifier can be fabricated from an oscillator by coating resonator facets using antireflection coating. In reality, removal of the feedback completely is not possible. But, the antireflection coating provides an increase of the lasing threshold. The device acts as travelling wave amplifier when the pumping rate is between initial threshold and the new threshold (after antireflection coating).

In the regime of the travelling-wave amplifier, the saturation of gain in presence of strong electromagnetic field occurs depending on the intensity of the field. Therefore, it can vary from an unsaturated value to almost zero in the high-intensity limit. The gain depends not only on the pumping rate but also on the intensity of waves during such behaviour.Based

on this difference between oscillator and amplifier, the gain coefficient should be taken accordingly for further calculations as shown in the Table 1.

Table 3.1. Calculated gain coefficient in the laser devices

Type	Regime	Gain	Comments
Oscillator	Above threshold	$g = g_{th}$	The threshold value (constant)
Travelling-wave amplifier	Below threshold	$g = g_0/(1 + I/I_{sat})$	g_0 is unsaturated value; I_{sat} is intensity parameter of saturation

3.7. Numerical Calculation of Ridge-Waveguide Modes Using finite element method (FEM)

To compute guided-mode solutions of the vector wave equation for the ridge waveguide structure, we use a Finite Element Method package FemSIM developed by Rsoft Design Group. FEM is generally advantageous in complex geometries and/or high index contrast materials. The FemSIM package from RSoft Design Group is a full-vector implementation for both propagating and radiation/leaky waveguide modes, and cavity modes can be found for both 2D Cartesian cross-sections and 3D BORs (bodies of revolution) in cylindrical coordinates. The method uses state-of the-art *hybrid edge/node elements* that allow for efficient separation of spurious modes from the physical ones. First and second order interpolant bases are provided for both rectangles and triangles. PEC or PML boundary conditions may be selected independently for each direction. It may be used to find all the modes or a small group of modes about a given wavelength.

The PML boundary conditions are chosen in our simulations. PML is an artificial absorbing layer for wave equation, commonly used to truncate computational regions in numerical methods to simulate problems with open boundaries, especially in the FDTD and

FEM methods. The key property of a PML that distinguishes it from an ordinary absorbing material is that it is designed such that waves incident upon the PML from a non-PML medium do not reflect at the interface, this property allows the PML to strongly absorb outgoing waves from the interior of a computational region without reflecting them back into the interior. In the below paragraphs, we showed the underlying equations and conditions used in finite element analysis.

3.7.1. The Electromagnetic Boundary Value Problem

We begin with the source-free time-harmonic form of the vector wave equation in an arbitrary, anisotropic, lossy medium [Jin 2002], [Saitoh 2002]:

$$\nabla \times \left(\frac{1}{s} \cdot (\nabla \times E) \right) - k_0{}^2 \varepsilon_r E = 0 \quad , \tag{3.21}$$

subject to vanishing field boundary conditions at the domain edges:

$$\hat{n} \times \mathbf{E} = 0 \tag{3.22}$$

The complex diagonal tensors, s and ε_r, represent coordinate-stretching and the dielectric material tensor, respectively. Throughout the domain, s is the identity tensor, but in the boundary layer it has the following form

$$\bar{s} = \left(\frac{s_y s_z}{s_x} \right) \hat{x}\hat{x} + \left(\frac{s_x s_z}{s_y} \right) \hat{y}\hat{y} + \left(\frac{s_x s_y}{s_z} \right) \hat{z}\hat{z} \quad , \tag{3.23}$$

$$s_{\alpha=x,y,z} = 1 - j \left(\frac{\alpha - L}{L} \right) \delta_{\max} \quad , \tag{3.24}$$

where $\delta_{\max}$ is the loss tangent, α is the distance from the edge, and L is the thickness of the boundary layer, known as the perfectly matched layer (PML). The tensor elements in the PML are matched to those in the rest of the domain according to the prescription

$$\overline{\varepsilon_2} = \varepsilon_1 \bar{s} \quad , \tag{3.25}$$

to produce arbitrarily small reflections at the PML interface for all frequencies and angles of incidence. The PML is terminated at the domain edge with a perfect electrical conductor (PEC) boundary condition [Schulz 1998].

3.7.2. Solution Using Finite Element Method

The Finite Element Method (FEM) does not solve the boundary value problem (3.21)–(3.24) directly, but rather a related one based on a variational expression, or functional, constructed from the operator of the differential equation (3.21). This functional in two dimensions, over a domain A, is given by [Koshiba 1994]

$$\boldsymbol{F}(\mathbf{E}) = \iint_A \left[(\nabla \times \mathbf{E})^* \cdot \frac{1}{\overline{\overline{s}}} \cdot (\nabla \times \mathbf{E}) - k_0{}^2 \mathbf{E}^* \cdot \overline{\overline{\varepsilon}} \cdot \mathbf{E} \right] dA \tag{3.26}$$

For propagating and leaky modes [Tsuji 1997], a separable field ansatz is assumed, $E(x, y, z) = E(x,y)\exp(-j\beta z)$, where β is the modal propagation constant along z.

Instead of finding an expansion basis over the entire domain, which can be difficult in general, the finite element method subdivides the domain into a collection of elements, for which a simple basis can be defined. This basis vanishes outside the element, so that the final solution is just a summation over the solutions of all the elements. For hybrid node/edge FEM, the transverse components are expanded in a vector (edge element) basis:

$$\mathbf{E}_T(x,y)e^{-j\beta z} = \sum_{\mathrm{i}=1}^{N}\sum_{i=1}^{N} \{U\hat{\mathbf{x}} + V\hat{\mathbf{y}}\} E_{Ti} \quad , \tag{3.27}$$

where E_{Ti} are the values of the field along each edge. The longitudinal component (perpendicular to the plane of the element) is represented by a scalar (node element) basis,

$$E_z(x,y)e^{-j\beta z} = \sum_{i=1}^{N} N_i E_{zi} \quad , \tag{3.28}$$

where Ez_{i} is the value of the field at node i. The basis dimension, N, depends on the geometry of the element and on the order of interpolation.

Lastly, the functional is minimized according to Eq. (3.29), yielding a matrix eigenvalue equation with β^2 as the eigenvalue, and the field component at the nodes and edges as the eigenvector:

$$\frac{\partial F}{\partial E_i} = 0 \quad . \tag{3.29}$$

Chapter 4

Application of NLI to improve sensitivity of rotation and other interferometer-based sensors

4.1. The nonlinear Sagnac effect

In this section, we briefly discuss the principle of operation of an active ring laser gyro and device a method to improve its sensitivity. Ring laser gyroscopes are rotation sensors which are highly accurate, lightweight devices with no moving parts. Ring laser gyros are used for navigation in various aircrafts, ships, spacecrafts, helicopters, etc. and can have sensitivity ranging from several turns per second to 10^{-3} degrees per hour. Semiconductor ring lasers (SRLs) are of particular interest because they can be monolithically integrated on a single chip [Laybourn 1999]. There are two basic versions of laser-based gyro devices: 1) active, utilizing a ring laser with measured frequency splitting between counter propagating modes (traveling waves); 2) passive, where a laser is used as an external source of monochromatic light, and phase shift of counter propagating waves is measured in the ring-type interferometer.

The ring laser gyros work on the principle of ***Sagnac effect*** where the phase shift or the shift of beating frequency between the two counter-propagating waves is directly proportional to the rotation rate of the gyro [Post 1967]. The slope sensitivity of an active laser gyro is directly proportional to the size of the gyro and inversely proportional to the group index, n_g of the medium filling the gyro [Eliseev 2005].In both cases, the size of the ring (actual circle or other closed circuit) is a parameter influencing the slope sensitivity (or gyroscopic factor) K of the gyro device. In the particular case of an air-filled active gyro, this sensitivity obeys the simple expression

$$K = \frac{d(\Delta\nu)}{d\Omega} = \frac{4A}{\lambda_0 L} \tag{4.1}$$

where $\Delta\nu$ is the frequency splitting of the counter propagating modes, Ω is the angular rotation rate, A is the area of the ring (or area of the ring projection to the plane perpendicular to the rotation velocity vector), λ_0 is the wavelength in vacuum, and L is the perimeter of the ring. The "size parameter" in this case is the ratio A/L, which is maximum for a circular ring ($A/L = R/2$, where R is the radius of the circle). The affordable sensitivity is achievable with the radius of about 10 cm and larger, whereas semiconductor laser physics allow the size of the laser to be about 10 μm. This potential for miniaturization cannot be used in full as the sensitivity decreases with decreasing R. Thus, other approaches should be found to overcome this barrier. A *monolithically-integrated* semiconductor ring laser can be characterized by the slope sensitivity K [Eliseev 2008]:

$$K = \frac{d(\Delta\nu)}{d\Omega} = \frac{4A}{n_g \lambda L} \tag{4.2}$$

where n_g is the group index of the medium filling the ring cavity, $n_g = n + \frac{\nu dn}{d\nu}$, n is the refractive index, and ν is the optical frequency. A very attractive possibility to *increase the slope sensitivity* appears if one can substantially *reduce the group index*. In linear (low-intensity) case, the group index is somewhat higher than the phase index (the refractive index) and it is equal to about 4.5 in materials such as GaAs (or composite materials such as AlGaAs, InGaAs, InGaAsP). By reducing n_g, an enhancement of the slope sensitivity can be achieved in a nonlinear regime of laser operation. As mentioned in the earlier sections, nonlinear perturbation of the effective group index occurs in spectral vicinity of a strong ("driving") wave, and the useful range of the anomalous dispersion is located at frequencies just above the optical frequency of the driving wave. The anomalous dispersion $\frac{dn}{d\nu} < 0$ is the necessary condition to reduce the group index. Under some conditions (optimal intensity of the driving wave),we obtain the point where group index passes zero value, it is known as a

point of *critically anomalous dispersion* (CAD). At the CAD point, the expected slope sensitivity becomes infinite. Therefore, the CAD point is not suitable for gyro operation, because of poor stability of the slope sensitivity. At an optimal spectral distance from the CAD point, one can obtain enhanced but stable sensitivity. This is the concept of usage of the ***nonlinear Sagnac effect*** for an increase in the gyro sensitivity by orders of magnitude, and/or for a decrease in the ring size, while keeping the desirable slope sensitivity.

4.2. Influence of dispersion on beat frequency splitting

In this section, we analyze the influence of NLI on the beat frequency splitting. Consider a laser operating at frequency ν_q corresponding to the longitudinal mode index q. We assume that the laser line is split into two components, namely high-frequency component $\nu_q + \Delta\nu_0$ and low-frequency component $\nu_q - \Delta\nu_0$, for example due to Sagnac effect. Here the initial splitting, or the beat frequency is $2\Delta\nu_0$, corresponding to a medium with no dispersion ($dn/d\nu = 0$). The influence of dispersion is taken into account by incorporating additional frequency shifts according to the known parametric effect, i.e, mode resonance shift due to perturbation of refractive index. The mode resonant frequency corresponds to

$$\nu_{mode} = cq/2nL \tag{4.3}$$

The frequency change due to perturbation of refractive index, n is given by

$$\delta\nu = (-cq/(2n^2L))\delta n = -(\nu_q/n)\delta n$$

The variation of refractive index is given by

$$\delta n = (dn/d\nu)\Delta\nu_0$$

Here $\Delta\nu_0$ is the primary or linear frequency shift, such as Sagnac related frequency shift. Hence, resonant frequency shift of the cavity mode of index q due to the dispersion is given by

$$\delta\nu = -(\nu_q/n)(dn/d\nu)\Delta\nu_0$$

The total shift in frequency is given by

$$\Delta\nu_0 + \delta\nu = \Delta\nu_0[1 - (\nu_q/n)(dn/d\nu)] \quad (4.4)$$

Hence, the high-frequency component of the splitting has shifted from $\nu_q + \Delta\nu_0$ to

$$\nu_q + \Delta\nu_0[1 - (\nu_q/n)(dn/d\nu)] \quad (4.5)$$

From the above expression, we can see that if the dispersion is normal (positive), the high-frequency component approaches central value ν_q, whereas if the dispersion is anomalous (negative), the frequency is shifted away from the central value. This means that the frequency splitting becomes larger due to anomalous dispersion. The above mentioned analysis is not comprehensive but it helps to understand the frequency splitting mechanism. We can make the following conclusions from our analysis:

a) Anomalous (negative) dispersion increases the beat frequency splitting of any origin including Sagnac effect

b) Normal (positive) dispersion decreases the beat frequency splitting

c) This behavior applies for lasers operating in both continuous wave regime as well as in the pulsed regimes

d) A result of this mechanism is appearance of group index term in the expression for Sagnac splitting

4.3. Wave beating as a measure of frequency splitting

If optical spectrum contains oscillation at two different frequencies, ν_0 and ν_1, one can measure the difference of these frequencies by registering the beating signal (at frequency $\nu = |\nu_0 - \nu_1|$). This frequency appears in the optical oscillation as a modulation frequency. The beating signal at frequency ν appears only during detection (type of rectification) of optical waves. At the photodetector, oscillation of electric field of light is represented as

$$E(t) = E_0 \sin(\nu_0 t) + E_1 \sin(\nu_1 t) \quad (4.6)$$

When squared, the result will contain term

$$2E_0E_1\sin(\nu_0 t)\sin(\nu_1 t) = -2E_0E_1[\cos(\nu_0+\nu_1)t - \cos(\nu_0-\nu_1)t] \quad (4.7)$$

There is an oscillating component of electrical response at the difference frequency $\nu = \nu_0 - \nu_1$ (last term). Investigation of this component is of interest due to the following reasons:

When frequency ν falls in RF or microwave range, it can be measured and studied with much higher accuracy than it is allowed in the optical spectroscopy. Also, the frequency resolution is better in the radio-frequencies than in optical frequencies.

The interference pattern inside the active region of the laser device is a particular case of appearance of the mode beating oscillations that are responsible for the NLI of modes. In this case, the "rectification" process is associated with response of electron density to intensity of electromagnetic oscillations (square rectification). This process is based on the proportionality of the stimulated emission rate to the photon density (as equivalent of intensity).

4.4. Factor of $1/n_g$

As it follows from expression (4.2), in order to increase the sensitivity scale factor, one should decrease the group index. There are various ways to modify the group index at the laser frequency. One of them is to find and to use the anomalous dispersion provided by material index or use combined index of system such as coupled cavities or use resonances of photonic crystals. These methods fall under the category of *static* dispersion. Another way to modify group index is through dynamic (induced) dispersion as a result of parametric interaction with driving wave. The NLI belongs to this version. Other dynamic techniques that can be successful in producing the superluminal light under influence of strong electromagnetic waves are nonlinear scattering, multiwave mixing, etc.

Let's consider a mode with frequency ν in a fabry-perot cavity whose length is L. A slight change in L leads to frequency shift which is calculated as follows:

The frequency of a mode with constant longitudinal index q is given by:

$$\nu_q = cq/(2nL)$$

where, c is the speed of light in vacuum, n is the refractive index, L is the length of the cavity.

The frequency shift due to shift of L (interferometer effect) is given by:

$$\frac{d\nu_q}{dL} = (cq/2)\left[\frac{d}{dL}(\frac{1}{nL})\right] = (cq/2)\left[\frac{d}{dL}(1/n)\frac{1}{L} + (1/n)(-1/L^2)\right]$$

$$= (cq/2)\left[\frac{-1}{n^2}\frac{dn}{dL}\frac{1}{L} - \frac{1}{nL^2}\right]$$

$$= -(\frac{cq}{2nL})\left[\frac{1}{n}\frac{dn}{dL} + \frac{1}{L}\right]$$

$$= -(\frac{cq}{2nL})\left[\frac{1}{n}\frac{dn}{d\nu}\frac{d\nu}{dL} + \frac{1}{L}\right]$$

$$\frac{d\nu}{dL} = -\frac{\nu}{n}\frac{dn}{d\nu}\frac{d\nu}{dL} - \frac{\nu}{L}$$

$$\frac{d\nu}{dL}[1 + \frac{\nu}{n}\frac{dn}{d\nu}] = -\frac{\nu}{L}$$

$$\frac{d\nu}{dL} = -\frac{n\nu}{L}\cdot\frac{1}{n_g}$$

Hence, it is shown that the rate of response of the laser to a nano-displacement of mirror is in reverse proportion to n_g. Formally, the enhancement of the frequency shift in the laser mode can go upto infinity. The concept of using the factor $1/n_g$ as a potential to improve the slope sensitivity is mentioned in several publications [Yum 2008], [Yum 2010], [Shahriar 2007], [Salit 2011], [Kotlicki 2012].The concept is based on the feature to increase the frequency shift in any interferometer system in the range of negative (anomalous) dispersion. It follows from this that the sensitivity of interferometer systems (including the Sagnac interferometer)

can be enhanced by acceleration of group velocity of light. According to [Shahriar 2007], supersensitive interferometer-based detection of gravitation waves is feasible using the anomalous dispersion and an increase of sensitivity by 10^6 times was reported.

4.5. Points of critically-anomalous dispersion

The situation where $n_g = 0$, and group velocity, v_g reaches infinity, seems very unusual and ambiguous. The group index is zero if the negative dispersion is sufficient to fulfill the condition

$$\frac{dn}{d\nu} = -\frac{n}{\nu} \tag{4.8}$$

In theory, calculated value of n_g can smoothly cross the zero line whereas the value of group velocity, which is inverse of group index has an infinite discontinuity ranging from $+\infty$ at positive side to $-\infty$ at negative side as shown in Fig.4.1.

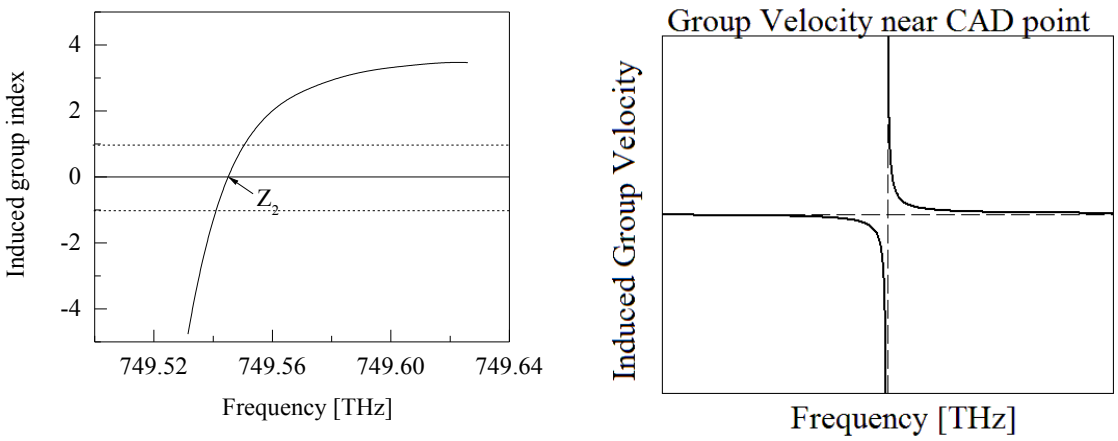

Fig.4.1. Perturbed group index (left) and group velocity (right) near Critically Anomalous Dispersion (CAD) point Z2.

In textbooks, it is advised not to consider this point or even the whole range of anomalous dispersion, where the usual physical sense is lost. The group velocity is, not in general, the velocity of signal or energy propagation and it can be greater than c, infinite, or negative

while still retaining its meaning as the velocity of nearly undistorted pulse propagation [Milonni 2004]. the velocity of a wave packet (or optical pulse).

The commonly used technique for measurement of group velocity, v_g is measurement of velocity of the peak of optical pulse (wave packet).This measurement technique is not applicable in circumstances where the pulse is subjected to significant distortion. It is well known fact that the dispersion, if any, leads to broadening of the pulse. This is the main reason for limitation of transmission of optical pulses in optical-fiber communication. The re-shaping of the pulse may cause difficulty in tracking the peak of the pulse. Therefore, the measurement of pulse velocity becomes ambiguous. Very strong re-shaping is unavoidable at the CAD point. According to the Fourier expansion, any pulse contains a set of spectral components covering a range of frequencies. The spectral width of pulse components is estimated as $1/\delta t$, where δt is the pulsewidth. In the CAD point, only certain component corresponding to central frequency matches the CAD conditions, whereas remaining parts of spectral components appear on opposite sides of the CAD point on the frequency scale. These components propagate in opposite directions. As a result, the pulse will be split or distorted so its movement cannot be easily interpreted.

Another anomaly of the CAD is indefinitely wide resonance at the point. This is the basis for construction of so called “white light cavity” [Kotlicki 2012]. If the lasing mode is involved in oscillation at CAD point, its spectral width will be broadened infinitely. One may expect that laser action in this case will not be observed due to very low spectral density of the laser emission.

4.6. Wave packet reshaping due to time-dependant saturation of gain or attenuation in the optical medium

The time dependant saturation of light-matter interaction (amplification or absorption) produces reshaping of the pulse that can mask phenomena associated with dispersion. In

experiments with ruby amplifier by [Basov 1966a],[Basov 1966b] the measured velocity of the pulse peak is found to be several times higher than *c* (6-9 times). The effect is interpreted as the result of re-positioning of the pulse which has a foregoing "tail" or precursor. During the passage of the pulse in the medium, the "tail" portion of the pulse absorbs the accumulated energy in the amplifier medium and gets strong amplification, whereas the remaining part of the pulse gets reduced amplification. The pulse peak appears in the "tail" and the old peak disappears. Formally, the observation looks like the superluminal propagation, but actually it is only a misinterpretation of the motion of pulse peak. It is characteristic of many slow/fast experiments with intense optical pulses in the saturable media, to observe the above mentioned pulse reshaping which results in ambiguous contribution to measurements of the group velocity. For instance, in [Wang 2000], using gain-assisted anomalous dispersion, superluminal light propagation, and even negative group index was demonstrated in atomic caesium gas.

The optical pulse passing through an amplifying medium, mimics fast or superluminal light; pulse reshaping happens where the peak of pulse shifts to front and even into the foregoing part. Contrary to this, the behavior of propagation of an optical pulse passing through a saturable or absorbing medium mimics slow light. The front part of the pulse is subjected to stronger attenuation when compared to the rest of the pulse and the pulse peak shifts to the end of the pulse. The modified light propagation through reshaping can be distinguished from nonlinear dispersion effect. Both slow light and fast light produced through pulse reshaping can't be observed in a single medium, only one of these effects can be observed in the medium, whereas both nonlinear dispersion induced slow and fast light can be observed in the same medium.

Phenomena associated with time-dependant absorption/amplification indicate a drawback in the formal approach of the interpretation of pulse behavior. To elaborate, there is

a risk of misinterpreting the data obtained by traditional observation of pulse peak, if one does not consider the reshaping effects. Due to this reshaping, the measurement of group velocity using observation of optical pulses becomes ambiguous.

4.7. Role of monochromatism of interacting waves

According to the basic model of NLI, both the driving and probe waves are considered as ideal monochromatic waves. In case of ring laser for rotation sensing with induced NLI, we also can use the model of monochromatic waves. This assumption corresponds to most important behavior of laser emission. On the other hand, the spectral width of the waves is important in the smoothening of the interference pattern that is a necessary step for producing the NLI. Also, the group velocity of ideal monochromatic waves cannot be measured without some modulation of wave. This modulation leads to the spectral broadening, the common approach is to manipulate the optical pulses that are not ideal monochromatic waves. The spectral width of pulse signal is determined by the pulsewidth, Δt, i.e, $\Delta\omega \sim 1/\Delta t$. The mechanism of propagation in the nonlinear medium should be considered in terms of multiple waves that represent the Fourier components of the envelope function. Usually, the group velocity is determined as the velocity of the peak point of the pulse. In the perturbed regime, such a possibility is restricted. One deals with steep variations of propagation parameters, and the analysis should be made taking into account all spectral components subjected to different action in the medium. In long-distance fiber optic communication, wavelength dependent refractive index is a well-known process. The pulse broadening occurs due to *dispersion of group velocity* (GVD). We have to notice that the pulse broadening is not just modification of the pulse shape. If different spectral components of the pulse move with different velocities, the pulse would be deformed or even destroyed. As an example, the pulse undergoes deformation when sign of n_g changes, it occurs when the optical frequency of the pulse coincides with the CAD point. The pulse is separated into parts travelling in opposite

directions. Appearance of multiple peaks of the pulse instead of single one makes the monitoring of the pulse peak to be ambiguous. The pulse evolution in the range of negative dispersion can impede the measurements of the group velocity. Such difficulty has been claimed as the reason to avoid the ranges of negative dispersion (where usual definition of group velocity becomes invalid).

Chapter 5

Modeling and analysis of NLI phenomenon in 1.55 µm laser devices

5.1. Introduction

In this section, we report numerical modeling of slow and fast light generation in RW semiconductor lasers and SOAs based on InGaAsP/InP material system designed to operate at ~1.55 µm. The choice of the 1.55 µm wavelength is motivated by its importance in the fiber-optical telecommunications. Perturbations in the effective phase index, effective group index, modal gain, and linewidth of the probe wave are computed as a function of detuning frequency between the two waves for a fixed driving wave intensity. Also, the driving wave intensity is varied and the corresponding frequency detuning between CAD points Z1 and Z2 is mapped in order to find zones of detuning related to slowing down, accelerating , or back reflection of the probe waves. The critically anomalous dispersion (CAD) points where n_g = 0, are found to form a loop, confining the zone of the back reflection. The numerically computed values of the perturbed group index are then compared with the delaying and advancing of pulse propagation, experimentally observed in a 1.55-µm SOA based on InGaAsP/InP [Pesala 2006]. According to our knowledge, the CAD point has been identified and explained for the first time in semiconductor optical amplifiers. The theoretical model agrees well with the experimental results. The probe wave experiences an additional delay (slow light) when the frequency is lower than the driving wave, and is advancing (fast light) when the frequency is higher than that of the driving wave.

5.2. Optical model of the amplifying medium

5.2.1. Vertical structure for guided waves

In this section, we analyzed two device structures. The first structure is taken from reference [Xu 1996], it is a triple-quantum-well (TQW) separate confinement heterostructure (SCH) with 4.5-nm thick $In_{0.58}Ga_{0.42}As_{0.9}P_{0.1}$ wells and 16-nm thick $In_{0.75}Ga_{0.25}As_{0.53}P_{0.47}$ barriers . It

is grown by organometallic vapor-phase epitaxy and has a low threshold current density of only 20 ±10 A/cm^2. The second structure is taken from reference [Eliseev 1994], it is a double-heterostructure (DH) SCH with 0.1-μm thick $In_{0.58}Ga_{0.42}As_{0.9}P_{0.1}$ active region surrounded by 0.15-μm thick $In_{0.72}Ga_{0.28}As_{0.62}P_{0.38}$ intermediate barrier layers. This structure was used to make fabry-perot cavity of various lengths to study the emission wavelength dependence on length and other material parameters. Complete sequences of the epitaxial layers for the TQW and SCH structures are given in Tables 5.1 and 5.2, respectively. The refractive indices for each layer were calculated using the formulae from reference [Broberg 1984]. The gain in both structures is assumed to peak at 1.55 μm. The vertical confinement is provided by the barrier and cladding layers, as listed in Tables 5.1 and 5.2.

Table 5.1. InGaAsP/InP TQW-SCH structure with the refractive index, *n* and thickness, *d* of each layer

Layer	Material	*n*	*d* [μm]
Cap	p^+-$In_{0.53}Ga_{0.47}As$	3.514	0.02
Cladding	*p*-InP	3.169	1.5
Confinement layer	$In_{0.85}Ga_{0.15}As_{0.32}P_{0.68}$	3.280	0.6
Outer barrier	$In_{0.83}Ga_{0.17}As_{0.37}P_{0.63}$	3.297	0.03
Active region	$In_{0.58}Ga_{0.42}As_{0.9}P_{0.1}$ QW	3.543	0.0045
Barrier	$In_{0.83}Ga_{0.17}As_{0.37}P_{0.63}$	3.297	0.016
Active region	$In_{0.58}Ga_{0.42}As_{0.9}P_{0.1}$ QW	3.543	0.0045
Barrier	$In_{0.83}Ga_{0.17}As_{0.37}P_{0.63}$	3.297	0.016
Active region	$In_{0.58}Ga_{0.42}As_{0.9}P_{0.1}$ QW	3.543	0.0045
Outer barrier	$In_{0.83}Ga_{0.17}As_{0.37}P_{0.63}$	3.297	0.03
Confinement layer	$In_{0.85}Ga_{0.15}As_{0.32}P_{0.68}$	3.280	0.6

Cladding	*n*-InP	3.169	1.5
Substrate	*n*-InP	3.169	----

Table 5.2. InGaAsP/InP DH-SCH structure with the refractive index, *n* and thickness, *d* of each layer

Layer	Material	*n*	*d* [μm]
Cap	p^{+}-$In_{0.53}Ga_{0.47}As$	3.514	0.05
Cladding	*p*-InP	3.169	0.9
Barrier	$In_{0.72}Ga_{0.28}As_{0.61}P_{0.39}$	3.388	0.15
Active region	$In_{0.58}Ga_{0.42}As_{0.9}P_{0.1}$	3.543	0.1
Barrier	$In_{0.72}Ga_{0.28}As_{0.61}P_{0.39}$	3.388	0.15
Cladding	*n*-InP	3.169	0.8
Buffer	$In_{0.72}Ga_{0.28}As_{0.61}P_{0.39}$	3.388	0.3
Substrate	*n*-InP	3.169	----

5.2.2. Lateral optical confinement

The lateral confinement is provided by the RW configuration as shown in Fig.5.1. The ridge-waveguide (RW) geometry is used because it is most popular laser design for development and also mass production. The advantage of this geometry is, one can control the modal content of the laser beam. The optimization of its parameters allows one to obtain spatial single mode emission. These parameters are 1) ridge width *w* and 2) thickness *h* of passive layer outside the ridge. The thickness *h* is controlled during the processing of the wafer, specifically by etching under the photolithographic mask. Proper value of *h* at given ridge

width provides sufficient lateral optical confinement to maintain the fundamental mode and prevent propagation of higher-order modes. We assume that both interacting waves during NLI in ridge waveguide laser geometry are transverse fundamental modes with maximum spatial overlapping but distinguished by the wavelength. In Fig.5.1, the region in black outside the ridge is the cover material which is assumed to be benzocyclobutene (BCB). The color code on the right indicates refractive index values of the layers of epitaxial structure.

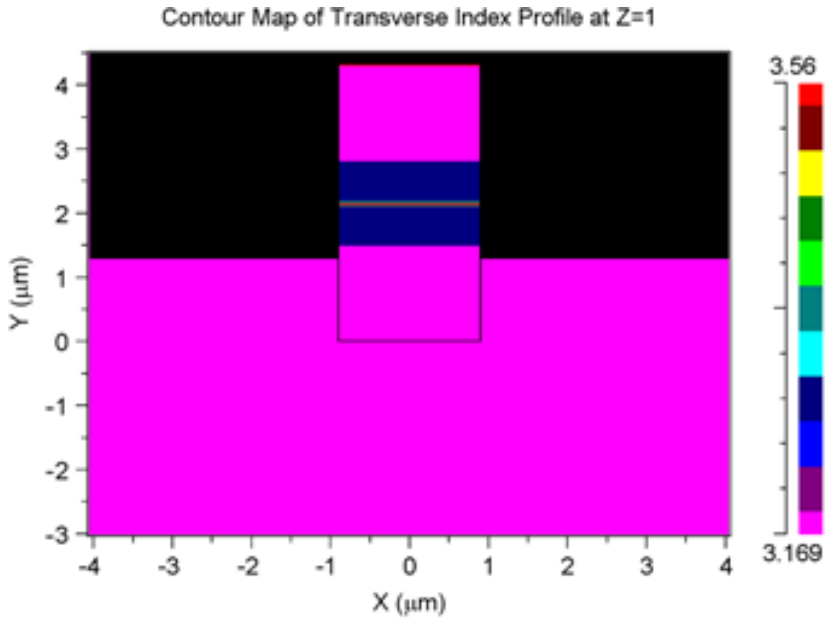

Fig. 5.1. Transverse refractive index profile of InGaAsP/InP QW ridge waveguide laser

The cross-section of the laser beam guided in the RW laser is shown in Fig. 5.2. The profile corresponds to the fundamental mode with limited penetration into passive regions outside the ridge. The monolithically-integrated ring lasers are designed based on RW geometry. It is a well-known fact that the bending losses can be avoided at sufficiently large radius of the ring. Thus, in optimized ring geometry there is no difference between curved and straight geometries of the RW. Therefore, the modal profiles are the same. The experimental demonstration of lasing in monolithically integrated lasers in ring (“race-track”)

configuration was made on LD-based optoelectronic integrated circuits (OEIC) operating in 1016-1020 nm wavelength range.

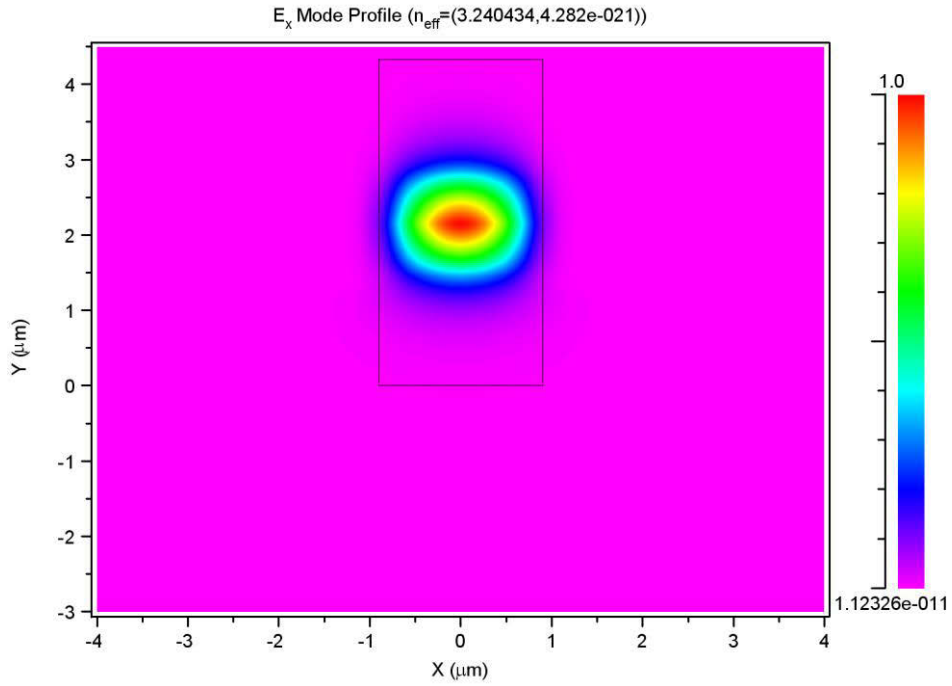

Fig.5.2. Fundamental mode of InGaAsP/InPbased QW ridge waveguide at 1.55 μm

5.3. Nonlinear perturbation theory and numerical simulations

The contribution of parametric interaction to the phase index is calculated using expression derived from perturbed dielectric permittivity. According to [Bogatov 1975], [Eliseev 2005], the perturbation of the real part *n* of the refractive index is given by Eqn.5.1 which is mentioned below:

$$\delta n = -\left|E_0\right|^2 B(N - N_0)(d\varepsilon'' / dN)(\alpha + \Omega/\gamma) / \left[2n\gamma(1 + \frac{\Omega^2}{\gamma^2}) \right] \qquad (5.1)$$

The main feature of guided wave analysis (in contrast to plane-wave approximation) is that the parametric interaction between the waves occurs only in the active region. Hence, the perturbation equation for refractive index is applicable only to the InGaAsP active region. The perturbed refractive index, δn is added to unperturbed refractive index, *n* in the active

region. Therefore, only the active region refractive index has to be modified due to NLI. The refractive index in the rest of the layers remains unchanged due to NLI. The refractive index values of all the epitaxial layers, including the active region (accounting for the change due to NLI) are calculated for wavelengths in the spectral vicinity of driving wave taking into account waveguide and material dispersion. The refractive index of the layers are then inputted into the mode solver of RSoft, called FemSIM and the perturbed effective index of the ridge waveguide is calculated numerically. FemSIM uses finite element analysis to compute the effective index of the mode. Table 5.3 gives the values of parameters used in numerical calculations of δn_{eff} and in modeling of the RW structures. Since, the NLI occurs only in active region in guided waves, the magnitude of NLI effect is reduced when compared to plane wave approach. The perturbed effective index is differentiated over the frequency and modified effective group index is then calculated using the relation 5.2. The computed effective group index contains contributions from the normal dispersion and the induced anomalous dispersion. However, the contribution due to the normal dispersion is quite small compared to the induced anomalous dispersion. The resulting perturbed effective group index increases to a certain value, then decreases and even passes through zero, as shown in Fig.5.4. This anomalous behavior of the effective group index of the probe wave leads to observations of slow and fast light in the semiconductor medium.

$$n_{\text{g,eff}} = n_{\text{eff}} + \omega \frac{dn_{\text{eff}}}{d\omega} \tag{5.2}$$

Table 5.3. Parameters used in numerical calculations

Parameter	Units	QW	SCH
Active layer thickness	μm	0.0135	0.1
Ridge width	μm	1.8	2
Etch depth	μm	3.0255	1.2

Optical frequency of driving wave, ν_s	THz	193.419	193.419
Linewidth broadening factor, α	-	5.4	5.4
Excess carrier density over the transparency level, $N - N_0$	cm^{-3}	2×10^{18}	2×10^{18}
Stimulated recombination coefficient, B	cm^2/V^2s	9.92	9.92
Initial relaxation rate, γ_0	1/s	10^9	10^9
dg/dN	10^{-16} cm^2	2.7	2.7
$d\varepsilon''/dN$	10^{-20} cm^3	-2.36	-2.36
Linear effective phase index	-	3.240	3.282
Linear effective group index	-	3.73	5.3

5.4. Calculation of effective group index and the flow chart

As mentioned earlier, in order to determine the group index of the probe wave we have to differentiate the perturbed phase index over the frequency to obtain the modified induced dispersion; then the modified dispersion is used to calculate the modal group index. This procedure for calculation of group index was used for all laser structures mentioned in this dissertation. A flowchart mentioning all the steps to calculate the modified effective group index is given below:

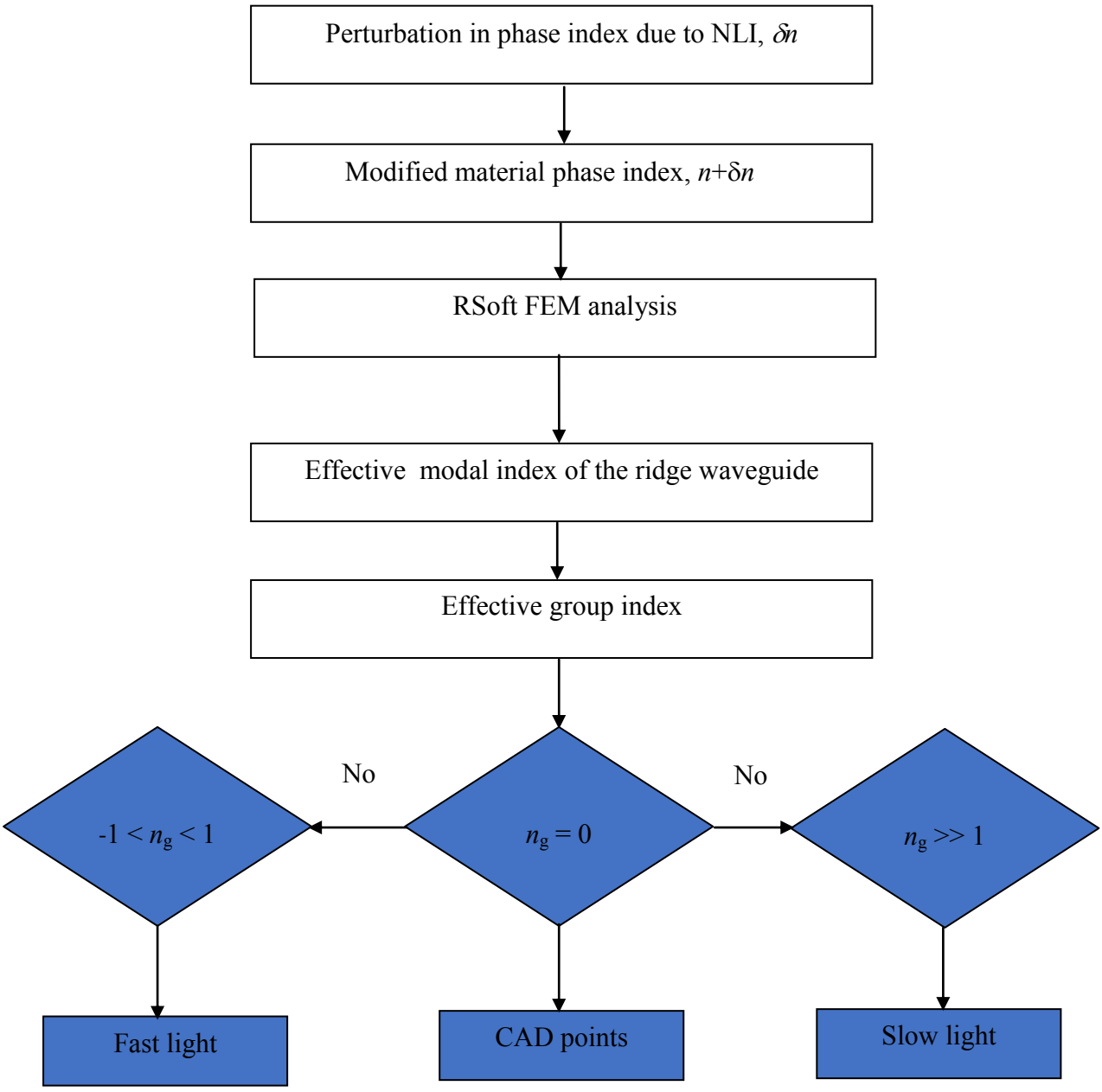

Fig.5.3. Flowchart to calculate the effective group index of a probe wave due to NLI in a ridge waveguide laser

5.5. Induced effective group index

The effective group index perturbation as a function of detuning frequency between the two waves for the TQW structure is shown in Fig. 5.4. The reference zero detuning line is at the driving wave frequency of 193.41935 THz. It is important to note that the parametric

interaction between the two waves leads to anomalous dispersion ($dn_{eff}/d\omega < 0$) of the probe wave. There is a range of frequencies higher than that of the driving wave, where anomalous dispersion leading to superluminal propagation ($v_g > c$) is induced. There are also CAD points, where the group index passes through zero.

We denote the CAD points in Fig. 5.4 as Z1 and Z2. The point Z1 is very close to the driving wave and in case of a laser it can fall within the frequency lock-in range. The point Z2 is separated from the driving wave frequency by several GHz. We can expect the following behavior: (i) the CAD point corresponds to an extremely fast light; the laser operation at this point is very unstable because the group velocity of the probe wave passes an infinite value and changes the sign; (ii) the gain is greatly reduced, since the fast wave weakly interacts with the active medium; and (iii) the spectral linewidth passes through an infinite peak. An experimental identification of the CAD point can be quite ambiguous.

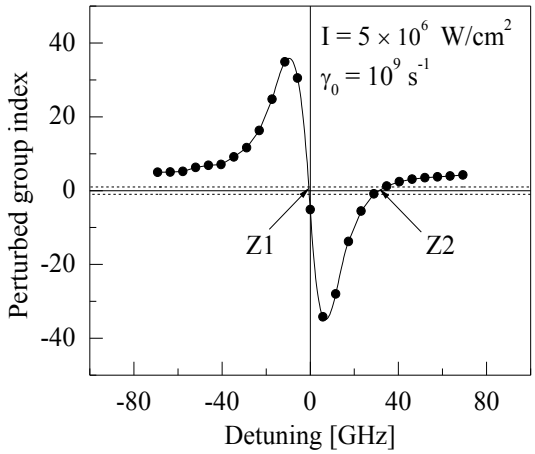

Fig. 5.4. Calculated spectrum of the perturbed effective group index as a function of detuning between the driving and probe waves for the TQW structure. The driving wave intensity is 5 MW/cm^2. Dotted lines around the zero line are drawn for $n_{g,eff} = \pm 1$. The band between these lines corresponds to superluminal propagation. Z1 and Z2 are the CAD points.

5.6. Induced modal gain spectrum

According to the CPO mechanism of parametric interaction, an exchange by photons causes variation of gain, depending on the detuning [Bogatov 1975], [Ishikawa 1982], [Ogasawara 1988], [Yamada 1989], [Su 2006]. The driving wave is scattered by a dynamic carrier grating, which is formed due to the interference between the driving and probe waves, and produces photons with energy equal to that of the probe wave. This results in additional modal gain at the probe wave frequency when the flow of converted photons is in the same direction as the initial probe wave. If the converted photons are directed in the opposite direction, the result is a suppression of the probe wave. The magnitude of this additional gain or suppression effect depends on the group velocity. The slowing of light propagation is associated with additional gain. The fast light reduces the interaction time and results in gain suppression. Thus, the spectral dependencies of group velocity and of induced gain are both asymmetric functions with respect to the driving frequency. The equation for calculation of induced gain is derived from the perturbation of dielectric permittivity mentioned in [Eliseev 2006]. The induced modal gain δG is given by Eqn. 5.3 which is mentioned here again:

$$\delta G = -2\pi B\left|E_0\right|^2 (N - N_0)(d\varepsilon'' / dN)(1 - \frac{\alpha\Omega}{\gamma}) / \left[n_{\text{eff}} c(1 + \frac{\Omega^2}{\gamma^2}) \right] \tag{5.3}$$

The induced modal gain as a function of detuning frequency between the driving and probe waves for the SCH TQW structure is shown in Fig. 5.5.

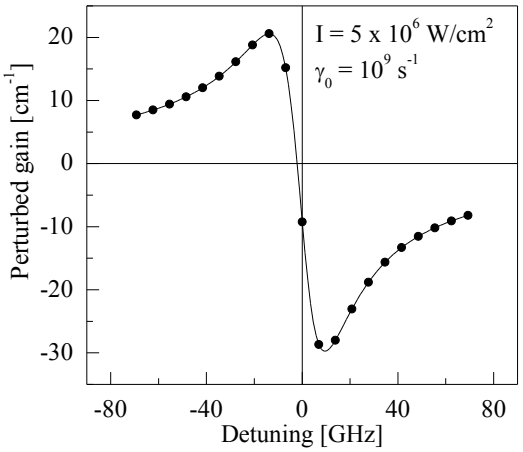

Fig.5.5. Calculated spectrum of the perturbed modal gain as a function of detuning between the driving and probe waves in the vicinity of the driving wave frequency (shown by the vertical line). The driving wave intensity is 5 MW/cm^2. The horizontal line represents the background, or unperturbed gain.

5.7. Induced spectral narrowing

In this section, we analyze the influence of the perturbed group velocity on the linewidth of laser emission of the probe wave. This influence includes both narrowing and broadening, depending on the frequency detuning. The nonlinear linewidth narrowing occurs in the case of the slow light. It can be explained as a result of increase in photon density in the mode under consideration. In this analysis, we assume the laser emission intensity to be fixed. The intensity is proportional to the photon density in the cavity and to the group velocity. When the group velocity is reduced (by parametric interaction), to maintain the fixed intensity, there will be an increase in the photon density. The spectral linewidth is inversely proportional to the photon density. Therefore, the new mechanism of linewidth narrowing (nonlinear narrowing) is a result of an increased photon density. When the group velocity is high, the photon density decreases to maintain the fixed intensity. Hence, there will be a nonlinear broadening in the case of fast light. This mechanism of induced linewidth narrowing or broadening works only if the power in the mode is fixed or is increasing. Therefore, it is valid

only for the laser operation regime, and not for the traveling wave regime in an amplifier, since the output intensity has to be fixed.

We have calculated the induced linewidth narrowing and broadening of the probe wave as a function of detuning between the driving and probe waves. The expression used for the calculation is as follows [Coldren 1995]:

$$\Delta\upsilon_{FW} = \frac{\left(\Gamma v_g g_{th}\right)^2 \eta_0}{4\pi P_0} n_{sp} h\nu(1+\alpha^2) \tag{5.4}$$

where Γ is the optical confinement factor, g_{th} is the threshold value of optical gain, η_0 is the single facet efficiency, P_0 is optical power, and n_{sp} is the spontaneous emission factor. The linewidth perturbation is calculated by substituting the perturbed v_g as a function of detuning in Eqn. 5.4. The other parameters used in this calculation are g_{th} = 100 cm^{-1}, Γ = 0.02, η_0 = 0.4, P_0 = 1 mW, n_{sp} = 2.6, α = 5.4 and $h\nu = 0.799$ eV. Fig. 7 shows a plot of the perturbed linewidth of the probe wave as a function of detuning between the driving and probe waves.

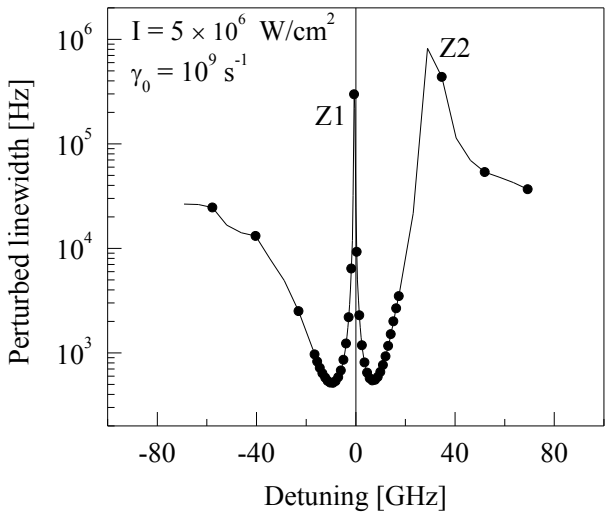

Fig. 5.6. Calculated spectrum of the perturbed linewidth as a function of detuning between the driving and probe waves. The vertical line at zero detuning corresponds to the driving wave frequency. The driving wave intensity is 5 MW/cm^2. The CAD points are Z1 and Z2.

5.8. Critically anomalous dispersion (CAD) plots

The frequency of CAD points Z1, Z2 is plotted by varying the driving wave intensity similar to our previous work [Kalagara 2012]. The CAD plots are made for both TQW-SCH and DH-SCH structures. The solid curves in Figs. 5.7 and 5.8 represent $n_g = 0$, the dotted contours around the solid curves represent $n_g = -1$ and 1. The region between the outermost and the inner dotted contours represents the region of *superluminal propagation*, where $v_g > c$. The shape of the loop corresponding to the CAD conditions is influenced by two factors. One is an increasingly nonlinear response with increasing intensity of the driving wave. Another factor is the relaxation-related broadening. Due to these two factors, the loop size rolls down and the effect diminishes at higher driving wave intensities. The influence of the driving wave intensity and the relaxation rate of carriers on the CAD loop is explained in more detail in [Kalagara 2012].

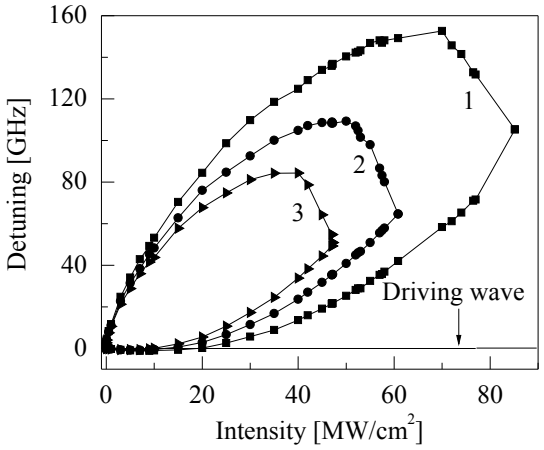

Fig. 5.7. Position of the CAD points Z1 and Z2 as a function of the driving wave intensity in the TQW-SCH structure. The initial carrier relaxation rate γ_0 is 10^9 s^{-1}. Curve 1 corresponds to $n_{g,eff} = 1$, curve 2 corresponds to $n_{g,eff} = 0$ and curve 3 corresponds to $n_{g,eff} = -1$. The solid horizontal line is at zero detuning, corresponding to the driving wave frequency.

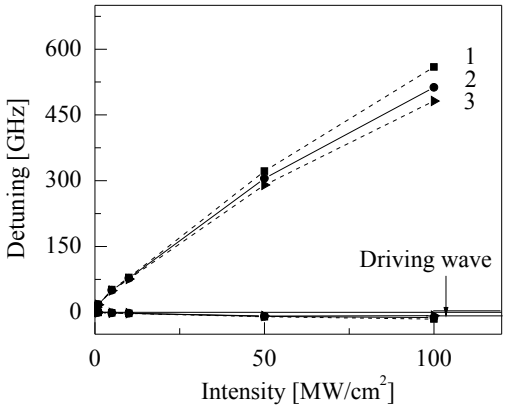

Fig. 5.8. Positions of the CAD points Z1 and Z2 as a function of the driving wave intensity in the DH-SCH structure. The initial relaxation rate of carriers $\gamma_0 = 10^9$ s^{-1}. The curve 1 corresponds to $n_{g,eff} = 1$, curve 2 corresponds to $n_{g,eff} = 0$ and curve 3 corresponds to $n_{g,eff} = -1$. The solid horizontal line denotes the driving wave, corresponding to zero detuning.

5.9. Catastrophic optical damage (COD)

It is very important to consider the catastrophic optical damage (COD) of the material that may occur typically at the laser facets at very high intensities, so that the computer simulation would not correspond to unrealistic conditions. Usually, the limitation of the intensity in GaAs-based lasers is on the level of 5-10 MW/cm^2. In lasers operating around 1.55 μm, these limitations are not well established and probably are somewhat higher. Also, the COD limitation depends on the pulse duration. Thus, we cannot indicate these limitations on plots, but we stop calculations at the intensity level above 80-100 MW/cm^2. As a result the curves of CAD-loops remain widely open in the case of the DH-SCH structure (see Fig. 5.8).

5.10. Comparison with experimental data

Experimental results on the delay of short pulses (1.3 ns long) through an SOA operating in the spectral range 1.52-1.57 μm have been reported in [Pesala 2006]. The time delay of the probe wave was observed to be perturbed under the influence of the driving wave. It increased or decreased, depending on the detuning frequency between the driving and probe

waves. It was demonstrated that the perturbed delay increased for negative detuning (the frequency of the probe wave lower than the frequency of the driving wave) and it decreased for positive detuning, as it was expected from the plane-wave theory [Uskov 2005]. In Fig. 5.9, the experimental data for the perturbed delay at the driving wave power of 1 mW are shown by square points, whereas the solid curve below is the numerically calculated perturbed effective group index, using the parameters given in Table 5.3 for the TQW-SCH structure. In the numerical simulation, the driving wave intensity was assumed to be around 10^5 W/cm^2. When $n_{g,eff}$ is positive, the delay is proportional to $n_{g,eff}$. The calculation of the actual delay has not been performed here, as the length of the SOA used in the experiments is not indicated in [Pesala 2006]. The zero delay line in Fig. 5.9 corresponds to the delay in absence of the driving wave. There is a good qualitative agreement between the calculated $n_{g,eff}$ and measured dependencies of delay versus detuning, with a few exceptions discussed below. The experimental data are missing within about 5 GHz range around zero detuning, due to the interference between the signal modulation frequency and the detuning frequency. In addition, when the detuning between the two waves is too small, they cannot be distinguished from each other, due to their finite linewidths.

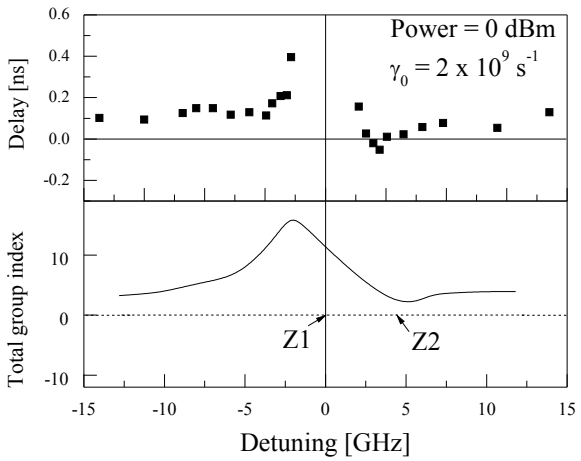

Fig.5.9. Comparison of total effective group index, $n_{g,eff}$ (linear plus nonlinear effective group index) calculated numerically for the TQW-SCH structure in this work (lower part) with

experimentally observed additional delay experienced by the pulse [5] (upper part). The driving wave intensity is 0.67×10^5 W/cm^2. The initial carrier relaxation rate γ_0 is 2×10^9 s^{-1}. Z1 and Z2 are the CAD points.

Calculation of the pulse delay for negative values of the effective group index also poses difficulty. The problem is that when the group index is negative, the model of parametric interaction does not predict the group velocity of a probe wave propagating in the same direction as the driving wave. Instead, the model describes a back-reflected wave. However, a forward-directed wave should still exist for the parametric interaction to occur. What is measured experimentally as the delay of pulse propagation is related to the forward-directed wave. Therefore, in the range of a negative effective group index, we have no reliable estimate of the perturbed delay. It can be seen in Fig. 5.9 that deviations between the calculated and measured data fall within the negative effective group index range. Satisfactory agreement for positive effective group index suggests the fitting parameters used in the simulation are adequate. We note that the fitted value of $\gamma_0 = 2\times10^9$ s^{-1} corresponds to the relaxation time of 0.5 ns. This value is in reasonable agreement with the CPO interaction model, where it has the meaning the lifetime of excess carriers in the active material.

Another issue when comparing simulation results with the reported data from [Pesala 2006] is the magnitude of the observed pulse advance within the positive detuning range, which was interpreted as a demonstration of superluminal propagation due to the influence of the driving wave. Under the conditions of increasing driving power, this advance reached about 300 ps [Pesala 2006]. Such result cannot be obtained in framework of our model. The reason is that the result for an unperturbed case in a traveling wave amplifier can differ from the perturbed pulse propagation time at most by the time it takes for an unperturbed pulse to traverse the length of the SOA. That maximum value corresponds to the advanced pulse traversing the

amplifier instantaneously. The unperturbed time τ of pulse passage is $n_{g0}L/c$, where n_{g0} is the unperturbed group index and L is the SOA length. For L = 1 mm, τ is ~18 ps. Therefore, the maximum advance for a mm-long SOA is expected to be 18 ps, which is much less than the reported 300 ps. While the actual length of the device used in the experiments was not given in [Pesala 2006], it is rather unlikely it was as long as 17 mm, which would be required to account for a 300 ps advancement using the nonlinear mode interaction model. It is possible that the observed pulse was somewhat reshaped during the propagation, which could account for this discrepancy.

5.11. Conclusion

The modeling of the parametric interaction of waves in an amplifying semiconductor medium is carried out numerically and analytically. The parametric interaction is considered in the two-wave approximation based on the coherent population oscillation. The results obtained allow us to interpret properties of semiconductor lasers and SOAs when two or more waves are present. The driving wave (assumed to be much stronger than the probe wave) influences the complex permittivity at the probe wave frequency, providing substantial modification of propagation parameters of the probe wave (gain, slowing, accelerating, or back reflection, and linewidth).

The numerical simulation was performed for InGaAsP/InP ridge-waveguide laser structures operating at the wavelength of ~1.55 μm. Thus, the results reported in [Kalagara 2012] are extended here to a wider spectral range.

In the framework of the CPO interaction, we computed perturbation of the complex effective refractive index and then calculated the modal gain and the effective group index at various intensities of the driving wave and various detunings between the interacting waves. Similar to the results reported in [Kalagara 2012] for InGaAs/AlGaAs/GaAs structures, the loops of critically anomalous dispersion are mapped on plots of detuning versus driving wave

intensity. The numerical simulation illustrates the ranges of threshold intensity of driving wave for the CAD points to appear, as well as maximum driving wave intensity at which the relaxation-related broadening reduces the magnitude of the nonlinear effect. As in [Kalagara 2012], we found that the laser structures with larger optical confinement demonstrate larger ranges of induced anomalous dispersion. In devices with a bulk active region, the maximum driving wave intensity exceeds the intensity of the catastrophic optical damage.

Comparison with the available experimental data leads to a qualitative agreement and it allows us to estimate the carrier relaxation rate γ_0, as the spectral range where nonlinear perturbation takes place is sensitive to the value of γ_0. Using the data on pulse delay between the pump and probe beams passing the SOA [Pesala 2006], we find the characteristic lifetime $1/\gamma_0$ of ~0.5 ns, which falls into standard range of recombination lifetimes for excess carriers in InGaAsP. This result indicates that the CPO model of parametric interaction is adequate.

Chapter 6

Modeling and analysis of nonlinear interaction (NLI) phenomenon in 1.016 μm and 0.88 μm laser devices

6.1. Introduction

In this section, the perturbation of optical characteristics of probe (weak) wave in presence of a strong driving wave is illustrated for GaAs/AlGaAs separate confinement heterostructure (SCH) operating at 0.88 μm and InGaAs/AlGaAs/GaAs double-quantum-well semiconductor (DQW) ridge waveguide laser operating at 1.016 μm using numerical modeling. The two laser structures are quite popular, InGaAs/AlGaAs/GaAs QW laser has the lowest value of recorded threshold current. Also, experimental data on beat frequency splitting due to nonlinear mode interaction in this laser system are available [Eliseev 2005a], which we will compare with our theoretical data in the future. The important feature of the present work is to calculate the actual perturbation of modal parameters, rather than using a simple approximation with plane wave parameters, as was done in [Eliseev 2006], [Eliseev 2005]. We demonstrate that the magnitude of the nonlinear effect depends on the laser structure. Also, illustrative calculations are carried out on the induced narrowing or broadening of the probe mode linewidth perturbed by nonlinear interaction.

6.2. Optical model of the amplifying medium

6.2.1. Vertical structure for guided waves

The lasing mode is confined to the active region (active waveguide) of the structure. The active medium is assumed be either bulk or two quantum well layers sandwiched between transparent passive barrier layers. Due to lower refractive index of these passive layers, the wave along the active layer is well confined (the vertical confinement). We consider here a DQW structure with two InGaAs QWs (d = 2×10 nm) separated by the 10-nm thick GaAs

barrier layers (operation wavelength is 1016 nm). Another type of guided structure we consider is a separate-confinement heterostructure (SCH) with a bulk 200-nm thick GaAs active region (operation wavelength is 880 nm). The laser structures have optical confinement factors of (~0.42 in SCH and ~0.035 in DQW). These two semiconductor structures with the epitaxial layers and the refractive indices [Adachi 1985] are shown in Tables 6.1 and 6.2 and also shown in Figs. 6.1 and 6.2 respectively. Because of significant index difference between the active region and cladding layers, the vertical confinement is of index-guiding type almost insensitive to gain and absorption in the layers.

Table 6.1. InGaAs/AlGaAs/GaAs DQW structure with the refractive index (n) and the thickness of the layers (d) in μm

Layer	Material/Doping	n	d
Cap	p^+ GaAs/3×10^{19}cm^{-3}	3.46	0.05
Cladding	p $Al_{0.3}Ga_{0.7}As$: C 5×10^{17} cm^{-3}	3.351	1.0
GRIN Cladding	Undoped $Al_xGa_{1-x}As$ x = 0.2-0.3	3.405 to 3.351	0.05
Cladding	$Al_{0.2}Ga_{0.8}As$	3.405	0.05
Barrier	Undoped GaAs	3.508	0.01
Active region	$In_{0.2}Ga_{0.8}As$	3.614	0.01
Barrier	Undoped GaAs	3.508	0.01
Active region	$In_{0.2}Ga_{0.8}As$	3.614	0.01
Barrier	Undoped GaAs	3.508	0.01
Cladding	$Al_{0.2}Ga_{0.8}As$	3.405	0.05
GRIN Cladding	Undoped $Al_xGa_{1-x}As$ x = 0.3-0.2	3.351to 3.405	0.05

Cladding	*n* $Al_{0.3}Ga_{0.7}As$:Te 5×10^{17} cm^{-3}	3.351	1.0
Buffer	$Al_{0.3}Ga_{0.7}As$	3.351	0.1

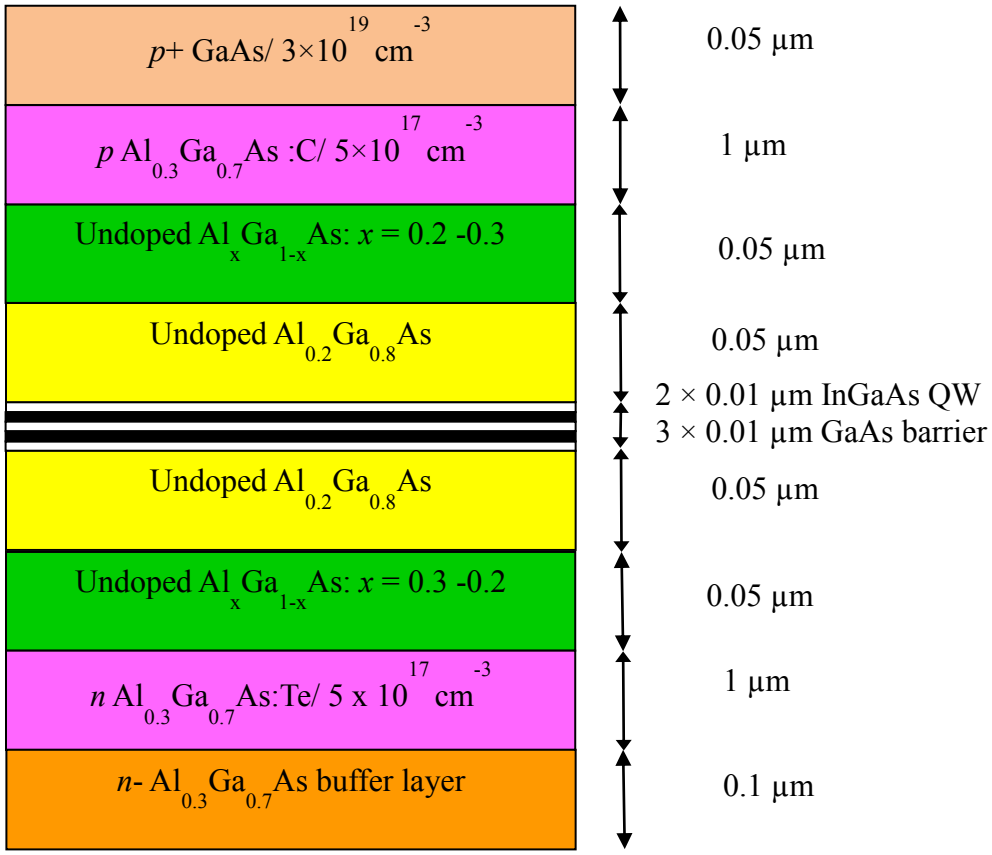

Fig.6.1.Epitaxial structure of InGaAs/GaAs/AlGaAs QW ridge waveguide structure

The vertical layers including active quantum wells or bulky layer are chosen accordingly, to obtain lasing in the desirable spectral range. LDs based on InGaAs double-quantum-well on GaAs substrate are known to be with lowest threshold current density among all other LDs, due to their lattice matched layers resulting in very low compressive stress. The spectral range of these LDs is from 970 to 1020 nm. It includes the most important wavelength of 980 nm that corresponds to laser-diode pumping of erbium-doped fber-amplifier (EDFA), which

has very wide range of applications in long-distance communication and also in laser technology.

Table 6.2. GaAs/AlGaAs SCH wafer structure with the refractive index (*n*) and thickness of the layers (*d*) in μm

Layer	Material/Doping	*n*	*d*
Cap	p^+ GaAs/3×10^{19}cm^{-3}	3.571	0.05
Cladding	*p* $Al_{0.3}Ga_{0.7}As$: C 5×10^{17} cm^{-3}	3.406	1.0
GRIN Cladding	Undoped $Al_xGa_{1-x}As$ x = 0.2-0.3	3.468 to 3.406	0.05
Cladding	$Al_{0.2}Ga_{0.8}As$	3.468	0.05
Active region	Undoped GaAs	3.619	0.2
Cladding	$Al_{0.2}Ga_{0.8}As$	3.468	0.05
GRIN Cladding	Undoped $Al_xGa_{1-x}As$ x=0.3-0.2	3.406 to 3.468	0.05
Cladding	*n* $Al_{0.3}Ga_{0.7}As$:Te 5×10^{17} cm^{-3}	3.406	1.0
Buffer	$Al_{0.3}Ga_{0.7}As$	3.406	0.1

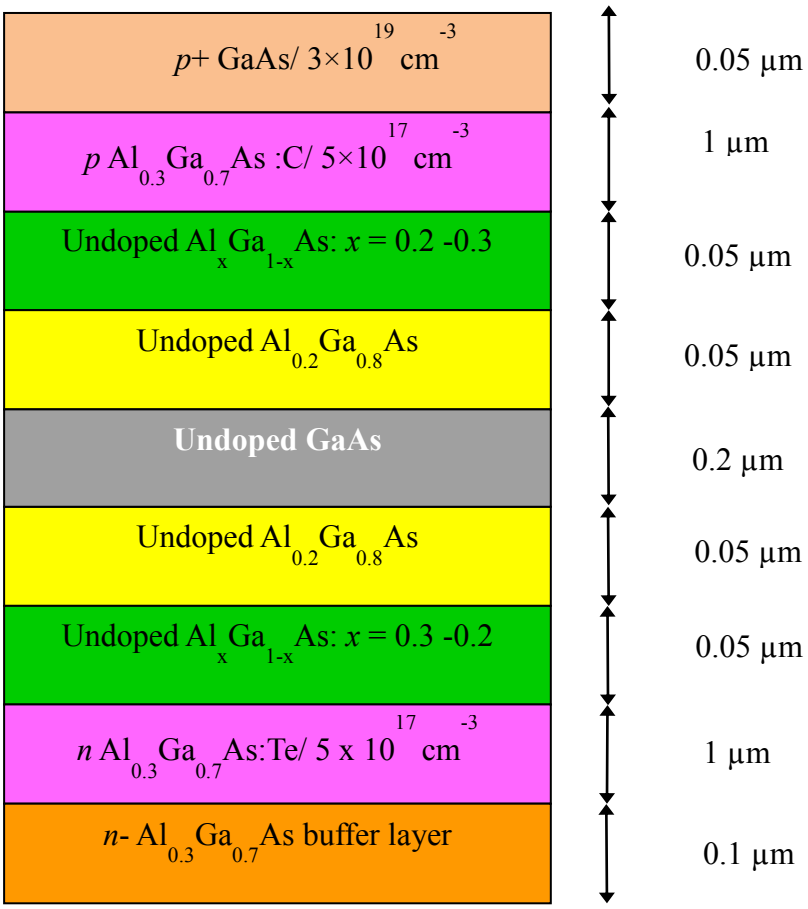

Fig.6.2. Transverse refractive index profile of InGaAs/GaAs/AlGaAs QW ridge waveguide structure

In Fig. 6.2 and table 6.2, the vertical structure of LD with bulky (200-nm thick) GaAs active region is shown. This laser structure is a double-heterostructure (DH) type. The laser structure is lattice-matched to substrate to avoid formation of interface defects. The laser emission is obtained in 850-890 nm range. We considered this LD since it is of larger optical confinement factor than the DQW LDs. The NLI effect is higher in this laser structure when compared to QW laser structure.

6.2.2. Lateral optical confinement

The transverse refractive index profile of RW structure is shown in Fig. 6.3. The active region is located under the ridge where the pumping current supplies excess carrier injection. The guided wave attenuates in lateral directions in accordance with eigen-functions of the wave equation which is solved numerically using FemSIM module, the modesolver of RSoft. An important parameter of the lateral confinement is the setback distance *h*, which is the

distance between the top active region interface and the surface outside the ridge. The strength of lateral confinement is usually determined by an interplay between sufficient and stable confinement for the fundamental mode, and suppression of higher order modes. The lateral confinement can be increased by decreasing *h*. We chose the parameter *h* so as to obtain single mode operation for both laser structures. All calculated optical characteristics are the modal parameters for the fundamental mode of the RW laser which is shown in Fig.6.4. The perturbation of material index occurs only in the active region, where the carrier density is subjected to the influence of local intensity of interfering fields of the driving and probe waves. Hence, the magnitude of the nonlinear effect is sensitive to the optical confinement as mentioned in the previous chapter.

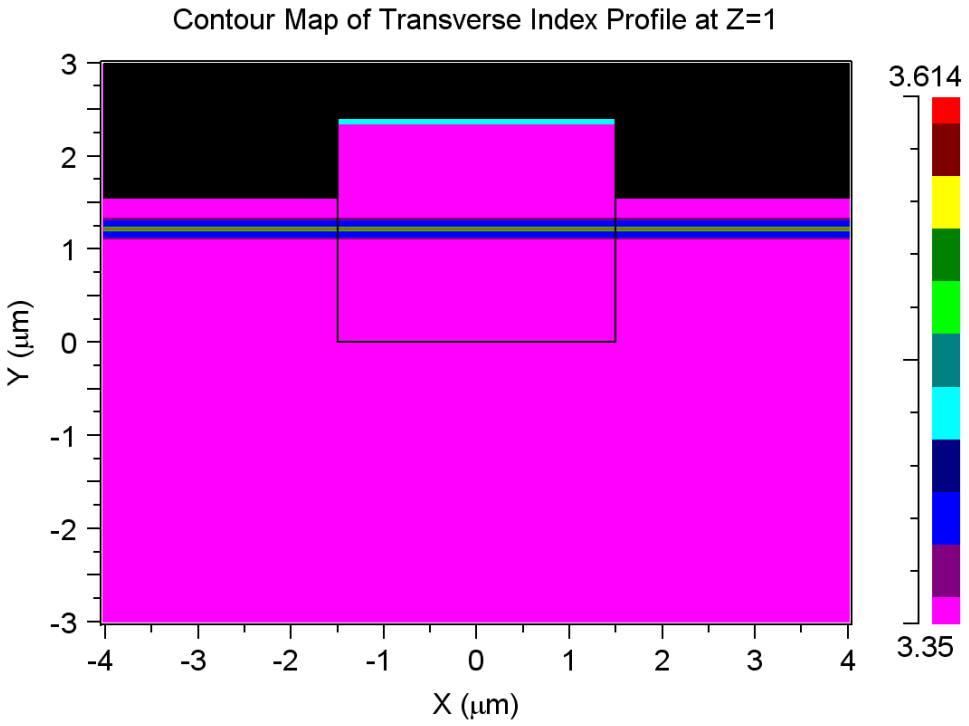

Fig.6.3.Transverse refractive index profile of InGaAs/GaAs/AlGaAs QW ridge waveguide structure

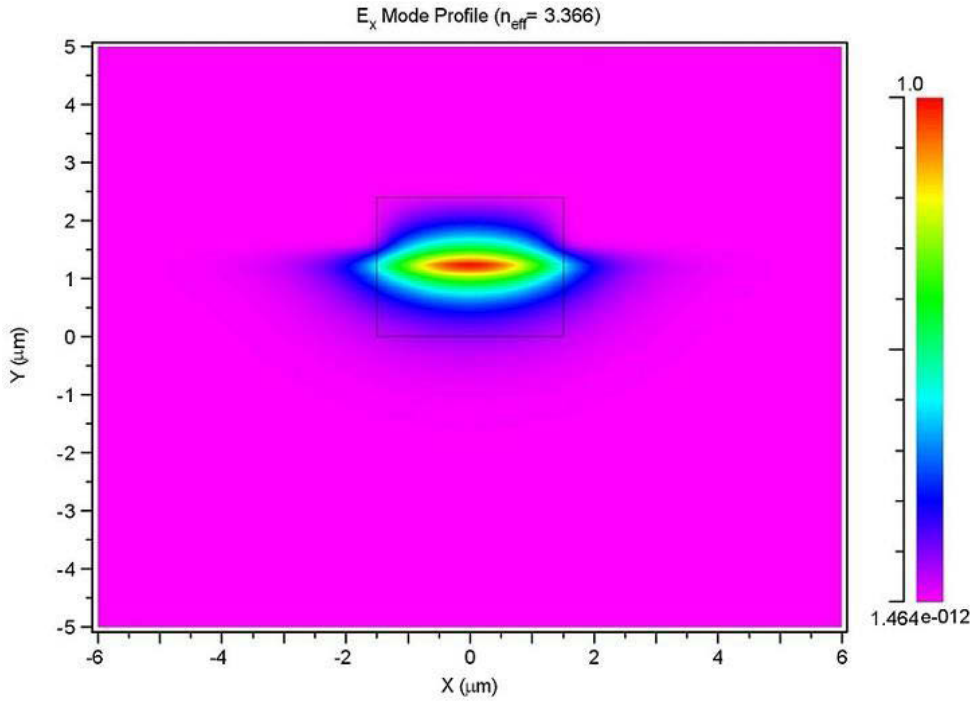

Fig.6.4.Fundamental modal profile of InGaAs/GaAs/AlGaAs QW ridge waveguide structure

6.3. Nonlinear perturbation theory and numerical simulations

According to [Eliseev 2005], the perturbation of the refractive index under two-wave interaction is given by Eqn.6.1 which is mentioned again here:

$$\delta n(\Omega) = -|E_0|^2 B(N - N_0)(d\varepsilon'' / dN)(\alpha + \Omega/\gamma) / \left[2n\gamma(1 + \frac{\Omega^2}{\gamma^2}) \right] \tag{6.1}$$

where E_0 is the electric field strength of the driving wave, B is the coefficient of stimulated emission, N is the carrier density, N_0 is the transparency carrier density, ε'' is the imaginary part of the relative dielectric permittivity, α is the linewidth broadening factor, γ is the rate of relaxation processes, and $\Omega = \omega_s - \omega$ is the detuning of probe wave with respect to the frequency ω_s of the driving wave.

The driving wave intensity depends on the carrier relaxation rate γ, which takes into account the spontaneous carrier relaxation rate and the stimulated recombination. The relaxation rate γ is expressed as $\gamma = \gamma_0 + B|E_0|^2$, where γ_0 is the initial carrier relaxation rate and B is the

coefficient accounting for an increase in the rate γ caused by stimulated recombination. An increase in γ leads to spectral broadening and to a decrease in the perturbation magnitude.

Table 6.3. Parameters used in numerical calculations

Parameter	Units	DQW	SCH
Active layer thickness	nm	2×10	200
Ridge width	μm	3	3
Setback distance, *h*	μm	0.31	0.3
Optical frequency of driving wave, ν_s	GHz	295078.74	340681.82
Line width broadening factor, α	-	3	3
Excess carrier density over the inversion threshold, $N - N_0$	$1/cm^3$	3×10^{18}	3×10^{18}
Stimulated recombination coefficient, *B*	cm^2/V^2s	40	40
Initial relaxation rate, γ_0	1/s	10^9, 5×10^9 10^{10}	10^9,10^{10}, 10^{11}
$d\varepsilon''/dN$	10^{-20} cm^3	-2.6	-2.6
Linear dispersion of phase index	μm^{-1}	-0.64	-0.76
Waveguide component of dispersion	μm^{-1}	-0.034	-0.05
Linear effective phase index	-	3.366	3.430
Linear effective group index	-	4.016	4.542

6.3.1. Spectra of perturbed effective phase index of probe wave

Eqn. 6.1 was used to calculate the steady-state perturbation of the material values of the phase index. Then the material values were included into the calculation of modal parameters of the RW structures, using numerical simulation by FemSIM mode solver. Finally, the effective group index was obtained by differentiation of the effective phase index. All

calculations were performed for laser devices operating at room temperature. Numerical parameters are collected in Table 6.3.

The operational gain is assumed constant, as it is automatically kept constant in a real steady-state laser. Spectrum of perturbed effective phase index is shown in Fig. 6.5 for a particular case of the driving wave intensity equal to 5 MW/cm^2. The index has a small bump located near the driving wave frequency. Meanwhile it is sufficient to produce a noticeable perturbation of the group index. The modal perturbation is numerically smaller than that of material perturbation, and it decreases with a decreasing optical confinement factor. We should emphasize here that our results are only to illustrate the nonlinear effect remembering that parameters used in calculations are valid for only particular cases.

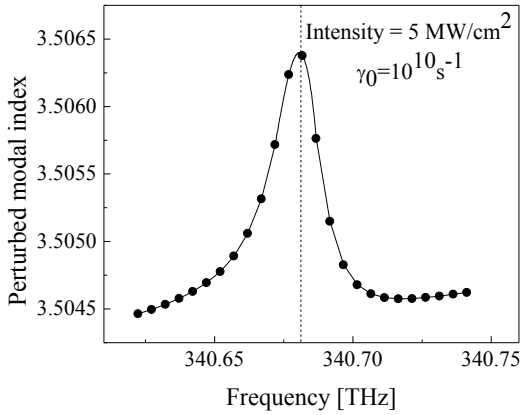

Fig. 6.5. Calculated spectrum of the perturbed modal index in SCH laser in the vicinity of the driving wave frequency 340.682 THz (shown by the dotted-dashed vertical line). The driving wave intensity is 5 MW/cm^2.The initial carrier relaxation rate γ_0 is 10^{10} s^{-1}.

6.3.2. Spectra of perturbed group index of the probe wave

Typical spectrum of the perturbed group index is shown in Fig. 6.6. When intensity of the driving wave is 5 MW/cm^2, there are two crossing points (Z1 and Z2) with a zero group index line, and each of them corresponds to what we termed critically anomalous dispersion. The band marked by dotted lines corresponds to a region of superluminal

propagation (the group index confined between –1 and 1).

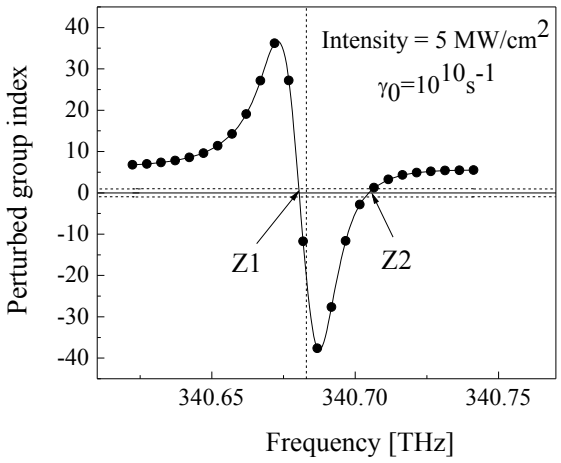

Fig.6.6. Calculated spectrum of the perturbed effective group index in the vicinity of the driving wave frequency 340.682 THz (shown by the dotted vertical line). The intensity of the driving wave is 5 MW/cm^2. Dotted lines around zero line are drawn for values -1 and 1. The band between these lines corresponds to superluminal propagation. Critically anomalous dispersion points are Z1 and Z2.

6.3.3. Spectra of perturbed gain of the probe wave

The modal gain of probe mode is perturbed by the nonlinear interaction in a manner shown in Fig.6.7. The asymmetric spectral shape has been found experimentally in [Bogatov 1975]. Additional nonlinear gain appears at the low-photon energy side of driving wave whereas at high-photon-energy side it will be suppression of the background gain. This behavior indicates the energy exchange between interacting waves. Namely, additional gain is resulted by photon conversion from driving wave to probe one. The additional nonlinear gain is probably one of origins of temporal instability of the laser action. An appearance of spectrally-shifted gain produces advantage of the mode competing against driving one. However, this advantage exists until the driving mode operates. If the driving mode were suppressed, the probe mode also will lose additional gain and it will be also suppressed. Then

the driving wave will get advantage to increase its intensity. Hence the interaction can produce cycles of mode switching in the free-run regime.

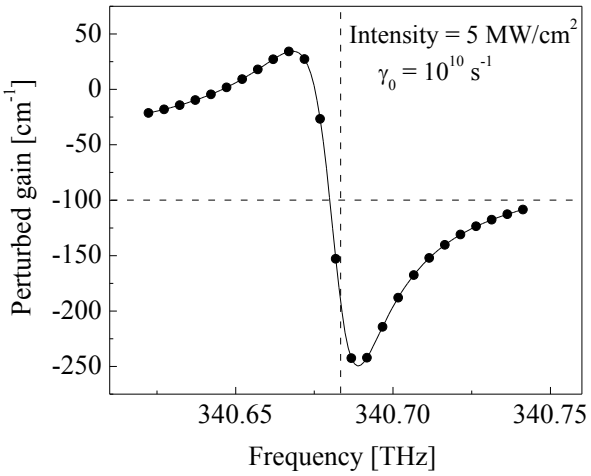

Fig.6.7. Calculated spectrum of the perturbed modal gain in the vicinity of the driving wave frequency 340.682 THz (shown by the dashed vertical line). The intensity of the driving wave is 5 MW/cm^2. Dashed horizontal line represents the background, or unperturbed, gain.

The gain suppression in the short-wavelength range may be understood as a result of emission of converted photons from the driving wave in direction opposite to the probe wave. Such behavior can be produced in traveling-wave amplifier and in unidirectional ring cavity. In the Fabry-Perot laser, the behavior is not simple because the laser emission propagates in both directions.

6.3.4. Spectra of perturbed linewidth of the probe wave

We consider behavior of spectral linewidth of laser emission in the probe wave under the influence of nonlinear wave interaction. According to [Coldren 1995], the linewidth $\Delta\nu$ is sensitive to the group velocity and is given by Eqn.6.2 which is mentioned again here

$$\Delta\upsilon_{FW} = \frac{\left(\Gamma v_g g_{th}\right)^2 \eta_0}{4\pi P_0} n_{sp} h\nu(1+\alpha^2) \qquad (6.2)$$

where v_g is the group velocity, Γ is the optical confinement factor, g_{th} is the threshold value of optical gain, η_0 is the single facet efficiency, P_0 is optical power, n_{sp} is the spontaneous emission factor [Coldren 1995], and α is the linewidth broadening factor.

In the previous section, we analyzed variation of the group index due to the nonlinear wave interaction; therefore we can make conclusions about corresponding variation of the linewidth. Assuming these variations occur at constant output power (of probe wave), we obtain the dependence of linewidth on the optical frequency as shown in Fig. 6.8. There are peaks (poles) of linewidth, corresponding to the points of the critically-anomalous dispersion. This fact indicates that it is impossible to observe the laser spectrum in that point. On the other hand, there are minima of linewidth where the wave interaction produces slow light. Thus, the nonlinear interaction leads to an induced spectral narrowing of probe-wave emission. In Fig. 6.8, this narrowing is about 30 times that of the unperturbed case. The narrowing may occur due to proper tuning of probe wave and by variation of power in the driving wave.

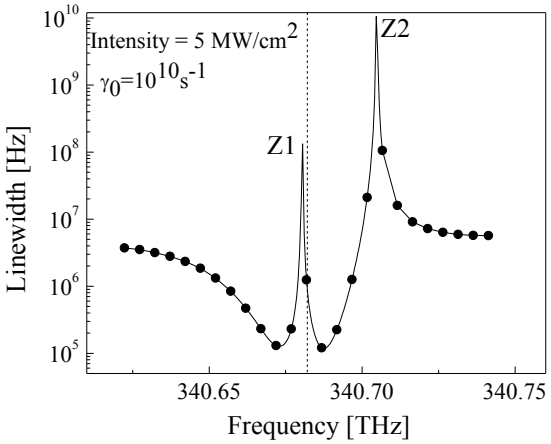

Fig. 6.8. Calculated spectrum of the perturbed linewidth in vicinity of the driving wave frequency 340.682 THz (shown by the dotted-dashed vertical line). The intensity of driving wave is 5 MW/cm^2.Critically anomalous dispersion points are Z1 and Z2

The induced narrowing/broadening phenomenon can be explained as a result of variation of the photon density in the probe mode influenced by the group velocity. If the emission power of the probe wave is fixed but group velocity decreases, this decrease corresponds to an increase of the photon density. We understand that the output optical power is proportional to the photon density multiplied by the group velocity. So the condition of fixed power immediately leads to an increase of photon density. Induced narrowing is the result of accumulation higher number of photons in mode with slow photons. The *Q*-factor of the mode under consideration is proportional to optical energy accumulated in the mode divided by the rate of loss of coherent emission energy. An increase of *Q*-factor corresponds to narrowing of the linewidth. In the case of fast light, similar relationships would lead to the spectral broadening. It is important to note that the regime of fixed power can be easily violated in practice because of influence of the group velocity on the optical gain. Thus, our assumption is valid only for a special case. A more detailed analysis will be needed for a general description of the spectral behavior.

6.3.5. Critically anomalous dispersion (CAD) loop

There is a small area on the diagram of probe wave frequency versus driving wave intensity, where the negative dispersion is sufficiently high. This area is contoured by the CAD lines of Z1 and Z2. They form closed loops ("CAD-loops"), as shown in Figs. 6.9 and 6.10.

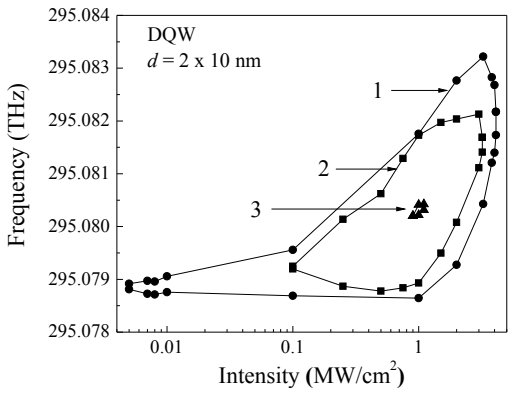

Fig. 6.9. Position of the CAD points Z1 and Z2 as function of laser emission intensity of the driving wave in the DQW laser structure. 1) $\gamma_0 = 10^9$ s^{-1};2) $\gamma_0 = 5\times10^9$ s^{-1}; 3) $\gamma_0 = 10^{10}$ s^{-1}.

The threshold of the CAD appearance increases from ~5 kW/cm^2 when $\gamma_0 = 10^9$ s^{-1} to ~1 MW/cm^2 when $\gamma_0 = 10^{10}$ s^{-1} in the case of DQW structure . The right-end closing of the loops depends also on the carrier relaxation rate and it shifts to lower intensities with increasing γ_0.

A superluminal behavior of the probe wave is expected at the Z-lines and in close vicinity of those lines. The influence of the relaxation rate is also demonstrated in the figures. Three different values of γ_0 are used in calculation. Increase of the initial relaxation rate leads to decrease of the area inside loop. The magnitude of the nonlinear interaction decreases with increase in relaxation rate. This is because the duration of scattering of the strong mode on the dynamic carrier density grating formed due to interference of the strong and weak modes is reduced because of shorter lifetime of carriers.

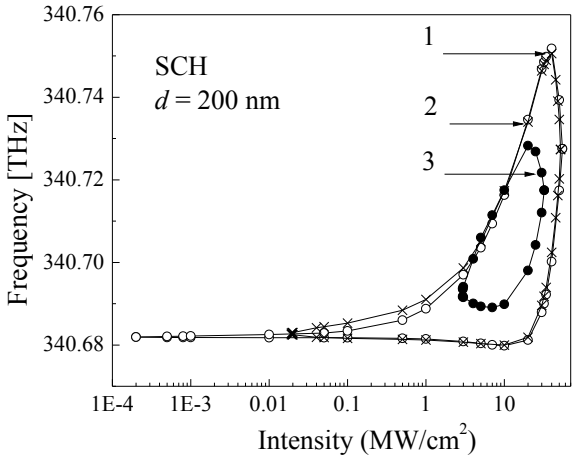

Fig. 6.10. CAD-map of the probe wave in the SCH-structure (a dependence of CAD frequency on the intensity of the driving wave): 1) $\gamma_0 = 10^9$ s^{-1}; 2) $\gamma_0 = 10^{10}$ s^{-1}; 3) $\gamma_0 = 10^{11}$ s^{-1}.

There is no CAD expected at γ_0 larger than 10^{10} s^{-1} in the case of DQW structure. This means that under the conditions considered in this study, any components of nonlinear interaction with higher relaxation rate do not produce the effect of CAD. At high intensities,

maximum limitation (~5 MW/cm^2) corresponds to a laser regime that is rather close to the limit of optical self-damage. The maximum width of the loop in Fig. 6.9 for the DQW structure is about 4 GHz.

6.3.6. Intensity threshold for superluminal propagation

As can be seen in Fig. 6.9, the CAD solutions appear at the intensity of driving wave exceeding approximately 5 kW/cm^2. This is an intensity threshold for a possible superluminal effect. Z-lines initially diverge to give a wider range of more than 4 GHz between Z_1 and Z_2. Then, the Z-lines converge with a further increase in the intensity, and finally collapse at ~4 MW/cm^2, so there are no CAD solutions above this power level. An increase in the initial carrier relaxation rate to 5×10^9 s^{-1} leads to an increase in the lower threshold of the CAD appearance to about 0.1 MW/cm^2. The broadening produces a decrease in the peak magnitude of the interaction effect. In particular, at $\gamma_0 > 10^{11}$ s^{-1}, there are no CAD points at all. The influence of initial relaxation rate on the CAD phenomenon is summarized in the Table 6.4.

Table 6.4. Influence of the initial relaxation rate on the threshold of CAD points in the SCH-structure

Initial carrier relaxation rate γ_0, s^{-1}	Intensity threshold of CAD points, kW/cm^2	
	SCH	DQW
10^9	0.2	5
5×10^9	10	100
10^{10}	~20	900
10^{11}	2940	No CAD points
10^{12}	No CAD points	No CAD points

6.3.7. Behavior in the CAD loop

When the probe wave frequency is varied with respect to the fixed driving frequency, crossing of the point Z1 corresponds to a change of sign of the group velocity as shown in Fig. 6.6. Inside the Z-loop one has a situation where group velocity is directed in opposite direction to the phase velocity. One interesting consequence of the wave interaction is that it produces the backscattering in the probe wave. The model of the wave interaction does not involve dissipation mechanism of probe wave; therefore the attenuation of the probe wave (as it follows from calculation of the imaginary part of the index) occurs by generation of photons in the opposite direction to the flow of the probe wave. In laser case the coherent backscattering of the beam should not produce significant problem except the correction of the actual value of the optical feedback. In contrast to this, in the optical amplifier the induced backscattering can be serious source of instability of the operation regime. The nonlinear backscattering can produce laser oscillation in the probe wave (on a higher-shifted frequency). This parasitic lasing in the amplifier is not desirable as it produces distortion of the output spectrum and takes power from driving wave

Some points of Z1 type appear very close to the zero detuning line .We don't consider the self-action of the wave in our approach (we assume that probe wave is much weaker than driving wave). Thus we should exclude from consideration the Z1 points which are closer to zero detuning than actual bandwidth of the driving wave. Hence, we emphasize here that for the experimental study of the behavior near CAD point requires very monochromatic waves for both driving and probe waves.

6.4. Discussion

6.4.1. Feasibility of superluminal behavior

Theoretical calculation and analysis of data on the group index perturbation under the influence of a strong (driving) monochromatic wave have been performed. The analysis

shows that in some frequency range (above the frequency of a driving wave) the group index decreases to negative values. The negative group velocity corresponds to reflection of the photon flow in direction opposite to direction of the phase velocity. In the intermediate region between negative and positive group index, there is a range for the index passing zero value and changing a sign. If the group index is between 1 and -1, one deals with superluminal propagation (formally the group velocity is higher than the light velocity in vacuum, *c*).

The magnitude of nonlinear perturbation depends on the intensity of the driving wave, the relaxation rate, and also on the optical confinement in the laser structure. In the case of a DQW laser, the superluminal regime seems to be achievable if the total relaxation rate of the population of operating energy levels is less than about 10^{10} s^{-1}. As the rate of stimulated recombination contributes to the relaxation rate, the increase of intensity above 3-5 MW/cm^2 leads to the broadening of the perturbation spectrum and to decrease of the magnitude of the interaction effect. It prevents the achievement of the superluminal effect at higher intensities. The power dependence of CAD points Z1 and Z2 forms two branches that appear at about 5 kW /cm^2, then split wider and come together to close the contour at > 5 MW/cm^2.The prediction of closing the CAD loop relates to the nonlinear effect of the pulsation of the population, but not to other possible mechanisms like the electromagnetic induced transparency (EIT).

This behavior is qualitatively the same in the laser structure with bulk active region (SCH with 0.2-μm thick active layer), but the threshold for the superluminal propagation is lower and the closing of the Z1-Z2 contour occurs at higher intensity. This can be explained by larger factor of optical confinement that provides stronger contribution of the nonlinear effect localized in the active layer. Therefore, the nonlinear perturbation of this type is more pronounced in laser structures with a larger optical confinement factor. Thus, in vicinity of the driving wave frequency, one can obtain anomalous behavior of the probe wave, namely,

the slow and fast propagation under influence of the driving wave. The range where CAD points are achievable is calculated numerically for different starting conditions. It is shown that the range of intensities is limited from the threshold of the nonlinear effect (typically in the range 5-10 kW/cm^2) to the upper limit (5-10 MW/cm^2) imposed by the spectral broadening due to stimulated recombination.

6.4.2. Limitation from optical damage

Calculations of nonlinear effects performed in this paper are neglecting practical limitations from the optical damage to the lasing facets or the semiconductor material. At high intensities of the driving wave, catastrophic optical damage (COD) can occur. It usually occurs at the facets of the diode laser (catastrophic optical mirror damage). The damage threshold depends on the pulse width, and it has the lowest value for continuous-wave operation. Also, the COD threshold depends on details of the laser structure; and becomes higher for structures with lower optical confinement factor. This is why we do not indicate the COD limit on the CAD maps in Figs. 6.9 and 6.10. The critical intensity of the COD is around 4 MW/cm^2 for GaAs-based lasers operating CW at 830 nm [Shinozaki 1989], while for InGaAs QW-based lasers values up to 20 MW/cm^2 have been reported [Eliseev 1996]. In pulse regime, higher peak intensities can be achieved, depending on the pulse width and the duty cycle.

6.4.3. Threshold for CAD appearance and catastrophic optical damage (COD) limitation

The CAD-map shown in Fig. 6.10 is for the SCH laser structure. This is a dependence of CAD frequency as a function of the light intensity of the driving wave. It forms a closed loop for each value of γ_0. Lower branch of the loop is formed by dependence of point Z1 and upper branch is formed by dependence of point Z2. Inside each loop one has the negative group index that means the back reflection of the probe wave. Maximum difference between

Z1 and Z2 branches (width of the loop) is about 50 GHz. Therefore, the anomalous propagation of the probe wave can be observed at relatively small detuning of probe wave from the driving wave (about 0.1 nm in the wavelength scale). An experimental study of the superluminal propagation can be carried out with two highly monochromatic waves coupled to the semiconductor amplifier from external sources. One wave serves as a driving wave whereas probe wave should be detuned from driving wave into higher-frequency side. In the semiconductor laser with external cavity, the mode spacing is quite small, so the probe mode appears in the near vicinity of the dominating mode (the latter serves as the driving wave).

6.5. Conclusion

A possibility to obtain the regime of critically anomalous dispersion is demonstrated by calculation of the perturbation of propagation parameters in the semiconductor laser structures of SCH and QW types. This prediction is based on the coherent population oscillation model in the semiconductor amplifying medium. As a result of these calculations, one can expect anomalous phenomena like superluminal propagation, infinite group velocity and slowed back propagation at the probe wave frequency that is detuned from the driving wave into shorter wavelength side by several GHz. The carrier relaxation rate is a very important factor, influencing the power range and detuning range within which the critically anomalous dispersion can be expected. At high intensity of the driving wave, the effect disappears due to a decrease in the magnitude of the nonlinearity and also due to spectral broadening. The treated effect is more evident in laser structures with higher optical confinement factor, as verified by comparing a separate confinement heterostructure with a double-quantum-well structure.

Chapter 7

Modeling and analysis of NLI in short-wavelength laser devices

7.1. Introduction: Factor of wavelength

In this chapter, the NLI in short-wavelength III-Nitride lasers, whose wavelength ranges from 0.37 μm to 0.45 μm is considered for the very first time. The goal of this study is to verify if III-Nitride lasers are more advantageous to be used as active elements of optical sensor devices, especially ring laser gyro. The wavelength is about 2 times shorter in III-Nitride lasers when compared to the more traditional GaAs-based lasers. This difference seems to be useful for improving the sensitivity of the ring laser gyro sensor. As mentioned in the previous sections, the slope sensitivity of an active ring laser gyro is inversely proportional to the wavelength, therefore shorter wavelength means higher sensitivity. Besides the direct influence of the wavelength, there is an indirect influence via material parameters which can be wavelength-sensitive. Thus the factor of wavelength is not simple and it needs to be investigated. Another example of an application of short wavelength III-Nitride lasers is in Laser Doppler velocimetry for measuring blood flow rate in a human body [Kliese 2010]. It has been demonstrated that these lasers can detect very slow motion, in the range of tens micrometers per second.

The main focus of this study is operation of room-temperature ridge-waveguide laser diodes based on InGaN/GaN materials. The optical model of such structure is presented below and NLI is calculated to demonstrate the feasibility of superluminal propagation to improve the slope sensitivity of a ring laser gyro.

7.2. Optical model of laser structure based on InGaN/GaN QW

7.2.1. Vertical structure for guided waves

Laser action has been demonstrated by QW's based on InGaN/GaN material systems in wavelengths ranging from 0.37 μm to 0.45 μm; which partially cover the short-wavelength spectrum [Nakamura 1997]. The InGaN/GaN multilayer QW structure consists of GaN (substrate, waveguide layers), AlGaN (cladding and barrier layers), InGaN (QW active layer, sometimes waveguide layers, and layers relaxing mechanical stress). Here are some of the features of the InGaN/GaN QW system:

a) The above mentioned layers are not lattice matched, hence hetero-junctions are under residual stress.

b) The density of dislocation in the nitride structures is usually very high when compared with lasers based on GaAs and InP materials. The defect density is around 10^6-10^8 cm^{-2} .

c) In spite of numerous defects and mismatch stress, lasing operation occurs in InGaN/GaN QW systems and such lasers are used for multiple applications. A famous example is the blue-ray disks.

The InGaN/GaN QW laser which we discuss here is grown on a sapphire substrate which is available in 2 inch diameter. Thus, ring laser gyroscopes with ring configuration of 1-2 cm radius can be made with the InGaN/GaN system. We also consider the possibility to use anomalous material dispersion which is observed in this laser system [Djurisic 2001].

The epitaxial structure of the InGaN based QW structure operating around 0.4 μm has been obtained from [Piprek 2002]. The epitaxial structure along with refractive index and thickness of the layers taken from [Piprek 2002] is shown in Table 7.1. The thickness of the n-type cladding is changed and the compliance layer and substrate is replaced by the cladding layer to avoid the ghost or substrate modes. Fig. 7.1 shows the modified structure with the epitaxial layers. The refractive index values of the $Al_xGa_{1-x}N$ layers as function of wavelength and concentration are calculated using the formulae from [Laws 2001]. The

refractive index of $In_xGa_{1-x}N$ layers is calculated using the formulae from [Laws 2001], [McGraw-Hill 2009].

Table 7.1. DQW structure based on InGaN/GaN with the refractive index (*n*) and the thickness of the layers (*d*) in micrometers

Layer	**Material/Doping**	***n***	***d***
Contact	*p* GaN / 2×10^{20} cm^{-3}	2.54	0.03
Cladding	*p* $Al_{0.14}Ga_{0.86}N$/GaN SL / 1×10^{20} cm^{-3}	2.35	0.6
Waveguide	*p* GaN / 5×10^{18} cm^{-3}	2.54	0.1
Stopper	*p* $Al_{0.2}Ga_{0.8}N$ / 1×10^{19} cm^{-3}	2.23	0.02
Barrier	*n* $In_{0.02}Ga_{0.98}N$ / 7×10^{16} cm^{-3}	2.59	0.01
Quantum well	*n* $In_{0.15}Ga_{0.85}N$ / 7×10^{16} cm^{-3}	2.8	0.004
Barrier	*n* $In_{0.02}Ga_{0.98}N$ / 7×10^{16} cm^{-3}	2.59	0.01
Quantum well	*n* $In_{0.15}Ga_{0.85}N$ / 7×10^{16} cm^{-3}	2.8	0.004
Barrier	*n* $In_{0.02}Ga_{0.98}N$ / 7×10^{16} cm^{-3}	2.59	0.01
Waveguide	*n* GaN / 7×10^{17} cm^{-3}	2.54	0.1
Cladding	*n* $Al_{0.14}Ga_{0.86}N$/GaN SL / 3×10^{18} cm^{-3}	2.35	0.6
Compliance	*n* $In_{0.1}Ga_{0.9}N$ / 3×10^{18} cm^{-3}	2.8	0.1
Substrate	*n* GaN / 3×10^{18} cm^{-3}	2.35	-

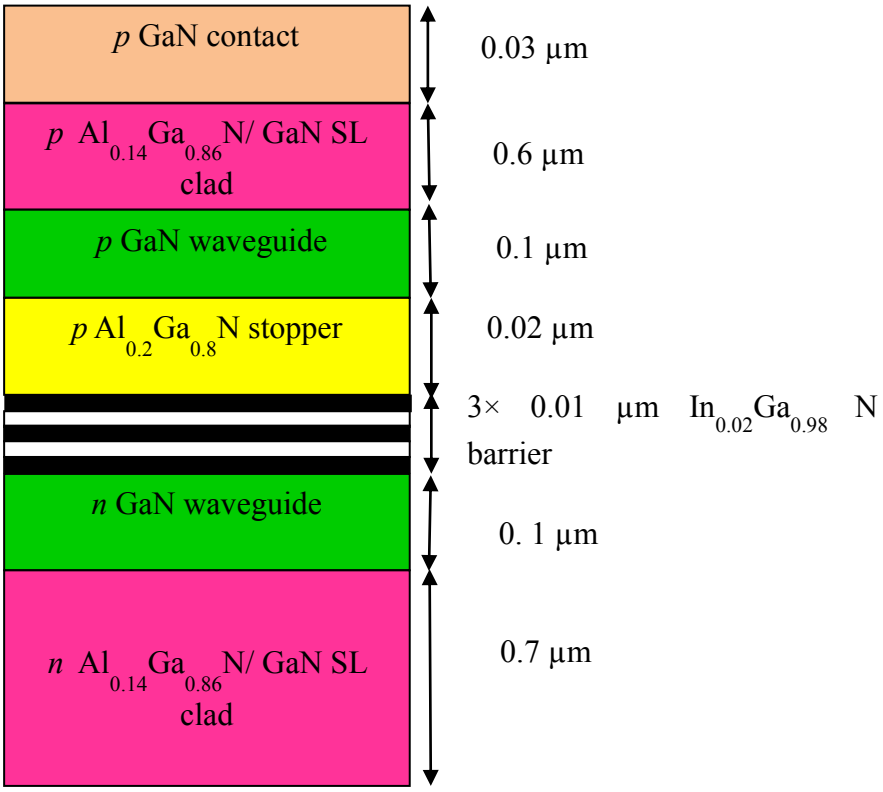

Fig. 7.1. Vertical structure of InGaN/GaN based QW laser showing epitaxial layers and their thicknesses

7.2.2. Lateral optical confinement

The lateral confinement is provided by the ridge waveguide structure. The parameters ridge width and the setback distance *h* influence the confinement of the mode. The setback distance *h* is the distance above the quantum well active region outside the ridge as shown in Fig.7.2.

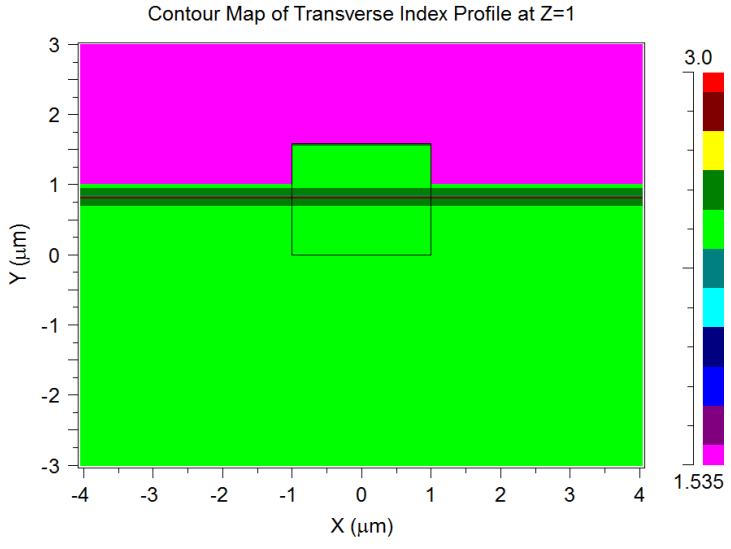

Fig.7.2. Transverse refractive index profile of InGaN/GaN based QW laser for *h* value of 0.19 μm

As the setback distance and ridge width are increased, the mode confinement decreases. We can obtain single mode operation by choosing an appropriate setback distance and ridge width. According to our calculations, an *h* value of 0.19 μm and ridge width of 2 μm gives single spatial mode operation. . At *h* value of 0.19 μm, the confinement of the first order mode disappears and we get only single mode operation. The *h* values are varied and the corresponding fundamental and first order modal profiles are calculated. In the nonlinear interaction model, we assume that both the driving and probe waves are operating in the single spatial mode regime. Hence, the spatial overlap between the modes is 100 %.

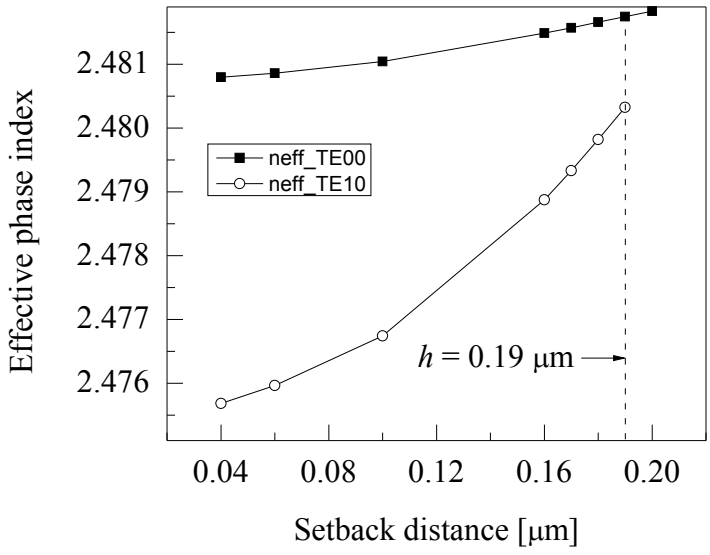

Fig.7.3. Dependence of effective phase index on the setback distance *h* for the fundamental and first-order modes in InGaN/GaN/AlGaN based QW laser.

The effective phase index n_{eff} is dependent on the lateral confinement of the ridge waveguide. The lateral confinement is influenced by the ridge width and the setback distance *h* as mentioned in the previous section. Fig.7.3. shows the dependence of effective phase index of the fundamental and the first order modes on the setback distance *h*. As the setback distance increases, the effective phase index increases and the confinement of the modes

decrease. For a setback distance *h* of 0.19 µm, the first order mode disappears. Hence, we get single spatial mode operation after a setback distance of *h* = 0.19 µm; which we used in our NLI calculations. The transverse modal profiles for fundamental and first order TE like modes are shown in Figs. 7.4 and 7.5 respectively. The colors on the right indicate the intensity values normalized to 1. The highest intensity value is denoted by red color and appears in the active region as shown in Fig 7.4. In Fig 7.5, which has the first order TE like mode, the highest intensity is outside the ridge; hence it's not a real modal profile.

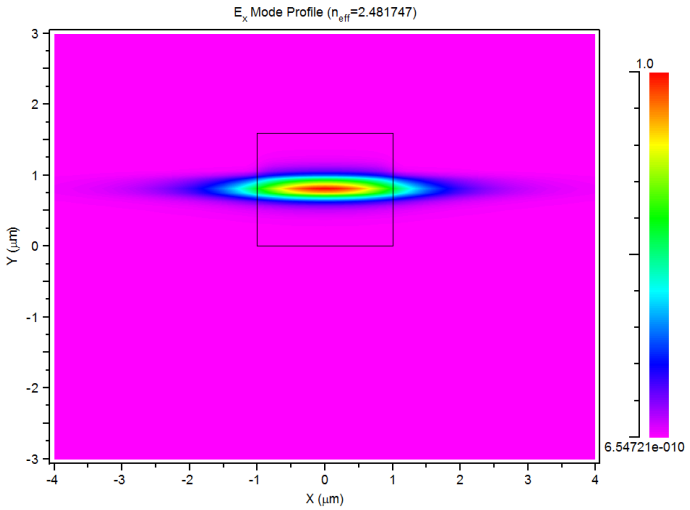

Fig.7.4. Fundamental TE like mode of InGaN based QW laser for *h* value of 0.19 µm

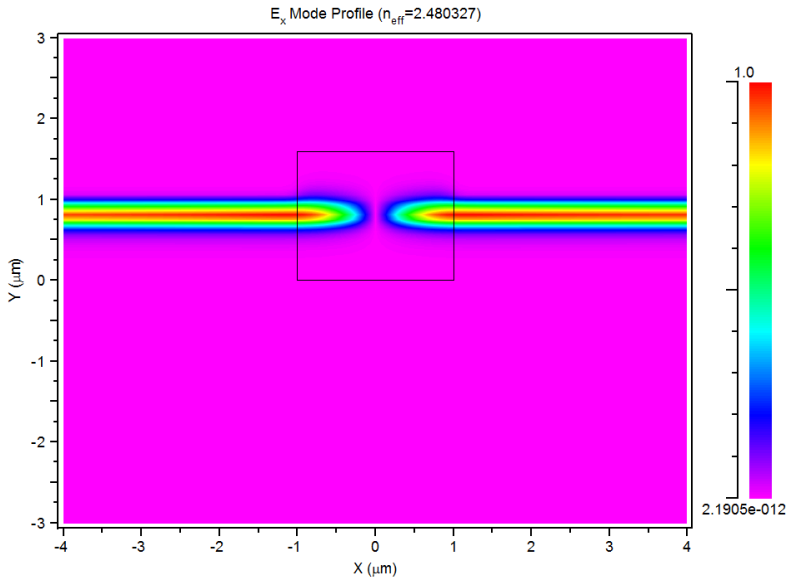

Fig. 7.5. First order TE like mode of InGaN based QW laser for *h* value of 0.19 µm

7.3. Estimation of slope sensitivity, K_0

The linear slope sensitivity K_0 of an active ring laser gyro is given by the Eqn.7.1 which is mentioned again here

$$K_0 = 4A/(\lambda L n_{g0}) \tag{7.1}$$

where, A is the ring area (area of projection of the ring on a plane perpendicular to the rotation axis), λ is the wavelength in vacuum, L is the length of ring perimeter, n_{g0} is the linear group index or the background value of group index, in the absence of a strong driving wave that provides the initial slope sensitivity.

In this section, we calculate the linear slope sensitivity, K_0 (i.e, in the absence of NLI) of the active ring laser gyroscope using Eqn. 7.1. K_0 is calculated for various laser systems having different active regions operating at different wavelengths. For a ring of radius 1cm, Table 7.2 shows the K_0 values. The slope sensitivity (scale factor) in laser gyro is in reverse proportionality to wavelength and group index. Hence, the background value of sensitivity, K_0 appears to be significantly larger in InGaN/GaN laser at 0.4 μm than the other lasers operating at 0.88, 1.016 and 1.55 μm due to lower wavelength of operation and lower group index. Hence, nitride-based lasers have definite advantages in terms of rotation sensitivity than longer-wavelength lasers.

Table 7.2. Calculated linear slope sensitivity, K_0 for various laser systems in the absence of NLI between the modes

Material system	Wavelength, λ [μm]	Active region thickness, d [μm]	n_{g0}	Linear slope sensitivity,K_0
InGaN/GaN/AlGaN DQW	0.4	0.008	3.18	~15720
GaAs/AlGaAs DHS	0.88	0.2	4.54	5004

InGaAs/GaAs/AlGaAs DQW	1.016	0.02	4.02	4902
InGaAsP/InP TQW	1.55	0.0135	3.73	3459
InGaAsP/InP DHS	1.55	0.1	5.3	2435

7.4. Material dispersion in GaN and InGaN

In this section, the nonlinear enhancement of rotation sensitivity is compared with effect of material dispersion that is rather prominent in nitride-based lasers. According to the empirical data on refractive index of GaN, there is relatively wide range of negative dispersion of the material refractive index just above the edge of intrinsic absorption, where inter-band absorption rises very steeply. This behavior is also extended to InGaN alloy in the vicinity of the absorption edge where the static dispersion is negative [Djurisic 2001].This situation can be used for obtaining a CAD point; it is more convenient to work with a stable or a static CAD point than a dynamic one. We inspect available data on negative dispersion in GaN and InGaN in order to design a ring laser device whose active region has both amplifying and CAD elements in the same material, e.g, InGaN. Therefore, we can use that specific wavelength range where dispersion is negative to obtain enhanced rotation sensitivity without applying any driving wave. In Table 7.3, we indicate ranges of negative dispersion where one can look for desirable CAD point, whereas more precise indication will need further investigation.

Table 7.3. Ranges of negative material dispersion in GaN and $In_xGa_{1-x}N$

Composition *x*	Wavelength, nm	Photon energy, eV	Reference
0	342 - 376	3.296 – 3.624	a)
0.1	390 - 420	2.952 - 3.179	b)
0.2	450 – 500	2.479 – 2.750	b)

0.3	530 - 630	1.968 – 2.339	b)

Fig.7.6 shows the spectral ranges of laser action and negative dispersion as function of $In_xGa_{1-x}N$ alloy composition, it is obtained from [Djurisic2001].

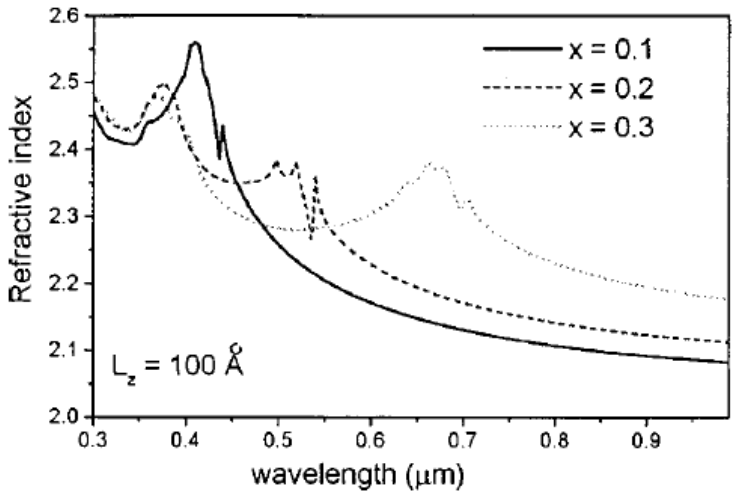

Fig.7.6. Phase index of $In_xGa_{1-x}N$ for various concentrations of indium. The static negative dispersion near the absorption edge for indium concentration, *x* of 0.2 is circled.

We consider the case of x = 0.2, and plotted the refractive index as function of frequency as shown in Fig.7.7.The group index corresponding to the phase index near the absorption edges circled in red and blue are plotted in Fig 7.8 and Fig.7.9 respectively.

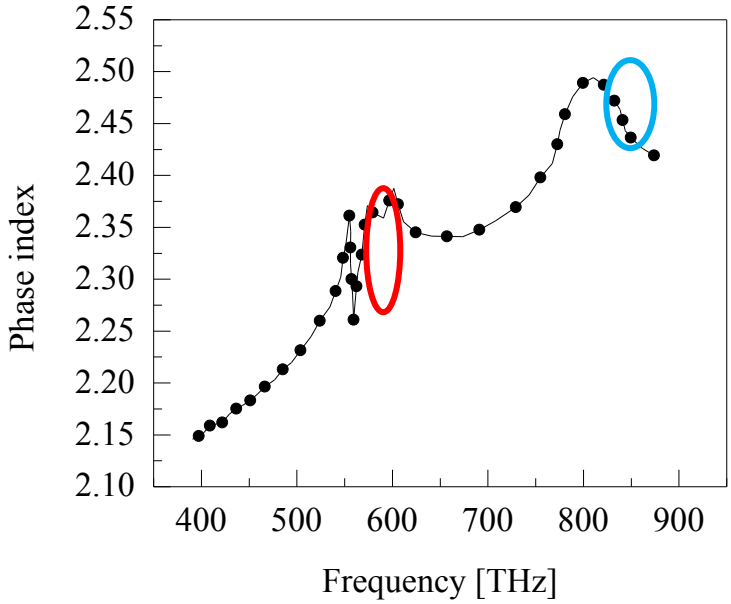

Fig.7.7. Calculated dependence of phase index on frequency for $In_{0.2}Ga_{0.8}N$ [Djurisic 2001]

The fast light region is where the group index is between -1 and 1 in the figure. In cases where there is no possibility to match these points in one device, it is possible to use two-section ring laser with one section for optical gain and another section for modified negative dispersion similar to [Kotlicki 2012]. The two sections should have different chemical content, and this can be difficult to construct monolithically. In contrast to this, in the case of nonlinear interaction one can get perturbed parameters at any spectral point of laser operation by proper tuning of the driving wave.

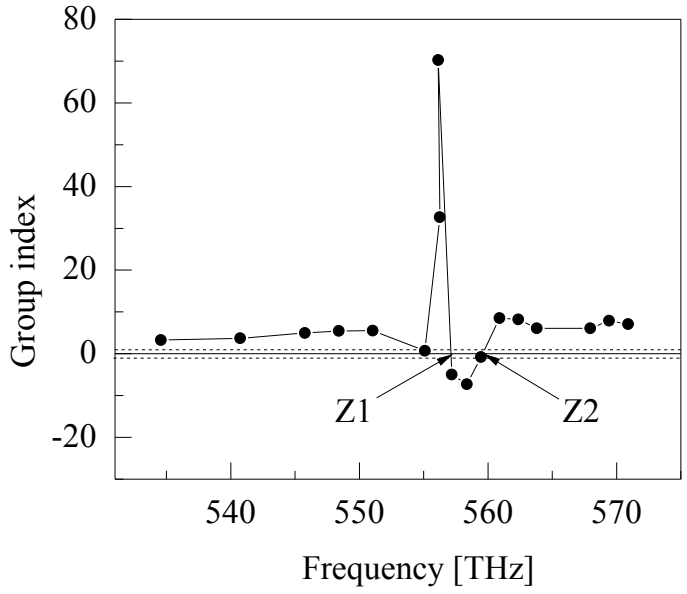

Fig.7.8. Calculated group index of $In_{0.2}Ga_{0.8}N$ near the absorption edge as circled in red in Fig. 7.7. Z1 and Z2 are the critically anomalous dispersion points.

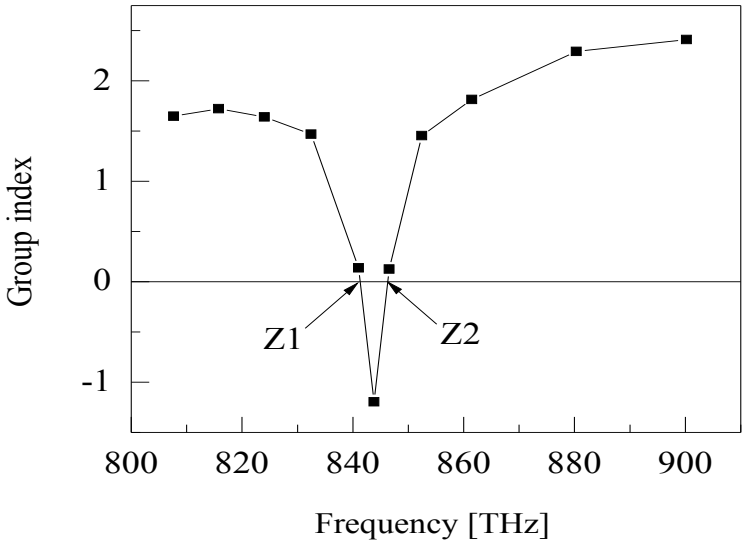

Fig.7.9. Calculated group index of $In_{0.2}Ga_{0.8}N$ near the absorption edge as circled in blue in Fig.7.7. Z1 and Z2 are the critically anomalous dispersion points.

7.5. Nonlinear perturbation theory and numerical simulations

7.5.1. Spectra of perturbed effective phase index and group index of probe wave

The perturbation in phase index of probe wave under the influence of driving wave calculated as a function of detuning frequency is given by eqn. 17 and is mentioned here again:

$$\delta n = -|E_0|^2 B(N - N_0)(d\varepsilon'' / dN)(\alpha + \Omega / \gamma) / \left[2n\gamma(1 + \frac{\Omega^2}{\gamma^2}) \right] \tag{7.2}$$

$$n_{g,eff} = n_{eff} + \omega \frac{\partial n_{eff}}{\partial \omega} \tag{7.3}$$

The perturbed value of phase index is added to the linear part of the phase index in the active region and the perturbed effective phase index, n_{eff} is calculated for detuning frequencies around the driving wave. Table 7.4 gives the values of parameters used in calculation of the perturbed phase index of Eqn.7.2 and also the parameters used for modeling of the ridge waveguide structures. FemSIM module developed by RSoft is used for numerical modeling and simulation of the RW laser structures in order to obtain perturbed effective phase index. The induced effective group index, $n_{\text{g,eff}}$ is calculated from perturbed effective phase index, n_{eff} given by Eqn.7.3 and is again mentioned here.

Table 7.4. Parameters used in numerical calculations

Parameter	**Units**	**QW**
Active layerthickness	μm	0.008
Ridge width	μm	2.0
Operational wavelength	μm	0.4
Optical frequencyof driving wave, ν_s	THz	749.5
Line width broadening factor, α	-	5.6
Stimulated recombination coefficient,*B*	cm^2/V^2s	0.973
Initial relaxation rate, γ_0	1/s	10^9
dg/dN	10^{-16} cm^2	1.3

$d\varepsilon''/dN$	10^{-21} cm^3	-2.32
Linear effective phase index	-	2.48
Linear effective group index	-	3.18

Fig. 7.10 shows the perturbed effective phase index on the left hand side and the modified effective group index on the right hand side. The phase index and group index are calculated for a particular case where the driving wave intensity is 5 MW/cm^2 and initial relaxation rate of carriers is 10^9 s^{-1}. From Fig. 7.10, we can observe that the effective phase index experiences perturbation only on the order of 10^{-4}. Since the perturbation occurs only in very narrow range of frequency, the induced dispersion dn/dv is very high. Hence, the small perturbation of phase index is enough to produce a significant modification of group index from the back ground level. The points Z1 and Z2 are the critically anomalous dispersion (CAD) points where the group index passes zero value.

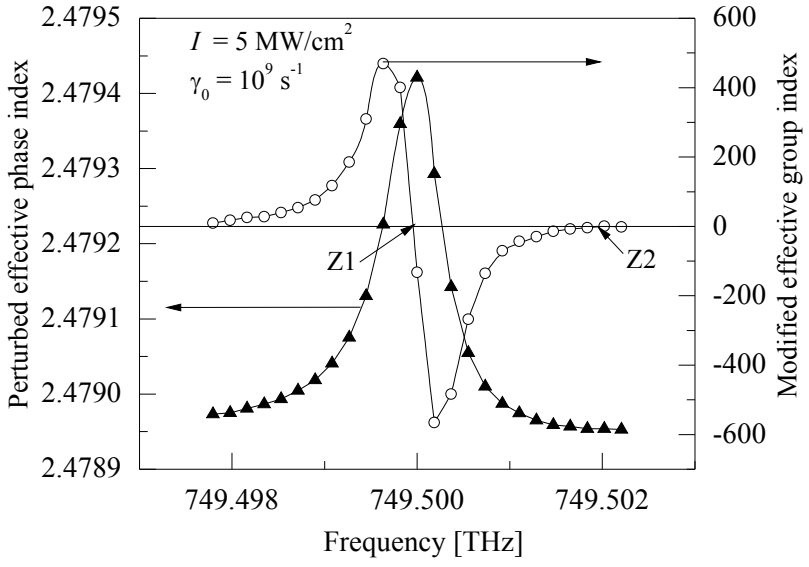

Fig.7.10. Calculated spectrum of the perturbed effective modal index and induced effective group index as a function of driving wave frequency for the InGaN/GaN/AlGaN QW

structure. The driving wave intensity is 5 MW/cm^2 and the initial relaxation rate is 10^9 s^{-1}. The dotted vertical line corresponds to the driving wave frequency of 749.5 THz.

7.5.2. Critically anomalous dispersion (CAD) loop

The CAD points Z1 and Z2 are plotted for various driving wave intensities in Fig. 7.11 similar to the previous sections. The dotted horizontal line represents the driving wave frequency. The CAD loop does not close even at very high intensity of 100 MW/cm^2 unlike in other laser structures based on GaAs, InGaAs [Kalagara 2012], [Kalagara 2013a] and InGaAsP [Kalagara 2013b]. The reason is the magnitude of nonlinear mode interaction in vicinity of the CAD point Z2 is higher for InGaN/GaN/AlGaN laser structure. This is due to the smaller *B* parameter which influences the decrease of relaxation rate under high intense driving wave. The shortening of the relaxation rate leads to increase of the interaction magnitude. There is an upper limit of diving wave intensity we can use due to the catastrophic optical damage. Experimental data on high-intensity limitation are available relating to the catastrophic optical damage (COD). According to [Takeya 2005], degradation phenomenon happens in blue-violet laser diodes at output power of 250 mW in continuous wave (CW) regime. The critical output intensity is measured to be ~4×10^7 W/cm^2. This value is about 10 times higher than that in AlGaAs lasers. The COD limit is even higher in diodes operating in a pulsed regime. According to these data, we indicate in Fig.7.11, a dotted line at driving wave intensity of 4×10^7 W/cm^2 and show calculated results up to 10^8 W/cm^2. The range between may be covered by pulse regimes.

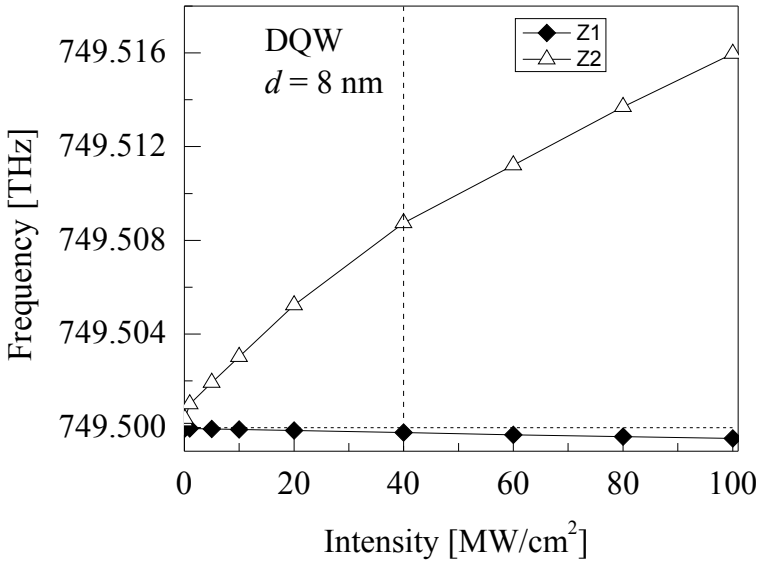

Fig.7.11. Position of the CAD points Z1 and Z2 as a function of the driving wave intensity in the QW structure. The initial carrier relaxation rate γ_0 is 10^9 s^{-1}. The dashed horizontal line corresponds to the driving wave frequency and the dashed vertical line corresponds to the catastrophic optical damage limit in CW regime.

Fig. 7.12 shows the peak of slowing and backward slowing as function of driving wave intensity. This data can be advantageous when the NLI is used for developing optical delay devices and for other slow-light applications as well as for optical devices based on the phase conjugation mechanism. It's seen here the intensity threshold for these effects is rather low and the detuning of reflection peak is of several GHz.

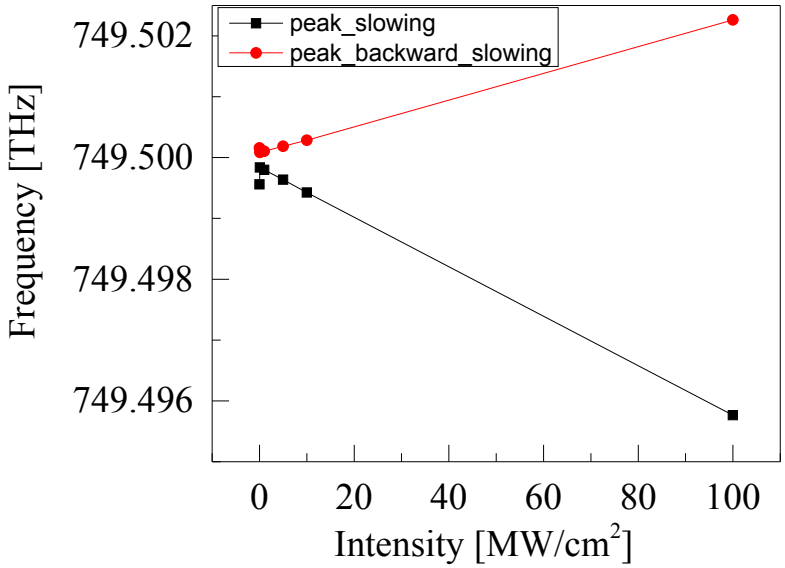

Fig.7.12. Peaks of slowing of forward and backward propagating waves. The initial carrier relaxation rate γ_0 is 10^9 s^{-1}.

7.6. Improvement in slope sensitivity in nonlinear regime in InGaN/GaN QW

In this section, we show the improvement in slope sensitivity of a ring laser gyro of radius 1cm to a rotation rate of 1 rad/s when operated in the nonlinear regime. The ring laser gyro is made up of InGaN/GaN QW materials system. From the results of table 6.2, we can conclude that InGaN- based lasers have higher linear slope sensitivity. When we take into account NLI effect, in the vicinity of CAD point, the slope sensitivity K is increasing steadily. At a proper detuning from CAD point Z2, we can obtain an increase of at least 10^3 times in the slope sensitivity as shown in Fig. 7.13. The dotted line in Fig.7.13 indicates the linear slope sensitivity

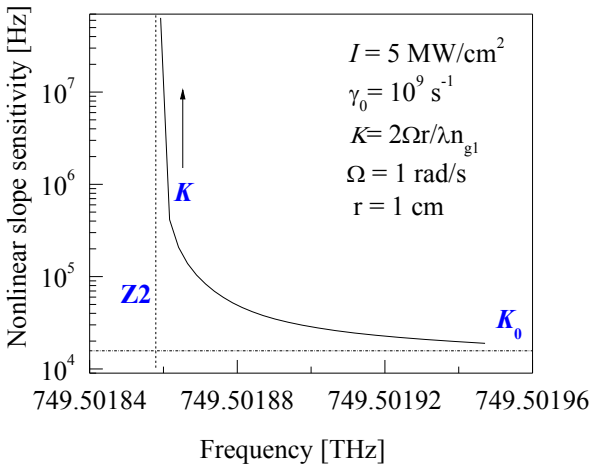

Fig. 7.13. Improvement in slope sensitivity in InGaN/GaN/AlGaN QW laser at 0.4 μm.

7.7. Conclusion

In conclusion, we present the theoretical analysis of conditions for the negative induced dispersion in order to obtain the superluminal propagation of emission of the probe wave in InGaN/GaN/AlGaN based lasers. The linear slope sensitivity of ring laser gyros made of InGaN/GaN/AlGaN material is higher due to the lower wavelength of operation and lower group index. Also, the nonlinear interaction between the modes in InGaN/GaN/AlGaN lasers is higher due to smaller values of *B* parameter when compared to the longer wavelength lasers. Thus, ring laser gyroscopes made of InGaN/GaN/AlGaN material system should act as better rotation sensors when compared to their longer wavelength counterparts. We also consider the possibility to use static (material) anomalous dispersion to obtain superluminal effect in InGaN-based lasers.

Chapter 8

Influence of second-order dispersion of group index

The aim of this section is to find a new expression for group index taking into account second order dispersion term. We also calculated the second order dispersion term for a particular set of parameters to determine if it's large enough to shift the CAD points and in turn affect the beat frequency splitting in a ring laser gyro. The group velocity of a wave is the velocity with which the overall shape of the waves' amplitudes known as the *modulation* or *envelope* of the wave propagates through medium.

8.1. Sagnac effect and influence of group index

The calculation of slope sensitivity and group index in a ring cavity filled with a semiconductor medium mentioned in this section is from [Eliseev 2006].Consider a homogenous circular ring cavity of radius *R,* for example an integrated optical waveguide in a semiconductor laser. Let's assume there are two counter propagating traveling waves, which are the independent modes of the laser cavity. They both have the same frequency ν_0 if the cavity is not moving and is given by the following expression:

$$\nu_0 = \frac{cq}{n_0 L} \tag{8.1}$$

Where, c is the velocity of light in vacuum, q is the longitudinal mode index, n_0 is the refractive index at frequency ν_0, L is the perimeter of the ring.

Now, let's assume the cavity is rotating with a constant angular velocity, Ω in clockwise direction. In this situation, the counter propagating waves have different frequencies due to change in the length at which the phase is reproduced. Hence, the phase velocities of the counter propagating waves also change. Since, we are interested in applications such as ring laser gyroscopes for navigation purposes, the rotation rate is quite low; hence $(\Omega R/c)^2$ is also quite low and therefore any relativistic effects can be ignored.

Consider a wave propagating in the same direction as the medium (clockwise). The length L^+ at which the phase is reproduced will be $2\Omega R+\Omega RT^+$, where, Ω is the angular rotation rate, R is the radius of the ring, T^+ is the round trip transit time, the term ΩRT^+ has to be added to $2\Omega R$ because the medium would have traversed an additional ΩRT^+distance. The phase velocity is given by:

$$V^+ = \frac{c}{n^+} + \alpha^+ \Omega R \tag{8.2}$$

Where, n^+ is the refractive index at the frequency ν^+, which is the new shifted frequency, α^+ is the drag coefficient. The equation for round trip transit time is given by:

$$T^+ = \frac{L^+}{V^+} = \frac{2\pi R + \Omega R T^+}{\frac{c}{n^+} + \alpha^+ \Omega R} \tag{8.3}$$

Solving for T+ gives the following expression

$$T^+ = \frac{2\pi R}{\frac{c}{n^+} - \Omega R(1-\alpha^+)} \tag{8.4}$$

Similarly, for the counter propagating wave, we have $L^- = 2\pi R - \Omega R T^-$; phase velocity, $V^- = \frac{c}{n-} - \alpha^- \Omega R$ and

$$T^- = \frac{2\pi R}{\frac{c}{n-} + \Omega R(1-\alpha^-)} \tag{8.5}$$

The frequencies of the counter propagating modes have to follow the conservation of the mode index, i.e, the mode numbers remain constant.

$$q = \nu_0 T_0 = \nu^+ T^+ = \nu^- T^-$$

Which gives

$$\Delta\nu = \nu^- - \nu^+ = \nu_0 T_0 \left(\frac{1}{T^-} - \frac{1}{T^+}\right) \tag{8.6}$$

Substituting equations 8.4 and 8.5, in equation 8.6, we get

$$= \frac{\nu_0 T_0}{2\pi R}[(\frac{c}{n^-} + \Omega R(1-\alpha^-)) - (\frac{c}{n^+} - \Omega R(1-\alpha^+))]$$

$$= \frac{\nu_0 n_0}{c}[\Omega R(2-\alpha^+ - \alpha^-) + \frac{c}{n^-} - \frac{c}{n^+}] \quad (8.7)$$

$\frac{c}{n^-} - \frac{c}{n^+} \approx \frac{-c}{n_0^{\,2}} \Delta\nu \frac{dn}{d\nu}$ is obtained by taking into account first order dispersion

Substituting in equation (8.7) and rearranging the terms gives the equation for Δν.

$$\Delta\nu(1 + \frac{\nu_0}{n_0} \cdot \frac{dn}{d\nu}) = \frac{2\Omega R \nu_0 n_0}{c}(1-\alpha)$$

Where, $\alpha = \frac{\alpha^+ + \alpha^-}{2}$ and the solution is given by:

$$\Delta\nu = \frac{2\Omega R \nu_0 n_0}{c}(1-\alpha)(1 + \frac{\nu_0}{n_0} \cdot \frac{dn}{d\nu})^{-1} \quad (8.8)$$

The drag coefficient according to Fresnel, when the source moves along with the cavity, is given by the following expression:

$$\alpha = 1 - \frac{1}{n^2} \quad (8.9)$$

Substituting equation (8.9) in equation (8.8) gives:

$$\Delta\nu = \frac{2\Omega R \nu_0}{c}[n_0(1 + \frac{\nu_0}{n_0} \cdot \frac{dn}{d\nu})^{-1}] = \frac{2\Omega R}{\lambda n_{g0}}$$

Where, $n_{g0} = n_0(1 + \frac{\nu_0}{n_0} \cdot \frac{dn}{d\nu}) = n_0 + \nu_0 \frac{dn}{d\nu}$ (8.10)

8.2. Influence of second order group index on Sagnac effect

The expression 8.11 which is given below is obtained from [Scorgie1993]

$$\frac{\Delta\omega}{\omega} = -\frac{1}{N}\left[\frac{4A\Omega}{\sigma c} + \Delta\right] \quad (8.11)$$

which gives the frequency splitting, Δω between clockwise and counter clockwise propagating waves in a ring resonator when we take into account only first order dispersion.

In Eqn.8.11, N is the mean value of the refractive index around the ring, A is the area of ring resonator **,** σ is the perimeter of the ring, Ω is the angular rotation rate, c is the velocity of light in vacuum, **Δ** is the mean value around the ring, of the difference between the two values of refractive index.Eqn.811 upon simplification gives ultimately the Eqn.8.10.

When we take into account second order dispersion in Eqn. 8.11, we obtain

$$\frac{\Delta\nu}{\nu} = \frac{-1}{n}\left[\frac{4A\Omega}{Lc} + \frac{dn}{d\nu}\Delta\nu + \frac{1}{2}\frac{d^2n}{d\nu^2}(\Delta\nu)^2\right] \tag{8.12}$$

Where, Δν is the frequency splitting between clockwise and counter clockwise propagating waves, ν is the central frequency; A is the area of ring resonator, L is the perimeter of the ring, Ω is the angular rotation rate, c is the velocity of light in vacuum.

After rearranging the above expression and substituting $c = \nu\lambda$, we obtain

$$\Delta\nu = \frac{-\nu}{n}\left[\frac{4A\Omega}{L\nu\lambda} + \frac{dn}{d\nu}\Delta\nu + \frac{1}{2}\frac{d^2n}{d\nu^2}(\Delta\nu)^2\right] \tag{8.13}$$

The below equations show the simplified steps of the above equation

$$\Delta\nu = -\frac{4A\Omega}{nL\lambda} - \frac{\nu}{n}\cdot\frac{dn}{d\nu}\Delta\nu - \frac{\nu}{2n}\cdot\frac{d^2n}{d\nu^2}(\Delta\nu)^2 \tag{8.14}$$

$$\frac{\nu}{2n}\frac{d^2n}{d\nu^2}\cdot(\Delta\nu)^2 + (1+\frac{\nu}{n}\frac{dn}{d\nu})\cdot\Delta\nu + \frac{4A\Omega}{nL\lambda} = 0 \tag{8.15}$$

$$(\Delta\nu)^2 + (1+\frac{\nu}{n}\frac{dn}{d\nu})\cdot\frac{2n}{\nu}\cdot\frac{1}{\frac{d^2n}{d\nu^2}}\cdot\Delta\nu + \frac{4A\Omega}{nL\lambda}\cdot\frac{2n}{\nu}\cdot\frac{1}{\frac{d^2n}{d\nu^2}} = 0 \tag{8.16}$$

$$(\Delta\nu)^2 + \frac{(n+\nu\frac{dn}{d\nu})}{n}\cdot\frac{2n}{\nu}\cdot\frac{1}{\frac{d^2n}{d\nu^2}}\cdot\Delta\nu + \frac{4A\Omega}{nL\lambda}\cdot\frac{2n}{\nu}\cdot\frac{1}{\frac{d^2n}{d\nu^2}} = 0 \tag{8.17}$$

Where, $n+\nu\frac{dn}{d\nu} = n_{g0}$, which is the first order group index. Substituting n_{g0} and $c = \nu\lambda$ in equation (8.16) gives the below equation,

$$(\Delta\nu)^2 + \frac{2n_{g0}}{\nu}\frac{1}{\frac{d^2n}{d\nu^2}}\cdot\Delta\nu + \frac{8A\Omega}{Lc}\cdot\frac{1}{\frac{d^2n}{d\nu^2}} = 0 \tag{8.17}$$

We now have a quadratic equation in $\Delta\nu$, and solving it gives the following equation

$$\Delta\nu = \frac{-\frac{2n_{g0}}{\nu}\frac{1}{\frac{d^2n}{d\nu^2}} \pm \sqrt{(\frac{2n_{g0}}{\nu}\frac{1}{\frac{d^2n}{d\nu^2}})^2 - 4\cdot\frac{8A\Omega}{Lc}\frac{1}{\frac{d^2n}{d\nu^2}}}}{2} \tag{8.18}$$

Rearranging the above equation leads to the following equation

$$\Delta\nu = \frac{-\frac{2n_{g0}}{\nu}\frac{1}{\frac{d^2n}{d\nu^2}} \pm \frac{2n_{g0}}{\nu}\frac{1}{\frac{d^2n}{d\nu^2}}\sqrt{1 - 4\cdot\frac{8A\Omega}{Lc}\frac{1}{\frac{d^2n}{d\nu^2}}\cdot\left(\frac{\nu}{2n_{g0}}\right)^2(\frac{d^2n}{d\nu^2})^2}}{2} \tag{8.19}$$

Simplifying the above equation leads to

$$\Delta\nu = -\frac{n_{g0}}{\nu}\frac{1}{\frac{d^2n}{d\nu^2}} \pm \frac{n_{g0}}{\nu}\frac{1}{\frac{d^2n}{d\nu^2}}\sqrt{1 - \frac{8A\Omega}{L\nu\lambda}\frac{1}{\frac{d^2n}{d\nu^2}}\cdot\frac{\nu^2}{{n_{g0}}^2}(\frac{d^2n}{d\nu^2})^2} \tag{8.20}$$

Further simplification leads to

$$\Delta\nu = -\frac{n_{g0}}{\nu}\frac{1}{\frac{d^2n}{d\nu^2}} \pm \frac{n_{g0}}{\nu}\frac{1}{\frac{d^2n}{d\nu^2}}\sqrt{1 - 2\cdot\frac{4A\Omega}{L\lambda n_{g0}}\cdot\frac{\nu}{n_{g0}}\frac{d^2n}{d\nu^2}} \tag{8.21}$$

$$\Delta\nu = -\frac{n_{g0}}{\nu}\frac{1}{\frac{d^2n}{d\nu^2}} \pm \frac{n_{g0}}{\nu}\frac{1}{\frac{d^2n}{d\nu^2}}\sqrt{1 - 2\cdot\Delta\nu_0\cdot\frac{\nu}{n_{g0}}\frac{d^2n}{d\nu^2}} \tag{8.22}$$

Assuming $2\cdot\Delta\nu_0\cdot\frac{\nu}{n_{g0}}\frac{d^2n}{d\nu^2} << 1$ (8.23)

i.e, $2\cdot\frac{4\Omega A}{L\lambda n_{g0}}\cdot\frac{\nu}{n_{g0}}\frac{d^2n}{d\nu^2} << 1$

$$\Omega << \frac{L\lambda {n_{g0}}^2}{8A\nu}\cdot\frac{1}{\frac{d^2n}{d\nu^2}} \tag{8.24}$$

When the rotation rate Ω satisfies the criterion (8.24), we can safely assume inequality (8.23). We will illustrate with an example. Lets consider the case of a monolithically integrated ring laser based on InGaN/GaN QW material system, of radius $r = 1cm$ and operating at $\lambda = 0.4\mu m$. The unperturbed group index, $n_{g0} = 3.2$

Substituting for $L = 2\pi r$ and $A = \pi r^2$, we get

$$\frac{L\lambda {n_{g0}}^2}{8A\nu} \cdot \frac{1}{\frac{d^2 n}{d\nu^2}} = \frac{\lambda^2 {n_{g0}}^2}{4rc} \cdot \frac{1}{\frac{d^2 n}{d\nu^2}}$$

Substituting the values of λ, n_{g0}, r and c we obtain,

$$\frac{\lambda^2 {n_{g0}}^2}{4rc} \cdot \frac{1}{\frac{d^2 n}{d\nu^2}} = 0.14 \times 10^{-18} \cdot \frac{1}{\frac{d^2 n}{d\nu^2}}$$

$$\frac{1}{\frac{d^2 n}{d\nu^2}} >> 0.14 \times 10^{-18}$$

Hence, the assumption is a valid assumption.

The equation (8.22) can be simplified using taylor series expansion

$$\sqrt{1+x} \approx 1 + \frac{x}{2} - \frac{1}{8}x^2$$

Where,

$$x = -2\Delta\nu_0 \cdot \frac{\nu}{n_{g0}} \frac{d^2 n}{d\nu^2}$$

$$\sqrt{1 - 2 \cdot \Delta\nu_0 \cdot \frac{\nu}{n_{g0}} \frac{d^2 n}{d\nu^2}} \approx 1 - \Delta\nu_0 \cdot \frac{\nu}{n_{g0}} \frac{d^2 n}{d\nu^2} - \frac{1}{2} \frac{\Delta {\nu_0}^2 \nu^2}{{n_{g0}}^2} \left(\frac{d^2 n}{d\nu^2}\right)^2$$

Plugging the above term in equation (8.22) gives the following

$$\Delta\nu = -\frac{n_{g0}}{\nu} \frac{1}{\frac{d^2 n}{d\nu^2}} \pm \frac{n_{g0}}{\nu} \frac{1}{\frac{d^2 n}{d\nu^2}} \left(1 - \Delta\nu_0 \cdot \frac{\nu}{n_{g0}} \frac{d^2 n}{d\nu^2} - \frac{1}{2} \frac{\Delta {\nu_0}^2 \nu^2}{{n_{g0}}^2} \left(\frac{d^2 n}{d\nu^2}\right)^2\right) \quad (8.25)$$

Further simplification of the above equation gives

$$\Delta\nu = -\frac{n_{g0}}{\nu}\frac{1}{\frac{d^2n}{d\nu^2}} \pm \left(\frac{n_{g0}}{\nu}\frac{1}{\frac{d^2n}{d\nu^2}} - \Delta\nu_0 - \frac{1}{2}\frac{d^2n}{d\nu^2}\frac{\Delta{\nu_0}^2\nu}{n_{g0}}\right) \tag{8.26}$$

Equation (8.26) gives the two roots of the quadratic equation (8.17).

Case 1: In this section, we consider the first root of the quadratic equation.

$$\Delta\nu = -\frac{n_{g0}}{\nu}\frac{1}{\frac{d^2n}{d\nu^2}} + \left(\frac{n_{g0}}{\nu}\frac{1}{\frac{d^2n}{d\nu^2}} - \Delta\nu_0 - \frac{1}{2}\frac{d^2n}{d\nu^2}\frac{\Delta{\nu_0}^2\nu}{n_{g0}}\right)$$

$$\Delta\nu = -\Delta\nu_0 - \frac{1}{2}\frac{d^2n}{d\nu^2}\frac{\Delta{\nu_0}^2\nu}{n_{g0}} \tag{8.27}$$

Case 2: In this section, we consider the second root of the quadratic equation.

$$\Delta\nu = -\frac{n_{g0}}{\nu}\frac{1}{\frac{d^2n}{d\nu^2}} - \left(\frac{n_{g0}}{\nu}\frac{1}{\frac{d^2n}{d\nu^2}} - \Delta\nu_0 - \frac{1}{2}\frac{d^2n}{d\nu^2}\frac{\Delta{\nu_0}^2\nu}{n_{g0}}\right)$$

$$\Delta\nu = \Delta\nu_0 - \frac{2n_{g0}}{\nu}\frac{1}{\frac{d^2n}{d\nu^2}} + \frac{1}{2}\frac{d^2n}{d\nu^2}\frac{\Delta{\nu_0}^2\nu}{n_{g0}} \tag{8.28}$$

The second case is not a valid solution. The reason is when $\frac{d^2n}{d\nu^2} = 0$, the second term on the right hand side of equation(8.28) increases infinitely.

The frequency splitting when we take into account second order dispersion is denoted by $\Delta\nu_1$ and given by the following expression:

$$\Delta\nu_1 = -\frac{4\Omega A}{L\lambda n_{g1}} \tag{8.29}$$

Where, Ω is the angular rotation rate, A is the area of ring resonator, L is the perimeter of the ring, λ is the central wavelength and n_{g1} is the group index approximated to second order.

Equation (8.29) can be written as:

$$-\frac{4\Omega A}{L\lambda n_{g1}} = -\frac{1}{2}\frac{d^2 n}{d\nu^2}\left(\frac{4\Omega A}{L\lambda n_{g0}}\right)^2 \frac{\nu}{n_{g0}} - \frac{4\Omega A}{L\lambda n_{g0}} \tag{8.30}$$

Upon simplification, we obtain the new group index after taking into account second order dispersion

$$n_{g1} = \frac{1}{\left|\frac{1}{n_{g0}} - \frac{1}{2}\frac{d^2 n}{d\nu^2}\Delta\nu_0 \frac{\nu}{{n_{g0}}^2}\right|} \tag{8.31}$$

The effect of second order dispersion also called, as the group velocity dispersion is very small. This is illustrated in the figures shown below. A ring laser gyro of radius 1 cm for various rotation rates is shown below. The 1st curve represents beat frequency splitting for group index when only first order correction is taken into account. The 2nd curve represents beat frequency splitting for group index when both first order and second order correction are taken into account. The second order beat frequency splitting is $\Delta\nu = \Delta\nu_0 - \frac{1}{2}\frac{d^2 n}{d\nu^2}\frac{{\Delta\nu_0}^2 \nu}{n_{g0}}$

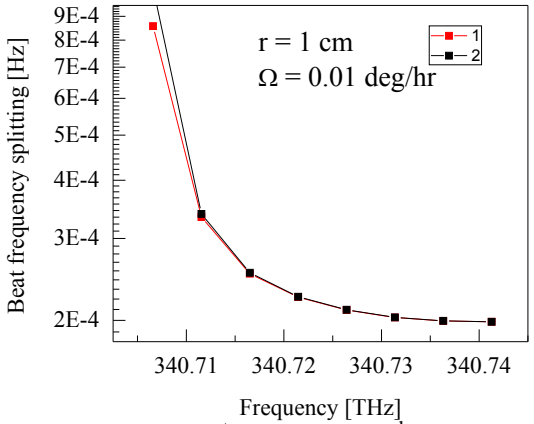

Fig. 8.1. Beat frequency splitting for 1st (red) and 2nd (black) order dispersion. The radius of ring, r = 1 cm, rotation rate, Ω = 0.01 deg/hr (aircraft navigation)

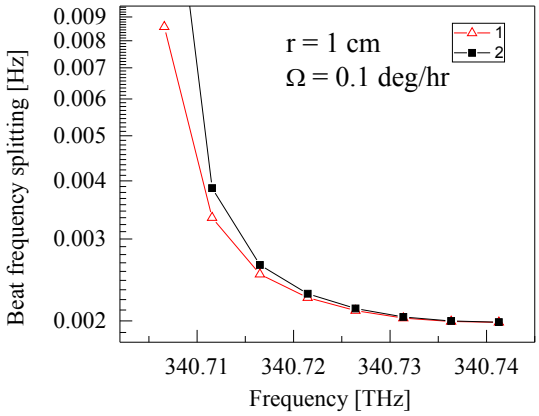

Fig 8.2. Beat frequency splitting for 1st (red) and 2nd (black) order dispersion. The radius of ring, r = 1 cm, rotation rate, Ω = 0.1 deg/hr (air-to-ground space craft)

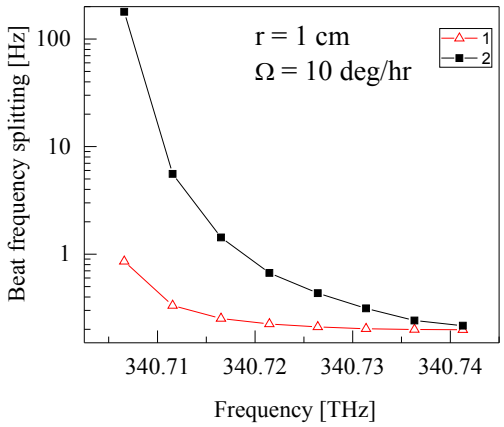

Fig. 8.3. Beat frequency splitting for 1st (red) and 2nd (black) order dispersion. The radius of ring, r = 1 cm, rotation rate, Ω = 10 deg/hr (aircraft navigation)

These results indicate that the effect of 2nd order correction depends on the rotation rate of gyro and the correction is negligible for navigation range.

Chapter 9

Conclusion and future work

9.1. Conclusion

The numerical modeling and analysis of parametric interaction of two-waves based on coherent population oscillation (CPO) in an amplifying semiconductor medium is carried out. The results obtained allow us to interpret optical properties of semiconductor lasers and SOAs when two waves are present in spectral vicinity. The driving wave, assumed to be much stronger than the probe wave, influences the complex permittivity at the probe wave frequency, providing substantial modification of parameters of the probe wave such as phase index, gain, linewidth and group index resulting in slow light, fast light, critically anomalous dispersion (CAD), super continuum emission, backward reflection, etc.

Superluminal light can be used for improving of sensitivity of rotation sensors and other interferometric sensors for detecting nano-displacement, ultra-low vibration, acceleration and even gravitational waves. In a monolithically integrated ring laser, in the non-linear regime, the Sagnac related response is infinity at critically anomalous dispersion (CAD) point. Therefore, by operating in the vicinity of critically anomalous dispersion (CAD) point, where we expect superluminal propagation, allows us to improve the sensitivity of ring laser gyros and interferometric sensors by manifolds. Hence, identification of critically anomalous dispersion (CAD) points is a crucial task of our project.

The numerical simulation of nonlinear interaction (NLI) was performed in various ridge-waveguide laser structures operating in the wavelength range of 0.4 μm to 1.55 μm. The most important feature of the present work is theoretically verifying the feasibility of obtaining superluminal propagation in ridge-waveguide lasers by calculating the actual perturbation of modal parameters, rather than using a simple approximation with plane wave parameters. In the framework of CPO interaction, we computed perturbation of effective

phase index, gain, group index and linewidth at various driving wave intensities for certain frequency detuning range between the interacting waves. Similar to results reported in Chapter 5 for InGaAsP/InP structures, loops of critically anomalous dispersion are made by plotting CAD frequencies versus driving wave intensity for all laser systems under consideration. The numerical simulation illustrates the ranges of threshold intensity of driving wave for the CAD points to appear, as well as maximum driving wave intensity at which the relaxation-related broadening reduces the magnitude of the nonlinear effect. Also, the CAD loops give information about the frequency ranges where we can observe superluminal propagation. We found that the laser structures with larger optical confinement demonstrate larger ranges of induced anomalous dispersion. In devices with bulky active region, the maximum driving wave intensity for observation of CAD points exceeds the intensity of the catastrophic optical damage.

Comparison of our theoretical data with available experimental data on perturbed pulse delay between the pump and probe beams travelling in a SOA lead to a qualitative agreement between the two and identification of CAD points for the very first time. The increase or decrease of the delay depending on the detuning between the waves indicates the phenomenon of slow and fast light. Since nonlinear interaction (NLI) is sensitive to the value of γ_0, it also allowed us to estimate the carrier relaxation rate γ_0, the spectral range where nonlinear perturbation takes place. From γ_0, the characteristic lifetime, $1/\gamma_0$ was found to be ~0.5 ns, which falls into standard range of recombination lifetimes for excess carriers in InGaAsP. This result indicates that the CPO model of parametric interaction is adequate.

Our main conclusions are as follows:

1. The nonlinear interaction (NLI) between a driving wave and a probe wave that are in close spectral vicinity in a semiconductor medium produces substantial perturbation of group velocity resulting in slow light, fast light, CAD and backward propagating light.

The numerical modeling of NLI is performed and feasibility of superluminal light is theoretically demonstrated in ridge waveguide lasers ranging from 0.4 μm to 1.55 μm. An important feature of the dynamically induced dispersion is to be able to produce perturbed propagation at any spectral range where optical transitions exist.

2. In addition to the group velocity perturbation, the gain and linewidth experienced by the probe wave also gets perturbed. In the slow light regime, additional gain and narrowing of line width are observed and in the fast light regime, additional suppression of gain and broadening of the linewidth are observed. The interpretation for the mechanism of additional narrowing due to NLI is given.
3. The magnitude of NLI was found to be sensitive to the driving wave intensity, frequency detuning between driving and probe waves, lifetime of carriers, optical confinement factor, driving wave wavelength and linewidth broadening factor. The CAD points which were shown to form a loop, are calculated at different laser wavelengths and for different values of background relaxation rate. Among all the laser structures considered, nitride-based lasers operating at 0.4 μm have the highest magnitude of NLI
4. The theoretical perturbed group index which we calculated is compared with available experimental data [Pesala 2005] on perturbed delay of optical pulse in InGaAsP/InP based SOA. The interpretation of the comparison of both data was done and critically anomalous dispersion (CAD) point has been identified for the first time.
5. Our calculations indicate the slope sensitivity of a monolithically integrated ring laser gyro whose radius is 1 cm and based on InGaAs-, GaAs-, InGaAsP-, InGaN- material systems, was improved by atleast 10^3 times, in the vicinity of CAD point.
6. The emission spectrum of laser operating at the CAD point is characterized by an infinite linewidth, also called as *super continuum* light or "white-light". Hence, due to the non-analytic behavior at the CAD point, it is not convenient for precise measurements, but we

can operate reasonably close to the CAD point. At the CAD point, very broad-band emission is observed and looks very similar to spontaneous emission. However, the spatial configuration of the supercontinuum emission corresponds to laser condition of high efficiency. Hence, the intensity can be orders of value higher in comparison to spontaneous emission sources and thermal sources. Also, the laser-emitted supercontinuum is characterized by very high speed performance.

9.2. Future work

The following areas listed here need further investigation:

Stable and reproducible operation regime near the CAD point has to be achieved and calculation of values of real parameters in optimal regime of NLI has to be performed.

Investigation of the regime of backward slowed propagation of light (n_g < -1) has to be performed from Einstein's causality point of view.

Experimental verification of nonlinear Sagnac response has to be performed.

Experimental verification of slow light related narrowing and fast light related broadening of the laser line has to be performed.

The nonlinear interaction of modes lead to anomalous splitting of mode beating line according to eqn. 9.1, where Δν is the mode spacing, c is the velocity of light in vacuum, n_g is the group index and L is the length of cavity

$$\Delta\nu = \frac{c}{2n_g L} \tag{9.1}$$

In the eqn 9.1, the mode spacing Δν, is in reverse proportion to group index, perturbation in group index resulting in slow and fast light, leads to perturbation of mode beating. Hence, the verification of slow/fast light can be done using experimental data on anomalous beat frequency splitting in InGaAs/GaAs/AlGaAs QW LD at 1.016 μm as shown in fig. 9.1 [Eliseev 2005a].

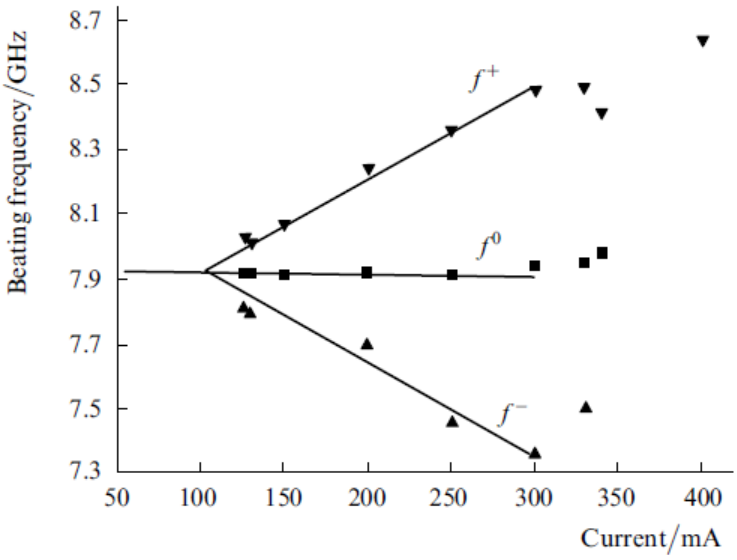

Fig.9.1. Position of the beating lines in the *f* band as functions of current in the QW laser. Cavity length, *L* = 5 mm, temperature, T = 15 ° C.

In fig. 9.1, the beat frequency is plotted as function of injection current in the laser, where the anomalous splitting of the difference-frequency line into three components f^+, f^0 and f^- is observed. The splitting increases with increasing optical power above the threshold.

REFERENCES

[Adachi 1985] S. Adachi, "GaAs, AlAs, and Al_xGa_{1-x} As: Material parameters for use in research and device applications," *J. Appl. Phys*., vol. 58, no. 3, pp. R1–R29, 1 Aug. 1985.

[Adachi 1992] S.Adachi, "Physical Properties of III-Y Semiconductor compounds," *John Wiley and Sons*.,1992

[Basov 1961] N. G. Basov, O. N. Krokhin, and Yu. M. Popov, *Sov. Phys., ZhETF*., vol.40 no.1879, 1961.

[Basov 1966a] N. G. Basov, R. V. Ambartsumyan, V. S. Zuev, P. G. Kryukov, and V. S. Letokhov, " Propagation velocity of an intense light pulse in a medium with inverted population," *Sov. Phys-Doklady*., vol.10, pp. 1039-1040, 1966.

[Basov 1966b] N. G. Basov, R.V. Ambartsumyan, V. S. Zuev, P. G. Kryukov, and V. S. Letokhov, "Nonlinear amplification of light pulses," *Sov. Phys. JETP*., vol.23, pp.16 - 22, 1966.

[Bogatov 1974] A. P. Bogatov, P. G. Eliseev, and B. N. Sverdlov, "Anomalous interaction of spectral modes of oscillation in semiconductor laser," *Kvant. Elektronika*., vol.1, no.10, pp.2286-2288, 1974.

[Bogatov 1975] A. P. Bogatov, P. G. Eliseev, and B. N. Sverdlov, "Anomalous interaction of spectral modes in a semiconductor laser," *IEEE J. Quant. Electron*., vol.11 , no. 7, pp. 510-515, Jul.1975.

[Bachert 1978] H. J. Bachert, A. P. Bogatov, and P. G. Eliseev, "Mode deformation in an injection laser due to self-focusing and its relation to the nonlinearity of the output characteristics," *Kvant. Elektronika*., vol.5, no. 30, pp. 603-608, 1978.

[Bazhenov 1981] V. Yu. Bazhenov, A. P. Bogatov, P. G. Eliseev et al., “Bistable condition and spectral tuning of injection laser with external dispersive cavity,” *Kvant. Elektronika*., vol. 8, no.4, pp. 853-859, 1981.

[Broberg 1984] B. Broberg and S. Lindgren, “Refractive index of In1-xGaxAsyP1-y layers and InP in the transparent wavelength region,’’ *J. Appl. Phys*., vol. 55, no. 9, pp. 3376–3381, 1 May 1984.

[Bahae 1989] M. Sheik-Bahae, A.A. Said, and E.W. Van Stryland, "High Sensitivity, Single Beam n_2 Measurements," *Opt. Lett.*, vol. 14, pp. 955-957, 1989.

[Bahae 1990] M. Sheik-Bahae, A.A. Said, T.H. Wei, D.J. Hagan, and E.W. Van Stryland, "Sensitive Measurement of Optical Nonlinearities Using a Single Beam," *IEEE J. Quant. Electron*., vol.26, pp.760-769, 1990.

[Boyd 1992] R. W. Boyd, "*Nonlinear Optics*," *Academ. Press* .,1992.

[Bigelow 2003a] M. S. Bigelow, N. N. Lepeshkin, and R. W. Boyd, “Observation of ultraslow light propagation in a ruby crystal at room temperature,” *Phys*. *Rev*. *Lett*., vol. 90, no. 11, pp. 113903-1–113903-4, 21 Mar. 2003.

[Bigelow 2003b] M. S. Bigelow, N. N. Lepeshkin, and R. W. Boyd, “Superluminal and slow light propagation in a room-temperature solid,” *Science*., vol. 301, no. 5630, pp. 200-202, 11 July 2003.

[Boyd 2009] R. W. Boyd, “Slow and fast light: Fundamentals and applications,” *J. Mod. Opt*., vol. 56, no. 18–19, pp. 1908–1915, 20 Oct. – 10 Nov. 2009.

[Coldren 1995] L. A. Coldren and S. W. Corzine, "*Diode Lasers and Photonic Integrated Circuits*," *John Wiley & Sons*., New York, 1995.

[Cao 2005] H. Cao, C. Liu, H. Deng, M. Benavides, V. Smagley, R.Caldwell, G. M. Peak, G. A. Smolyakov, P. G. Eliseev, and M. Osinski, “Frequency beating between

monolithically integrated semiconductor ring lasers," *Appl. Phys. Lett.*, vol. 86, no. 041101, 2005.

[Djurisic 2001] Aleksandra B. Djurisic, and E. Herbert Li, "Dielectric function models for describing the optical properties of hexagonal GaN," *J. Appl. Phys.,* vol. 89, no.1, pp. 273-282, 2001.

[Eliseev 1970] P. G. Eliseev, "Waveguide theory of lasers on homojunctions and heterojunctions," *Preprint FIAN Lebedev Physics Institute*., vol. 30, 1970.

[Eliseev 1987] P. G. Eliseev and A. P. Bogatov, "Phenomena in semiconductor lasers associated with non-linear refraction and the influence of current carriers on the refractive index," *The Nonlinear Optics of Semiconductor Lasers*., pp. 19–69, edited by N.G. Basov, *Nova Sci. Publ*., Commack, N.Y,1987.

[Eliseev 1994] P. G. Eliseev, A. E. Drakin, and W. Pittroff, "A study of laser emission wavelength variations in 1.5 μm InGaAsP/InP BRS laser diodes: Theoretical model and experiment," *IEEE J. Quantum Electron*., vol. 30, no. 10, pp. 2271–2276, Oct. 1994.

[Eliseev 1996] P. G. Eliseev, "Optical strength of semiconductor laser materials," *Progress Quantum Electron.*, vol. 20, no. 1, pp. 1–82, 1996.

[Eliseev 2005a] P. G. Eliseev, C. Liu, H. Cao, and M. Osinski, "Spectral perturbations in a semiconductor laser: I. Anomalous splitting in the mode-beating spectrum," *IEEE* J.*Quant.Electron.*, vol. 35, no.9, pp.787-790, 2005.

[Eliseev 2005b] P. G. Eliseev, "Spectral perturbations in semiconductor laser, II. Nonlinear interaction of modes," *Quant. Electron.*, vol. 35, no. 9, pp.791-794, 2005.

[Eliseev 2006] P. G. Eliseev, "On the calculation of the gyro-factor in semiconductor ring laser," *Quant. Electron*., vol. 36, no. 8, pp. 738-749, Aug, 2006.

[Eliseev 2006] P. G. Eliseev, H. J. Cao, C. Y. Liu, G. A. Smolyakov, and M. Osiński, "Nonlinear mode interaction as a mechanism to obtain slow/fast light in diode lasers" *Physics and Simulation of Optoelectronic Devices XIV* (M. Osiński, F. Henneberger, and Y. Arakawa, Eds.), *Proc. SPIE*., vol. 6115, Art. 61150U (9 pp.), Jan. 2006.

[Eliseev 2007] P. G. Eliseev and M. Osiński, "Influence of nonlinear dispersion of the refractive index on the Sagnac effect in semiconductor ring lasers", *Physics and Simulation of Optoelectronic Devices XV* (M. Osiński, F. Henneberger, and Y. Arakawa, Eds.), *Proc. SPIE*., vol. 6468, pp. 64680B-1 – 64680B-8, 22-25 Jan. 2007.

[Eliseev 2007] P. G. Eliseev, and M. Osiński, "Effects of dispersion on the optical drag effect in a laser gyro," *Techn. Digest, 27th Annual Conf. Lasers & Electro-Optics CLEO*., Paper QTuB4, 6-11 May 2007.

[Eliseev 2008] P. G. Eliseev, "Theory of nonlinear Sagnac effect," *Opto-Electron. Rev*., vol. 16, no. 2, pp. 118–123, 2008.

[Faxvog 1970] F. R. Faxvog, C. N. Y. Chow, T. Bieber, and J. A. Carruthers, "Measured pulse velocity greater than *c* in a neon absorption cell," *Appl. Phys. Lett.,* vol. 17, no. 5, pp. 192–193, 1970.

[Feketa 1986] D. Feketa, K. T. Chan, J. M. Ballantyne, and L. F. Eastman, "Graded-index separate-confinement InGaAs/GaAs strained-layer quantum well laser grown by metalorganic chemical vapor deposition," *Appl. Phys. Lett*., vol. 49, no. 24, pp.1659-1660, 1986.

[Gibbs 1979] H. M. Gibbs, S. L. McCall, T. N. C. Venkatesan, A. C. Gossard, A. Passner and W. Wiegmann, "Optical bistability in semiconductors," *Appl. Phys.Lett*., vol. 35, no.6, pp. 451-453, 1979.

[Gan 2004] K. G. Gan and John E. Bowers, "Measurement of gain, group index, group velocity dispersion, and linewidth enhancement factor of an InGaN multiple quantum-

well laser diode," *IEEE Photonics Technology Letters*., vol. 16, no. 5, pp. 1256-1258, 2004.

[Henry 1982] C. H. Henry, "Theory of the linewidth of semiconductor lasers," *IEEE J. Quant. Electron*., vol.18, no.2, pp. 259-264, 1982.

[Harris 1992] S. E. Harris, J. E. Field, and A. Kasapi, "Dispersive properties of electromagnetically induced transparency," *Phys*. *Rev. A.*, vol. 46, no. 1, pp. R29-R32, 1992.

[Hau 1999] L. V. Hau, S. E. Harris, Z. Dutton, and C. H. Behroozi, "Light speed reduction to 17 metres per second in an ultracold atomic gas," *Nature*., vol. 397, no. 6720, pp. 594–598, 1999.

[Ishikawa 1982] H. Ishikawa, M. Yano, and M. Takusagawa, "Mechanism of asymmetric longitudinal mode competition in InGaAsP/InP lasers," *Appl. Phys. Lett*., vol.40, no.7, pp. 553-555, 1982.

[Jin 2002] J. Jin, "*The Finite Element Method in Electromagnetics*," *John Wiley & Sons*., 2nd Ed, New York, 2002.

[Koshiba 1994] M. Koshiba, S. Maruyama, and K. Hirayama, "A vector finite element method with the high-order mixed-interpolation-type triangular elements for optical waveguiding problems," *IEEE J. Lighwave Technol.*, vol. 12, no. 3, pp. 495, 1994.

[Kliese 2010] R. Kliese, Y. L. Lim, T. Bosch, and A. D. Rakić, "GaN laser self-mixing velocimeter for measuring slow flows," *Optics Lett*., vol. 35, no. 6, pp. 814-816, 2010.

[Kotlicki 2012] O. Kotlicki, J. Scheuer, and M. S. Shahriar, "Theoretical study on Brillouin fiber laser sensor based on white light cavity," *Optics express*., vol. 20, no. 27, pp. 28234-28248, 2012.

[Kalagara 2012] H. Kalagara, P. G. Eliseev, and M. Osiński, "Numerical simulation of nonlinear mode interactions in ridge-waveguide semiconductor lasers," *Physics and Simulation of Optoelectronic Devices XX* (B. Witzigmann, M. Osiński, F. Henneberger, and Y. Arakawa, Eds.), *Proc. SPIE*., vol. 8255, Art. 82550D (9 pp.), 2012.

[Kalagara 2013a] H. Kalagara, P. G. Eliseev, and M. Osinski, "Induced Anomalous Dispersion in Semiconductor Lasers," *IEEE J. Special Topics in Quant Electron.,* vol. 19, no. 4, pp. 150250-8, 2013.

[Kalagara 2013b] H. Kalagara, P. G. Eliseev, and M. Osiński, "Slow/fast light due to induced dispersion in 1.55 μm semiconductor lasers," *Proc. SPIE*., vol. 8619, pp. 86190, 2013.

[Laybourn 1999] P. J. Laybourn, M. Sorel, G. Giuliani, and S. Donati, "Integrated semiconductor laser rotation sensor," *Optoelectronics' 99-Integrated Optoelectronic Devices, International Society for Optics and Photonics*., pp. 322- 331, March 1999.

[Laws 2001] G. M. Laws, E. C. Larkins, I. Harrison, C. Molloy, and D. Somerford, "Improved refractive index formulas for the AlxGa1−xN and InyGa1-yN alloys," *J. Appl. Phys*., vol. 89, no. 2, pp. 1108-1115, 2001.

[Miller 1979] D. A. B. Miller, S. D. Smith, A. Johnston, "Optical bistability and signal amplification in a semiconductor crystal: application of new low power nonlinear effect in InSb," *Appl. Phys. Lett*., vol. 35, pp. 658-660, 1979.

[Miller 1981] D. A. B. Miller, S. D. Smith, and C.T. Seaton, "Optical bistability in semiconductors," *IEEE J. Quant. Electron*., vol.17, no.3, pp.312-317, 1981.

[Milonni 2004] P. W. Milonni, "*Fast light, Slow light and left-handed light*", *Institute of Physics Publishing*., 1st Ed, Philadelphia, 2004.

[Ogaswara 1984] N. Ogasawara, R. Ito, K. Tone, and H. Nakae, “Dispersion of the linewidth enhancement factor in semiconductor injection lasers,” *Jap. J. Appl. Phys*., vol.23, pp.518L-520L, 1984.

[Osinski 1987] M. Osinski and J. Buus, “Linewidth broadening factor in semiconductor lasers, An Overview,” *IEEE J. Quant. Electron*., vol. 23, no. 1, pp. 9-29, 1987.

[Ogaswara 1988a] N. Ogasawara and R. Ito, “Longitudinal mode competition and asymmetric gain saturation in semiconductor injection lasers. 1. Experiment,” *Jpn. J. Appl. Phys*. *Pt. 1*., vol. 27, no. 4, pp. 607-614, 1988.

[Ogaswara 1988b] N. Ogasawara, and R. Ito, “Longitudinal mode competition and asymmetric gain saturation in semiconductor injection lasers. 2. Theory,” *Jpn. J. Appl. Phys*. *Pt. 1*., vol. 27, no. 4, pp. 615–626, 1988.

[Okawachi 2005] Y. Okawachi, M. S. Bigelow, J. E. Sharping, Z. M. Zhu, A. Schweinsberg, D. J. Gauthier , R. W. Boyd, and A. L. Gaeta, “Tunable all-optical delays via Brillouin slow light in an optical fiber,” *Phys. Rev. Lett*., vol. 94, no. 15 , pp. 153902-1–153902-4, 2005.

[Osinski 2006] M. Osiński, H.-J. Cao, C.-Y Liu, and P. G. Eliseev, “Monolithically integrated twin ring diode lasers for rotation sensing application*s*,” *J. Cryst. Growth*., vol. 288, pp. 144-147, 2006.

[Post 1967] E. J. Post, “Sagnac Effect,” *Rev. Mod. Phys*., vol. 39, no. 2, pp. 475-493, 1967.

[Piprek 2002] J. Piprek and S. Nakamura, "Physics of high-power InGaN/GaN lasers," *Proc. Optoelectronics IEEE*., vol. 149, no. 4, pp. 145-151, 2002.

[Palinginis 2005] P. Palinginis, F. Sedgwick, S. Crankshaw, M. Moewe, and C. J. Chang-Hasnain, “Room temperature slow light in a quantum-well waveguide via coherent population oscillation,” *Opt. Express*., vol. 13, no. 99, pp.09–15, 2005.

[Pesala 2006] B. Pesala, Z. Y. Chen, A. V. Uskov, and C. Chang-Hasnain, “Experimental demonstration of slow and superluminal light in semiconductor optical amplifiers,” *Opt. Express*., vol. 14, no. 26, pp. 12968–12975, 2006.

[Rowe 2003] M. Röwe, P. Michler, J. Gutowski, V. Kümmler, A. Lell, and V. Härle, "Influence of the carrier density on the optical gain and refractive index change in InGaN laser structures," *physica status solidi*., vol. 200, no. 1, pp. 135-138, 2003.

[Shinozaki 1989] K. Shinozaki, A. Watanabe, R. Furukawa, and N. Watanabe, “High-power operation of 830-nm AlGaAs laser diodes,” *J. Appl. Phys*., vol. 65, no. 8, pp. 2907–2911, 1989.

[Schulz 1998] D. Schulz, C. Glingener, M. Bludszuweit, and E. Voges, “Mixed finite element beam propagation method,” *IEEE J. Lighwave Technol.*, vol. 16, no. 7, pp. 1336, 1998.

[Saitoh 2002] K. Saitoh and M. Koshiba, “Full-vectorial imaginary-distance beam propagation method based on a finite element scheme: Application to photonic crystal fibers,” *IEEE J. Quantum Electron*., vol. 38, no.7, pp. 927, 2002.

[Song 2005] K. Y. Song, M. Gonzalez Herráez, and L. Thévenaz, “Observation of pulse delaying and advancement in optical fibers using stimulated Brillouin scattering,” *Opt. Express*., vol. 13, no. 1, pp. 82–88, 2005.

[Sharping 2005] J. E. Sharping, Y. Okawachi, and A. L. Gaeta, “Wide bandwidth slow light using a Raman fiber amplifier,” *Opt. Express*., vol. 13, no. 16, pp. 6092–6098, 2005.

[Su 2006] H. Su, P. Kondratko, and S. L. Chuang, “Variable optical delay using population oscillation and four-wave-mixing in semiconductor optical amplifiers,” *Opt. Express.*, vol. 14**,** no. 11, pp. 4800–4807, 2006.

[Shahriar 2007] M. S. Shahriar, G. S. Pati, R. Tripathi, R., Gopal, V., Messall, and K. Salit, "Ultrahigh enhancement in absolute and relative rotation sensing using fast and slow light," *Phys. Rev. A*., vol.75, no.5, pp.053807- 053817, 2007.

[Shahriar 2007] M. S. Shahriar, G. S. Pati, and M. Messal, "Demonstration of interferometer sensitivity varying as the inverse of the group index," *Proc. SPIE*., vol. 6482, pp.64820L-1-9, 2007.

[Salit 2011] M. Salit, K. Salit, and P. Bauhahn, "Prospects for enhancement of ring laser gyroscopes using gaseous media," *Optics express*., vol.19, no. 25, pp.25312-25319, 2011.

[Thompson 1972] G. H. B. Thompson, "A theory of filamentation in semiconductor lasers including the dependence of dielectric constant on injected carrier density," *Opto-Electron*., vol. 4, pp. 257-310, 1972.

[Tsuji 1997] Y. Tsuji and M. Koshiba, "Guided-mode and leaky-mode analysis by imaginary distance beam propagation method based on finite element scheme," *IEEE J. Light. Technol.*, vol. 15, no. 9, pp. 1728, 1997.

[Taguchi 1998] K. Taguchi, K. Fukushima, A. Ishitani, and M. Ikeda "Optical inertial rotation sensor using semiconductor ring laser," *Electronics Letters.,* vol.34, no.18, pp. 1775-1776, 1998.

[Takeya 2005] M. Takeya, T. Hashizu, and M. Ikeda, "Degradation of GaN-based high-power lasers and recent advancements," *Proc. SPIE*., vol. 5738, pp. 63- 71, 2005.

[Uskov 2005] A. V. Uskov and C. Chang-Hasnain, "Slow and superluminal light in semiconductor optical amplifiers," *Electronics Letters*., vol. 41, no.16, pp. 55-56, 2005.

[Van Stryland 2009] E. Van Stryland, D. Williams, and W. Wolfe, "Handbook of Optics," edited by Michael Bass, *McGraw-Hill*., vol. 4, 3rd Ed, 2009.

[Westbrook 1986] L. D. Westbrook, "Measurements of *dg*/*dN* and *dn*/*dN* and their dependence on photon energy in 1.5 μm InGaAsP laser diodes," *IEE Proc. J. OptoElectron*., vol. 133, no. 2, pp. 135-142, 1986.

[Wang 2000] L. J. Wang, A. Kuzmich, and A. Dogariu, "Gain-assisted superluminal light propagation," *Nature*., vol. 406, no.6793, pp. 277-279, 2000.

[Witzigmann 2006] B. Witzigmann, V. Laino, M. Luisier, U. T. Schwarz, G. Feicht, W. Wegscheider, K. Engl et al, "Microscopic analysis of optical gain in InGaN/GaN quantum wells," *Appl. Phys*., vol. 88, no. 2, pp. 021104, 2006.

[Xu 1996] L. Xu, D. Garbuzov, S. Forrest, R. Menna, R. Martinelli, and J. Connolly, "Very low internal loss, 1.5 μm wavelength SCH-MQW InGaAsP/InP laser diodes with broadened-waveguides," *Lasers and Electro-Optics Society 9th Annual Meeting Conf. Proc*., vol. 1, pp. 352–353, Nov. 1996.

[Yamada 1989] M. Yamada, "Theoretical analysis of nonlinear optical phenomena taking into account the beating vibration of the electron density in semiconductor lasers," *J. Appl. Phys*., vol.66, no.1, pp.81-89, 1989.

[Yum 2008] H. N. Yum, M. Salit, G. S. Pati, S. Tseng, P. R. Hemmer, and M. S. Shahriar, "Fast-light in a photorefractive crystal for gravitational wave detection," *Optics express*., vol. 16, no. 25, pp. 20448-20456, 2008.

[Yum 2010] H. N. Yum, M. Salit, J. Yablon, K. Salit, Y. Wang, and M. S. Shahriar, "Superluminal ring laser for hypersensitive sensing," *Optics express.,* vol. 18, no. 17, pp.17658-17665, 2010.

[Zhu 2007] Z. Zhu, D. J. Gauthier, and R. W. Boyd, "Stored light in an optical fiber via stimulated Brillouin scattering," *Science*., vol.318, no. 5857, pp.1748-1750, 2007.

Publications

1. M. Osiński, G. A. Smolyakov, F.-H. Chu, H. S. Kalagara, and E. Mercado-Sotelo, "*Strongly injection-locked semiconductor ring lasers for ultrafast transmitters (Invited Paper)*", Technical Digest, International Photonics Conference, 8-10 December 2011, Tainan, Taiwan.
2. F.-H. Chu, L. Naznin, H. Kalagara, G. A. Smolyakov, and M. Osiński, "*Bending losses and modal properties of serpentine and bent waveguides*", Physics and Simulation of Optoelectronic Devices XX (B. Witzigmann, M. Osiński, F. Henneberger, and Y. Arakawa, Eds.), SPIE International Symposium on Integrated Optoelectronic Devices OPTO 2012, San Francisco, California, 23-26 January 2012, Proceedings of SPIE, Vol. 8255, Paper 825511 (9 pp.).
3. H. Kalagara, P. G. Eliseev, and M. Osiński, "*Slow/fast light due to induced dispersion in 1.55 μm semiconductor lasers*", Physics and Simulation of Optoelectronic Devices XXI (B. Witzigmann, M. Osiński, F. Henneberger, and Y. Arakawa, Eds.), SPIE International Symposium on Integrated Optoelectronic Devices OPTO 2013, San Francisco, California, 4-7 February 2013, Proceedings of SPIE, Vol. 8619, Paper 86190N (9 pp.).
4. H. Kalagara, P. G. Eliseev, and M. Osiński, "*Induced anomalous dispersion in semiconductor lasers*", IEEE Journal of Selected Topics in Quantum Electronics, Special Issue on Semiconductor Lasers, vol. 19, no. 4, Art. 1502508 (8 pp.), July/August 2013.
5. H. Kalagara, P. G. Eliseev, and M. Osiński, "*Numerical modeling of improvement in slope sensitivity of InGaN-based ring laser rotation sensor*", Physics and Simulation of Optoelectronic Devices XXII (B. Witzigmann, M. Osiński, F. Henneberger, and Y. Arakawa, Eds.), SPIE International Symposium on Integrated Optoelectronic Devices

OPTO 2014, San Francisco, California, 3-6 February 2014, Proceedings of SPIE, Vol. 8980, Paper 89800U (9 pp.).

6. H. Kalagara, G. A. Smolyakov, and M. Osiński, "*Rate equation analysis of Q-modulated strongly injection-locked whistle-geometry ring lasers*", IEEE Journal of Selected Topics in Quantum Electronics, Special Issue on Semiconductor Lasers, November/December 2015 (in print).

7. F.-H. Chu, H. Kalagara, G. A. Smolyakov, and M. Osiński, "*Reciprocity principle and nonequivalence of counterpropagating modes in whistle-geometry ring lasers*", accepted for Physics and Simulation of Optoelectronic Devices XXIV (B. Witzigmann, M. Osiński, and Y. Arakawa, Eds.), SPIE International Symposium on Integrated Optoelectronic Devices OPTO 2016, San Francisco, California, 13-8 February 2016.